RIPARIAN ZONE EVAPOTRANSPIRATION USING STREAMFLOW DIEL SIGNALS

by

Ethan Thomas Geisler

A thesis

submitted in partial fulfillment

of the requirements for the degree of

Master of Science in Hydrologic Sciences

Boise State University

May 2016

BOISE STATE UNIVERSITY GRADUATE COLLEGE

DEFENSE COMMITTEE AND FINAL READING APPROVALS

of the thesis submitted by

Ethan Thomas Geisler

Thesis Title: Riparian Zone Evapotranspiration Using Streamflow Diel Signals

Date of Final Oral Examination: 02 December 2015

The following individuals read and discussed the thesis submitted by student Ethan Thomas Geisler, and they evaluated his presentation and response to questions during the final oral examination. They found that the student passed the final oral examination.

James P. McNamara, Ph.D.	Chair, Supervisory Committee
Shawn G. Benner, Ph.D.	Member, Supervisory Committee
Alejandro N. Flores, Ph.D.	Member, Supervisory Committee

The final reading approval of the thesis was granted by James P. McNamara, Ph.D., Chair of the Supervisory Committee. The thesis was approved for the Graduate College by John R. Pelton, Ph.D., Dean of the Graduate College.

ACKNOWLEDGEMENTS

I would like to acknowledge and thank the students and faculty at Boise State University. I would like to acknowledge the financial support provided by the Boise State Geosciences Department. I would particularly like to thank my advisor Dr. Jim McNamara for allowing me the opportunity to be part of the Boise State Geosciences Department and all the help in the creation of this thesis. I would like to thank my committee members, Dr. Shawn Benner and Dr. Lejo Flores, for their added insight into the project and help in the completion of my thesis.

I would like to thank Pam Aishlin, at Boise State University, for everything she has done to help me with learning instrumentation and her guidance in performing hydrologic studies. She puts in a lot of work to acquire the data for thesis projects like this and it wouldn't be possible without her work.

I would like to also thank Dr. Patrick Burkhart, at Slippery Rock University, who encouraged me to become a scientist as an undergraduate at Slippery Rock University. His passion for science has inspired many individuals, and I strive to exemplify the same passion and inspiration in my work as a scientist.

Last but not least, I would like to acknowledge my family and friends who supported me along the way in following my endeavors. I would like to thank my wife, Elissa, who has been there for me throughout this entire process. I also would like to thank my parents, Dave and Linda, for all their support and encouragement.

ABSTRACT

Riparian zones are crucial regions of semi-arid and arid watersheds. In the summer, riparian zones provide an important habitat for the watershed since they have sufficient water supply throughout the year. However, little is known about the impact of riparian zone evapotranspiration (ET) at a watershed scale. The use of streamflow diel signals can provide a more thorough understanding of riparian zone processes, particularly evapotranspiration. The streamflow diel signals were analyzed for Dry Creek Experimental Watershed (DCEW), for the summer of 2014, to determine riparian evapotranspiration. The riparian zone evapotranspiration was compared to a spatially distributed evapotranspiration model to determine the influence of riparian ET, in comparison to watershed scale ET. The analyses showed that streamflow diel signals were complex and varied in both space and time. The amplitude of the diel signals played a key role in understanding riparian processes and showed that plant transpiration, water availability, and diel signal mixing all had an effect on the amplitude throughout the watershed. The diel signal was most accurate in the headwaters of the catchment, where diel signal mixing was at a minimum. Based on the headwaters of the catchment, riparian ET attributed up to 11% of the watershed scale ET. When taking into account the uncertainty associated with the spatially distributed ET model, the amount of riparian ET was negligible compared to watershed scale ET. Meteorological data and sap flux calculations support the conclusion that there was little riparian ET relative to watershed scale ET. Although riparian ET was minor compared to watershed scale ET, it was a

relatively large portion of streamflow during low flow in DCEW. The research provided insight into the analysis of diel signals and possible factors affecting diel signal characteristics.

TABLE OF CONTENTS

LIST OF TABLES

LIST OF FIGURES

LIST OF ABBREVIATIONS

ET	Evapotranspiration
DCEW	Dry Creek Experimental Watershed
LG	Lower Gauge
C2M	Confluence 2 Main
C2E	Confluence 2 East
C1W	Confluence 1 West
C1E	Confluence 1 East
VMC	Volumetric Moisture Content

1. INTRODUCTION

Evapotranspiration (ET) is an important flux of water from semiarid watersheds that can account for up to 90 percent of the exports from a watershed annually (e.g., Chauvin et al. 2011). Quantifying ET is important to understand water resources and land and atmospheric interactions, especially in complex mountainous terrain. Evapotranspiration, however, is difficult to measure in complex mountainous terrain. Generally, ET cannot be measured directly. Rather, ET must either be computed as a residual in the water balance or estimated based on meteorological observations.

Heterogeneity within a watershed can present challenges when calculating watershed scale ET with meteorological observations. Standard reference ET equations are commonly used to calculate the potential ET. However, this is not necessarily the actual evapotranspiration of the watershed (Allen et al. 1998). Spatial variability in moisture, at a watershed scale, can cause a divergence between actual ET and potential ET. Subsequently, understanding the water availability within an environment is an important step when estimating watershed scale ET.

ET is a function of the energy flux and the water supply within the system. Energy limited systems have ample water supply but lack the energy to evaporate the water from the system. On the other hand, water-limited systems have ample energy supply but lack sufficient water supply to meet the energy demand. Semi-arid and arid regions are typically water limited, particularly during the summer. Water-limited systems have been shown to have spatial variability in soil moisture (Williams &

McNamara 2009), which leads to spatial variability of actual ET. Although it is a challenge to estimate the actual evapotranspiration from within a watershed, there have been recent studies that have assimilated soil moisture, vegetation, and elevation to provide an adequate estimate of watershed scale (Chauvin et al. 2011; Parham 2015; Stratton et al. 2009; Wilson et al. 2001). However, these studies rarely focus on the riparian zone ET and its impact on the overall watershed scale ET estimate.

The riparian zone is a distinct ecohydrologic region and presents a challenge when modeling ET in a complex mountainous watershed. Although the riparian zone is a small proportion of semi-arid watersheds, in recent years, it has been observed that riparian zone vegetation affects streamflow (Cadol et al. 2012; Bond et al. 2002; Boronina et al. 2005 Gribovszki et al. 2010; Lundquist & Cayan 2002). The effect that riparian zones have on streams is particularly evident during low flow conditions within the watershed. During low flow conditions, the riparian zone has water availability, which hillslopes do not. This creates variability within the watershed and it may be useful to focus on the riparian zone and hillslopes separately to understand the influence that each region has on watershed scale ET.

Hillslopes and riparian zones are regions that have distinct differences in water availability. Hillslopes are thought to be truly water limited and have a finite supply of soil moisture for parts of the year (Smith et al. 2011). Conversely, the riparian zone is thought to have water availability throughout the year, with access to streamflow, hyporheic flow, and local groundwater (Gregory et al. 1991). This is important in regard to ET because the riparian zones have the water availability to evapotranspire throughout the entire year and particularly during the driest time of the year.

Recent studies have focused on the water sources used by vegetation and the connection between hydrology and vegetation, particularly within the riparian zone (McCutcheon 2015; McDonnell et al 2014; Renée Brooks et al. 2009; Snyder & Williams 2000). Subsequently, vegetation uptake has been shown to impact streamflow over the course of a day (Gribovzski et al. 2010). Streams throughout the world exhibit this daily fluctuation in streamflow, due to various factors that are often referred to as diel signals (Gribovzski et al. 2010). The diel signals within semi-arid and arid regions, during the summer, have been attributed to evapotranspiration in multiple studies (Gribovszki et al. 2010; Lundquist & Cayan 2002). However, little is known about the effects these diel signals have at a watershed scale. Diel signals have been used in past studies to estimate the riparian zone area of influence by comparing sap flux estimates within a small catchment (Bond et al. 2002). Other studies have used them to model evapotranspiration from the watershed (Boronina et al. 2005; Cadol et al. 2012).

More recent studies have focused on the process by which these diel signals are transmitted from vegetation to the stream channel. Research on the timing and amplitude of diel signals have produced a more thorough understanding of the link between vegetation and streamflow (Federer 1973; Graham et al. 2013; Szeftel 2010; Tabacchi et al 2000; Wondzell et al. 2007). Although the use of diel signals has provided insight into streamflow processes, it is still uncertain as to how well diel signals perform in calculating ET. The amplitude and lag time between different diel signals may offer key information into the effectiveness of diel signals in estimating evapotranspiration.

Installed within vegetation, sap flow has allowed for an increased understanding of vegetation transpiration, controls on streamflow diel signals, and riparian zone

processes. Studies, using sap flow, have calculated transpiration estimates from different regions within a watershed (Oishi et al. 2010; Schaeffer et al. 2000; Granier 1987). Sap flow has also been used to determine diel signal timing and correlations to streamflow (Graham et al. 2013). These studies show the importance of understanding the link between hydrology and vegetation within a watershed.

The purpose of this study was to determine the importance of riparian zone ET relative to watershed scale ET. To achieve this, the riparian zone ET was calculated using the "missing streamflow" from streamflow diel signals. The riparian ET estimates were then compared to a spatially distributed Penman-Monteith ET model based on elevation and vegetation distributions. The study modified the Penman-Monteith ET model with soil moisture to determine a growing season to calculate an estimate of actual watershed scale ET. Additionally, to understand the effectiveness and limitation of using diel signals to estimate riparian zone ET, meteorological and sap flux diel signals were measured in conjunction with streamflow diel signals. The study was able to provide spatial and temporal estimates of riparian zone evapotranspiration within the Dry Creek Experimental Watershed relative to watershed scale ET estimates. Analyzing the riparian zone's meteorological, sap flux, and streamflow data allowed us to determine the importance of riparian zone ET within the watershed.

Background

Evapotranspiration has been modeled in various ways, but recently the FAO 56 Penman-Monteith has become a common method for estimating ET with meteorological variables (Allen et al. 2006).

Equation C.1 $$ET_{gr,can} = \frac{\Delta(Rn - G) + \rho_a c_p * \frac{(e_s - e_a)}{r_a}}{\lambda(\Delta + \Upsilon(1 + \frac{r_s}{r_a})}$$

where Δ is the slope of the saturation vapor pressure temperature relationship, Rn is net radiation, G is soil heat flux, p_a is the mean air density at constant pressure, c_p is the specific heat of the air, (e_s-e_a) is the vapor pressure deficit of the air, r_a is the aerodynamic resistance, γ the psychometric constant, and r_s is the surface resistance.

The standardized reference ET equation provides a consistent method for calculating ET in various environments for hydrological, ecological, and agricultural studies. The idea of a reference crop was introduced to prevent the need to calibrate the Penman-Monteith method to numerous regions (Allen et al. 1998). Utilizing the reference crop equation presents the assumption of a well-watered grass of uniform height that is completely shading the ground. This assumption is violated in most cases but nevertheless has been shown to provide an accurate calculation under a range of conditions (Allen et al. 1998; Goodrich et al. 2000).

Estimating watershed scale ET in a complex mountainous terrain adds variability to the estimate that can be accounted for with a modified Penman-Monteith equation. Watershed soil moisture varies depending on elevation and the time of the year (Smith et al. 2011). The variability in soil moisture conditions in water-limited environments can affect the reference ET calculation (Allen et al. 1998). Complex environments, at a watershed scale, have shown that soil moisture limits plant production during the summer months when ET is at its highest demand (Smith et al. 2011). To account for the decoupling of atmospheric demand and soil moisture availability, research has focused on the effects of soil moisture on the growing season (Emanuel et al. 2010). A growing

season can be used to modify the Penman-Monteith reference ET calculation and account for the variability in soil moisture throughout the watershed.

The vegetation distribution within a watershed has also been shown to factor into the calculation of watershed scale ET (Allen et al. 1998). The Penman-Monteith equation has been modified in past studies to account for different plant physiological characteristics (Graham et al. 2010; Parham 2015). This was done by adjusting the surface resistance of the crop to provide an accurate estimate of canopy reference ET and grass reference ET. Implementing an ET calculation, modified by vegetation cover, has been shown to be an effective method in calculating watershed scale ET in a complex mountainous terrain (Chauvin et al 2011; Parham 2015; Stratton et al. 2009).

Diel fluctuations in both streamflow and groundwater have been used to estimate evapotranspiration (Bond et al. 2002; Boronina et al. 2005; Cadol et al. 2012; Fahle & Dietrich 2014; Gribovszki et al. 2008; Loheide 2008; White 1932). Diel signals have been documented as being caused by changes in hydraulic conductivity within a stream channel due to water temperature (Constantz et al. 1994; Lundquist and Cayan 2002), precipitation patterns (Wain 1994; Sulistyowati et al. 2014), snowmelt cycles (Gribovszki et al. 2006; Lundquist and Cayan 2002; Muntzner et al. 2015), and evapotranspiration (Blaney 1965; Bren 1997; Czikowsky & Fitzjarrald 2004; Reigner 1965; Tschinkel 1963; White 1932). In semi-arid environments, during the summer months, diurnal signals in streamflow and groundwater have been attributed to evapotranspiration (Butler et al. 2007; Dahm et al. 2002; Gribovszki et al. 2010; Lundquist and Cayan 2002).

Early observations of diel fluctuations caused by evapotranspiration were first documented by Blaney et al. (1930) and attributed the diel fluctuations to phreatophytes

and hydrophytes that had access to the water supply in an arid environment. Diel signals were analyzed for groundwater loss by White (1932) in shallow wells in southeast Utah. White developed a method to estimate the amount of groundwater loss based on these diel fluctuations. White's work has been modified throughout the years to include more refined measurements of aquifer characteristics and soil texture (Cadol et al. 2012; Loheide 2008).

A collection of studies has observed diel signal processes after vegetation removal from various regions of the watershed. The studies compiled by Bren (1997) explained that the diel fluctuations were a product of riparian and near riparian vegetation. Dunford and Fletcher (1947) observed an elimination of the streamflow diel signal after vegetation was cut along the stream bank with a buffer of 15-50 meters. Two separate studies (O'Loughlin et al. 1982; Lawrence 1990) observed that the streamflow diel signal was eliminated and flow increased within the stream after a fire removed vegetation within each watershed. Bren (1997) conducted a similar study in a small forested catchment where hillslope vegetation was removed. From these studies, it was concluded that the removal of hillslope vegetation did not change the streamflow diel fluctuation and in some cases increased the amplitude of the diel signal. The culmination of these studies concluded that diel signals were a product of riparian zone vegetation and could be exclusively attributed to the near riparian and riparian zone vegetation.

Although the study by Bren (1997) showed a major relationship between riparian zone processes and streamflow diel signals, there have been studies in the past that have attributed hillslope processes to streamflow diel signals (Barnard et al. 2010; Moore et al. 2011). Barnard et al. (2010) performed an irrigation study that showed a link between

hillslope soil moisture and streamflow diel signals. Moore et al. (2011) analyzed hillslope soil moisture to determine the effect on streamflow diel signals. Although these studies relate hillslopes process to streamflow diel signals, the coupling occurred during periods of high soil moisture which allowed for a connection between the hillslope and stream. Moore et al. (2011) stated that transpiration during the summer may cause a decoupling of hillslope soil moisture and streamflow diel signals. A study by van Meerveld et al. (2015) supported this idea with a conclusion that hillslopes were disconnected from the stream most of the time except for large precipitation events. Based on these results and the study occurring within a semi-arid watershed during the summer months, it could be assumed that the near riparian and riparian zone vegetation are the major control on the diel signal. This is particularly the case during the summer months when evapotranspiration is the major export from the watershed. It should be noted, for this study and future studies, that hillslope processes could have some influence on diel signals depending on hillslope soil moisture.

Research has recently focused on plant-water interactions within the riparian zone. To do this, studies have focused on understanding the diel signal and calculating the “missing streamflow” lost to vegetation. The “missing streamflow” within a diel signal is calculated by finding the potential baseflow without vegetation uptake and interpolating between the maximum daily discharges. The “missing streamflow” is the difference between the potential baseflow and the actual baseflow. Research by Bond et al. (2002) used the “missing streamflow” within the diel signal in conjunction with sap flow measurements to determine the riparian area of influence throughout the summer. Boronina et al. (2005) used the diel signal to calculate a volumetric ET estimate for a

catchment in Cyprus. Cadol et al. (2012) used streamflow diel signals with a modification of the White method to determine transpiration rates from the watershed based on a recharge rate for precipitation-free periods. Gribovszki et al. (2008) used a modified White method and groundwater diel signals to estimate riparian evapotranspiration. The interaction between vegetation and streamflow is evident throughout these studies. However, there are questions that remain within these methods and ideas.

The characteristics of the diel signal change throughout the baseflow with respect to lag time and amplitude. This variability was the focus of Wondzell et al. (2007) and has been mentioned in other streamflow diel signal studies (Bond et al. 2002; Szeftel 2010). It has been observed in various forested catchments that as baseflow decreases the lag time between peak meteorological measurements or sap flow measurements and minimum streamflow increases (Graham et al. 2013). The same holds true for the amplitude, which shows that as baseflow decreases through summer the amplitude of the streamflow diel signal also decreases (Szeftel 2010). The observations of the variability in amplitudes and lag times bring into question how these diel signals are transferred to the streamflow. Multiple theories have been brought to light in the recent studies of streamflow diel signals.

The theories on the mechanism of diel signal transfer were summarized in a study by Graham et al. (2013) in which the various hypotheses were tested in separate watersheds. The first theory being a saturated wedge hypothesis in which the vegetation changes the head gradient next to the stream. As the flow decreases, so too does the head gradient, therefore causing the temporal variability (Burt 1979). The second hypothesis

of riparian interception theorizes that the riparian zone captures the subsurface flow that would otherwise enter the stream. Additionally, as conditions become dryer, the velocities of the subsurface flow decrease, therefore, slowing down the transfer time to the stream (Bren 1997). The third, flow path migration theory, provides the idea that the flow path shifts to a lower permeability medium with dryer conditions, therefore causing a slower transfer of signal (Bond et al. 2002). The last hypothesis, in which Wondzell et al. (2007) theorized that stream velocity is the main reason for this discrepancy, stated that as baseflow decreased so did the stream velocity. Therefore, the decrease in stream velocity creates a slower transfer of the diel signal downstream and the downstream amplitudes become dampened by upstream signals because signals are out of phase. This was supported by Graham et al. (2013) with research conducted in three different catchments, showing there could be influences from the first three hypotheses, but mainly the increase in lag time throughout the baseflow could be attributed to a dampening of diel signals throughout the summer.

Szeftel (2010) used these ideas to focus on riparian and hillslope hydraulic connectivity within a nested catchment design. His findings were similar to those of Wondzell et al. (2007), but he also obtained additional spatial variability information based on nested streamflow gauges. This allowed for a comparison of different drainage basins along the same stream channel. Szeftel (2010) found that lag times increased throughout the low flow season with decreasing flow, but the lag times did not correspond to the drainage basin area. Within the nested catchment, the average amplitude correlated well with drainage basin area at high flows, but correlation decreased through the low flow season. The nested catchment design provided insights

into diel signal processes that were not observed before with independent stream gauging sites.

These studies used diel signals to estimate and describe watershed processes. Further research would provide more insight into how these processes affect other watersheds. The Dry Creek Experimental Watershed provides a useful resource for this type of analysis due to the fact it has had previous studies on soil moisture (Smith et al. 2011), plant-water interactions (McCutcheon 2015), mass balance (Aishlin & McNamara 2011; Parham 2015), and streamflow studies (Frye 2013). The permanent instrumentation of streamflow gauges, soil moisture instrumentation, and meteorological stations allowed for an in-depth analysis on the controls of the diel signals. This study included the work of previous studies that provided a foundation to implement a refined analysis on watershed processes.

2. METHODS

Approach

The goal of this study was to determine the contribution of riparian ET compared to watershed ET at a watershed and sub-watershed scale during the baseflow season. To achieve this, watershed scale ET was modeled using a weighted average approach that included meteorological data distributed across different vegetation types and elevation profiles. Riparian zone ET was modeled in DCEW using streamflow diel signals to calculate the "missing streamflow" due to vegetation use. The proportion of riparian ET compared to watershed scale ET was computed for the entire watershed and four sub-watersheds.

The watershed or catchment ET (ET_c) was computed for five watersheds and six different precipitation-free periods, where there was no precipitation input to the system. Catchment ET_c (mm/day) was computed as the average rate over the duration of the period and was the weighted sum of the average daily rate of hillslope evapotranspiration, $ET_{h,}$ and the average daily rate of riparian evapotranspiration, $ET_{r.}$

Equation C.2 $$ET_c = ET_h W_h + ET_r W_r$$

where the average daily hillslope evapotranspiration, $ET_{h,}$ was weighted by relative hillslope area, W_h, and average daily rate of riparian evapotranspiration, ET_r, was weighted by relative riparian zone area, W_r. The sum of the weights (W_h and W_r) was equal to one.

Equation C.3 $$W_r = \frac{Area_{rip}}{Area_{Total}}$$

Equation C.4 $$W_h = \frac{Area_{hill}}{Area_{Total}}$$

Equation C.5 $$W_r + W_h = 1$$

The properties of the streamflow diel signals were analyzed to understand the dynamic controls on the streamflow diel signal. Streamflow diel signals were compared to meteorological and sap flux diel signal measurements to observe the timing of diel signals to determine lag times. The streamflow diel signal amplitudes were also analyzed on a daily time period. The lag time and amplitude of the streamflow diel signals were calculated spatially and temporally to determine influences on the streamflow fluctuation throughout the baseflow. The added insight into the diel signal properties provided an idea of the effectiveness and limitations of the diel signal method in estimating riparian zone ET.

Study Site

The study site was Dry Creek Experimental Watershed (DCEW), located in southwest ID, approximately 20 km North of Boise, ID. DCEW ranges in elevation from approximately 1000 meters to 2100 meters and annual precipitation varies from 300 mm in the lower elevation of the watershed up to 1000 mm in the highest elevations (DCEW 2015). The watershed drains approximately a 27 km^2 area and is instrumented with seven stream monitoring sites and five meteorological stations (DCEW 2015). Soil moisture measurement sites are paired on adjacent north and south facing aspect hillslopes at four elevations within the watershed and are also instrumented at multiple meteorological sites (Figure B.1). The watershed has a semi-arid climate with most of the precipitation

occurring during the winter months and evapotranspiration exceeding precipitation during the summer months.

This study focused on the outlet of the entire watershed (Lower Gauge) along with four other stream gauging sites (Confluence 1 East, Confluence 1 West, Confluence 2 Main, and Confluence 2 East) shown in Figure B.2. Each gauging site was used to divide the watershed into sub-watersheds for a refined analysis with a nested catchment design.

The meteorological stations range from approximately 1100 meters to 2100 meters. For this study, four of the five permanent meteorological stations were used for analysis in the study (Lower Weather, Treeline, Lowe Deer Point, and Bogus Ridge), ranging in elevation of 1150 to 2100 meters. All meteorological stations measured air temperature, relative humidity, solar radiation, net radiation, wind speed, and wind direction. The data from these sites were used in the Penman-Monteith models to calculate hillslope ET (ET_h).

Vegetation within DCEW varies with elevation and topography (DCEW, 2015). Lower elevations are dominated by mainly grass, shrubs, and sagebrush (*Artemisia spp.*) on the hillslopes, while higher elevation hillslopes are predominantly ponderosa pine (*Pinus ponderosa*) and Douglas-fir (*Pseudotsuga menziesii*). Lower elevation riparian zones consist of deciduous trees and bushes such as yellow willow (*Salix lutea*), black cottonwood (*Populus trichocarpa*), water birch (*Betula occidentalis*), mountain alder (*Alnus viridis*), and mountain Maple (*Acer spicatum*). Higher elevation riparian zones contain a mix of deciduous and conifer trees (DCEW 2015; Graham et al. 2013; Loughridge 2014).

Watershed and sub-watershed scale studies have been performed in the past within DCEW on an annual timescale. Annual water balance studies were performed by Aishlin & McNamara (2011) to determine net recharge utilizing a chloride mass balance approach for the 2005-2009 water years. The study calculated ET as a residual from the water balance and showed that ET accounted for up to 70% of the precipitation in the watershed. Stratton et al. (2009) ran a Soil Water Assessment Tool (SWAT) model that calculated ET accounting for approximately 39% and 44% of the precipitation respectively for the 2006 and 2007 water years. Similarly, a ten-year water balance study was performed by Parham (2015) to determine the influence of DCEW evapotranspiration on net recharge. The study used an elevation and vegetation distribution method, similarly described in this study, to calculate watershed scale ET for the 2001-2012 water years. The study showed that ET accounted for an average of 48% of the hypsometrically distributed precipitation. Based on these studies, it was revealed that ET plays a large role in DCEW's annual water balance.

Hillslope Evapotranspiration (ET_h)

The average daily hillslope evaporation during the study period was computed by weighting the Penman-Monteith equation (Equation C.1) by vegetation and elevation. The first step was to compute vegetation-weighted evapotranspiration ET_v for every hour, i, at each meteorological station (sta) as the weighted sum of evapotranspiration from two vegetation classes: grass/shrub and canopy.

Equation C.6
$$ET_{v,i}(sta) = ET_{can,i}W_{can} + ET_{gr,i}W_{gr}$$

where weight factors W_{can} and W_g are computed as the fraction of the entire catchment occupied for each vegetation class (see Vegetation Class section and Table A.1). ET_{can}

and ET_{gr} are computed using modifications of the Penman-Monteith equation (see Reference Evapotranspiration section). The result of this step, $ET_{v,i}$(sta), produced an estimate of evapotranspiration that would occur in the catchment if that specific meteorological station represented the entire catchment. Equation C.6 is computed every hour at the four meteorological stations used for the study (Lower Weather, Treeline, Lower Deer Point, and Bogus Ridge).

Secondly, hourly $ET_{v,\,i}$ (sta) computations were distributed by elevation using the hypsometric method. Hourly vegetation-weighted ET within an elevation zone, $(ET_{v,\,i)\,z}$, was computed using a linear relationship between $ET_{v,\,i}$ (sta) and station elevation, z_{sta}.

Equation C.7 $$\left(ET_{v,i}\right)_z = mz + b$$

Equation C.7 was solved for specified elevation zone spanning the range of elevations in the respective catchment using the midpoint elevation of each zone, z_{mid}, and then multiplied by an elevation weight factor, W_z, to produce vegetation and elevation weighted hourly hillslope evapotranspiration.

Equation C.8 $$ET_{h,i} = \sum_{z=1}^{Z} \left(ET_{v,i}\right)_z W_z$$

Elevation weight factors consisted of 100-meter elevation zones ranging from 1100 to 2200 meters. The elevation weight factors for the watershed and each sub-watershed were computed using a digital elevation model in ArcMap 10.3.

The third step was to compute the average daily hillslope evapotranspiration, ET_h, by summing 24 hourly values of hillslope evapotranspiration, $ET_{h,i,}$ for each day, d, and then computing the average of all days within a period of interest.

Equation C.9 $$ET_h = \frac{1}{D}\sum_{d=1}^{D}\left[\sum_{i=1}^{24} ET_{h,i}\right]_d$$

Reference Evapotranspiration

Two separate Penman-Monteith reference evapotranspiration estimates, ET_{can} and ET_{gr}, were calculated for five meteorological sites in order to apply a hypsometric model to account for elevation and vegetation within DCEW. The Penman-Monteith equation was used to calculate two different estimates of ET for two different vegetation types (Equation C.1).

Grass reference evapotranspiration (ET_{gr} in Equation C.1) was calculated to determine grass and shrub evapotranspiration within DCEW. This method has been used in the past within DCEW to determine the significance of watershed scale ET within DCEW (Parham 2015) and also by others to inform hydrological, ecological, and agricultural studies (Allen et al. 2006). The method assumes a well-watered green crop of uniform height that completely covers the surface. Although these assumptions are violated within DCEW, the method is easily applied with meteorological variables and was adjusted for the growing season. The FAO Penman-Monteith is recommended as the standard equation to calculate reference ET (Allen et al. 1998). For further information on FAO Penman-Monteith method and application, refer to Parham (2015) and Allen et al. (1998).

The second equation modified the Penman-Monteith model to represent the evapotranspiration from canopy vegetation. Due to physiological differences between grasses and trees, grass reference ET was not an appropriate calculation for a canopy ET estimate (ET_{can}). Conifer and deciduous vegetation are physiologically different from

grasses and shrubs, and must be modified to account for this difference in the evapotranspiration model. The canopy surface resistance term was modified within the Penman-Monteith model, and the canopy surface resistance was substituted for surface resistance in Equation C.1. Values of canopy surface resistance and aerodynamic resistance for the canopy reference ET (ET_{can}) were obtained from Parham (2015) and Graham et al. (2013) for consistency with past studies in DCEW. The canopy reference ET (ET_{can}) was calculated to determine canopy evapotranspiration for the hypsometric ET model within DCEW (Equation C.6).

Growing Season

The growing season was determined to convert the estimate of grass reference ET (ET_{gr}) to an estimate of actual grass reference ET. To estimate actual ET, soil water storage was analyzed throughout the summer months to determine the beginning and end of the growing season. Smith et al. (2011) showed that the timing of wilting point within DCEW varied with elevation. For this study, four soil pits were chosen in adjacent locations to meteorological stations to determine the growing season at each meteorological station to modify grass reference ET (ET_{gr}). Soil moisture storage calculations were made within the profile using Equation C.10.

Equation C.10

$$\mathbf{S} = \sum_{\boldsymbol{i=1}}^{\boldsymbol{N}} \mathbf{b_i}\Theta_\mathbf{i}$$

where b is the discrete thickness of the soil layer and Θ is the volumetric moisture content (VMC) of that soil layer, i, and N is the number of soil layers. Integration of the VMC throughout the depth of the profile provided an estimate of total soil moisture within the soil profile.

The growing season was initiated when the upper 5 cm of the soil profile reached an average daily temperature of 5°C. The end of the growing season was determined by the same method used by Smith et al. (2011), in which a change of slope in the soil moisture determined the wilting point of the soil. When the soil reached the wilting point, it was considered to be the end of the growing season based on the lack of available water throughout the soil profile, and the grass reference ET (ET_{gr}) model was shut off. The ET model was allowed to turn on again if the soil moisture reached a level above the wilting point at any point after the end of the growing season.

The calculations of canopy reference ET (ET_{can}) and growing season modified grass reference ET (ET_{gr}) provided a range of ET estimates to account for the vegetation and moisture variability within the watershed. These methods have been shown to provide an adequate estimate of watershed scale ET within DCEW in the past (Parham 2015).

Vegetation Class

Canopy and grass vegetation cover were calculated for the entire watershed and subset for each sub-watershed (Table A.1). The vegetation distribution was determined for DCEW watershed using remotely sensed imagery from Landsat 8 OLI/TIRS (acquired Sept 13, 2014) and NAIP imagery, acquired from USGS EarthExplorer. Landsat 8 imagery was preprocessed using ENVI 5.1 and subset to include an area slightly larger than DCEW to reduce classification analysis time. National Agriculture Imagery Program (NAIP) imagery was used for aerial observations of regions of interest and plots to train the classification. The NAIP imagery was overlaid on Landsat imagery to define both training plots and ground truth plots. Accuracy assessments were

completed with the use of NAIP imagery ground truth data. The mahalanobis classification method produced an overall accuracy of 87.7% for the Landsat imagery. The vegetation distribution in Figure B.3 was used to calculate a weighted value for grass reference ET (W_{gr}) and canopy reference ET (W_{con}) (Table A.1).

The results of the Landsat analysis for DCEW vegetation distribution was compared to previous watershed scale vegetation data and had comparable results (Loughridge 2014; Stratton et al. 2009). A sensitivity analysis was performed for different vegetation weights to determine if changes in vegetation cover altered ET calculations significantly. The sensitivity analysis showed little variation when vegetation cover was varied throughout the watershed for the short precipitation-free time periods.

Meteorological Instrumentation

Four permanent meteorological sites were used to calculate watershed scale ET using a hypsometric approach with a relative vegetation class distribution. In addition to the permanent meteorological stations, an additional temporary automated meteorological station programmed with a CR1000 logger (Campbell Scientific) was installed in the riparian zone of DCEW approximately 100 meters Northwest of Confluence 1 gauging station (B.8). The station was equipped to measure and record net radiation (NR-LITE2, Campbell Scientific), solar radiation (MK 1-G Sol-A-Meter, Matrix Solar), precipitation (CS700, Hydrologic Services), relative humidity (HMP60, Vaisala), temperature (HMP60, Vaisala), wind speed, and wind direction (034B, Met One). The sensors were installed two meters above the ground surface and recorded on an hourly timescale. The station was placed in an open area void of vegetation, but within the riparian zone, to simulate the same energetic environment that the riparian canopy receives. This allowed

for the most accurate measurement of riparian zone meteorological fluxes without interference from riparian zone canopy cover. This station was used to compare with meteorological hillslope sites to determine different meteorological fluxes between the two regions within the watershed.

Riparian Evapotranspiration (ET_r)

Streamflow at each sub-watershed was measured using stage-discharge relationships maintained in routine operations of the DCEW. Data, metadata, and methods are available through the DCEW website (earth.boisestate.edu/drycreek).

There is an assumption within the "missing streamflow" method that there is no additional input of water to the system that is modifying the diel signal, such as precipitation. To consider this assumption of no input of water to the watershed, the sub-watersheds were analyzed for only precipitation-free periods during the 2014 summer baseflow. The periods were chosen during the baseflow by analyzing the hydrograph in conjunction with precipitation measurements to find several consecutive days with no precipitation occurring. These periods were classified as precipitation-free periods and there were determined to be six precipitation-free periods with consecutive days of no measured precipitation.

Riparian zone evapotranspiration was calculated using the streamflow diel signal from the hydrograph. Figure B.4 shows an example of the diel signal from DCEW at Confluence 1 East for a precipitation-free time period. Previous research has shown the riparian zone vegetation to be the main contributor to the streamflow diel signals (Bren 1997). To estimate streamflow diel signal influences, studies in the past have used methods to determine the "missing streamflow" from within the diel signal (Bond et al.

2002; Boronina et al. 2005; Cadol et al. 2012). The method assumes that missing streamflow estimations at a catchment outlet represent the riparian evapotranspiration from the entire riparian zone.

Hydrographs were detrended to remove the impact of long-term recession based on the median daily streamflow value according to Graham et al (2013). The detrended discharge was the difference between the instantaneous discharge value and the median daily value.

The hydrograph was converted to volume per hour for each hourly time step to account for the entire discharge of that time step. Figure B.5 shows the variables and data used to calculate the "missing streamflow." The potential discharge (Q_p) was computed for every hour, i, by linearly interpolating between the maximum daily discharges, $Q_{max,d}$.

Equation C.11 $$\boldsymbol{Q_{p,i} = Q_{max,d} - \left(Q_{max,d} - Q_{max,d+1} \left[\frac{(t_i - t_{i+1})}{t_{Q_{max,d}} - t_{Q_{max,d+1}}} \right] \right)}$$

where $Q_{max,d}$ is the daily maximum discharge for the day and $Q_{max,d+1}$ is the daily maximum for the following day. Taking into account the time of the maximum daily discharge ($t_{Qmax,d)}$ for each day and adding the value to the daily maximum discharge, $Q_{max,d}$. Linearly interpolating between the daily maximum for each day provided a potential discharge, $Q_{p,i}$, (m^3/hr).

Riparian evapotranspiration, ET_r, (m^3/hr) was then computed for every hour by calculating the difference between potential discharge, $Q_{p,}$ (m^3/hr) and actual discharge, $Q_{a\,(}m^3$/hr) at every hour. The difference between the potential and actual discharge was determined to be the "missing streamflow" due to vegetation uptake (ET_r) in a volume per hour (m^3/hr). The "missing streamflow" was theoretically the volumetric quantity of water lost to the atmosphere through riparian zone evapotranspiration. Riparian

evapotranspiration was then converted to a length per time (m/hr) by distributing the ET_r over the portion of the watershed that influences the diel signals, which in this case was assumed to be the riparian area, $Area_{rip}$ (m^2). Once riparian ET (ET_r) is converted from a volume per time (m^3/hr) to length per time (m/day), it is then converted from meters/day to mm/day for consistency with hillslope ET estimates performed above.

Equation C.12 $$\boldsymbol{ET_{r,i} = \frac{Q_{p,i} - Q_{a,i}}{Area_{rip}}}$$

where ET_r is the hourly riparian evapotranspiration in mm/hour. Average daily riparian evapotranspiration, ET_r, is then computed by summing 24 hourly values of riparian evapotranspiration, $ET_{r,i,}$ for each day, d, and then computing the average of all days within a period of interest as shown in Equation C.13.

Equation C.13 $$\boldsymbol{ET_r = \frac{1}{D}\sum_{d=1}^{D}\left[\sum_{i=1}^{24} ET_{r,i}\right]_d}$$

The method was limited within various sub-watersheds due to a lack of streamflow present at the gauging station. Gauging stations, Confluence 1 East and Confluence 2 Main, provided estimates throughout the summer since they had sufficient streamflow throughout the 2014 baseflow season.

Riparian Area

Previous research has showed that the riparian area is the major influence on streamflow diel signals (Bren 1997). To determine the area of influence for the diel signals, it can be concluded based on research by Bren (1997) that diel signals can be almost exclusively attributed to the riparian zone and near riparian zone vegetation, particularly in semi-arid regions. Based on this conclusion, along with an analysis of precipitation-free periods only, the riparian zone within DCEW was calculated for the

entire watershed and four sub-watersheds.

The riparian area, for this study, was defined as the area adjacent to the stream that had a slope of less than 25°. A slope of less than 25° was an arbitrary value chosen based on the ability for lateral flow of water to contribute to the stream. The analysis was performed using ArcMap 10.3 and the riparian area was determined based on a thirty-meter stream buffer and a slope less than 25° (Figure B.6). Table A.2 shows the riparian zone area compared to each respective sub-watershed area, along with the percent of the riparian zone for each sub-watershed. The riparian zone calculation provided an estimation of influence to compare to the watershed area when calculating ET.

To determine the weights of the riparian zone (W_r) and the hillslope (W_h), the calculated riparian zone area was computed as a percentage of the total watershed area (Equation C.2). The hillslope weight was calculated as the difference between the total watershed and riparian zone area estimated above. Together the weights of the hillslope (W_h) and riparian zone (W_r) were equal to one (Equation C.5) and applied to the model in Equation C.2.

The slope chosen was an estimate based on direct observations of the stream channel within DCEW. The model was based on calculating the area adjacent to the stream where hyporheic zone flow could be affected by shallow soil vegetative uptake. The model provided an adequate interpretation of riparian zone area throughout the watershed. The lower elevations of DCEW, where hillslopes are dominated by grasses and shrubs and the riparian area is composed of deciduous trees, had a well-defined narrow riparian area. The higher elevations of the watershed had a wider riparian zone along the stream where the riparian zone and hillslopes were less defined since the

hillslopes are vegetated with conifer trees. The riparian zone area, for this study, is considered an estimate since there is a fluctuation in the riparian zone area throughout the year (Bond et al 2002). The uncertainty within the estimate was accounted for and is discussed later in the paper. The estimate of the riparian area allowed for a comparison of ET based on streamflow diel signals and a spatially distributed meteorological ET model.

Diel Signal Properties

Diel signal characteristics of hydro-meteorological variables were used to add insight into the spatial and temporal variability of ET. The diel signals of meteorological and sap flux measurements were analyzed for lag times between maximum daily hydro-meteorological measurements and minimum streamflow. This timing provided a lag time between the transfer of the signal from vegetation or atmosphere to the streamflow. The streamflow measurements were also analyzed for amplitude to determine controls throughout the baseflow. The properties of these diel signals were evaluated to provide a clearer understanding of the dynamic controls on the streamflow diel signals.

Sap Flux

Sap flux was monitored within both riparian and hillslope vegetation. The riparian sap flux was installed in the spring of 2014 and the hillslope sap flux was installed in spring 2013. Riparian sap flux was instrumented in multiple trees of four water birch (*Betula occidentalis*) and two Douglas-firs (*Pseudotsuga menziesii*) at a location adjacent to Confluence 1 in DCEW (Figure B.7). Hillslope sap flux (HS Sap Flow) was instrumented in two different Douglas-fir trees (*Pseudotsuga menziesii*) near Lower Deer Point meteorological station in the upper elevations of DCEW (Figure B.1). Both sites utilized a Dynamax FLGS-TDP XM100.

The instrumentation used heat dissipation probes to record the velocity of sap flow at breast height on the instrumented trees. The velocity of the sap flow was then converted to volume of sap flux per time by multiplying by the sapwood area. For this study, sapwood area was inferred to be 60% of the basal wood area. This estimate was determined based on previous sapwood estimate in Douglas-fir stand provided by Bancalari et al. (1987). The sap flux estimates were used to compare both hillslope and riparian vegetation throughout the base flow, as well as to analyze sap flow diel signals.

Amplitude and Lag Time

The properties of the diel signal, such as the amplitude and the timing of the signal, were analyzed to understand the processes that control streamflow diel signals. With the timing of the diel signal, it was important to determine the time of minimum streamflow in reference to a peak meteorological or sap flux measurements and calculate that as the lag time. For this study, the lag time was calculated in reference to the difference in time between peak net radiation at C1E meteorological station and the minimum daily discharge at each streamflow gauge. Each streamflow gauge was referenced to C1E net radiation for consistency in the analysis.

Amplitudes were calculated daily for each site, as well as an average over the six precipitation-free periods. The amplitudes were calculated by the difference between the daily maximum and daily minimum streamflow for the same day and dividing the difference by two (Wondzell et al. 2010). The amplitudes at each gauging site were compared throughout the watershed to determine factors that may influence the amplitude variability. This, in turn, helped to determine how the diel signals were influenced through space and time.

3. RESULTS

Hydro-Meteorological Data

Streamflow

Streamflow was measured throughout the year, but analyzed from May 2014 until October 2014, particularly during the baseflow. Confluence 1 East and Confluence 2 Main gauging stations had adequate streamflow throughout the analysis. The three other gauging stations (LG, C2E, and C1W) had little to no streamflow at some point during the baseflow (Figure B.8). All streamflow receded during May, reaching a low flow, and then recovered around October. Streamflow throughout the watershed responded to precipitation events with numerous local peaks observed during the baseflow.

All precipitation-free periods greater than three days were determined based on meteorological measurements of precipitation. There were six total precipitation-free periods of various lengths. Starting dates for the precipitation-free periods used in the analysis were 5/29/14, 6/20/14, 6/28/14, 7/25/14, 9/1/14, and 10/1/14 (Figure B.8, highlighted in gray). Confluence 2 East and Confluence 1 West had periods that were shorter lengths, relative to other gauging stations, due to inadequate streamflow for the entire precipitation-free period.

Meteorological Variables

The riparian meteorological station was used in conjunction with streamflow and sap flux estimates to determine controls on streamflow diel signals. Figure B.9 illustrates the occurrence of diel signals in measured meteorological variables, particularly relative

humidity, temperature, and net radiation, throughout the summer.

Elevation controlled multiple meteorological variables throughout the summer. Figure B.10 shows the trends of mean annual relative humidity, temperature, and net radiation with respect to the elevation at each meteorological site. The average temperature decreased at each meteorological site with an increase in elevation. The average relative humidity increased with an increase in elevation. The average net radiation at the meteorological stations had little variation between elevations except for Treeline (1610 meters), which had a slightly higher measurement relative to the other stations.

Sap Flux

Sap flux was calculated for two hillslope Douglas-firs, four riparian water birch, and two riparian Douglas-firs. Data gaps were present within riparian sap flux because the instrumentation did not have an adequate power source throughout the summer. The riparian sap flux power failure occurred in late June 2014, late August 2014, and early October 2014, and is the reason for data gaps in the sap flux (Figure B.11). Hillslope sap flux had no such power failure and provided good data throughout the analysis period.

The riparian and hillslope sap flux data both showed a decrease in transpiration through the summer. The riparian sap flux showed a reduction in the daily peak from the early summer to late summer. A large amount of transpiration occurred early in the summer followed by a relative decrease in transpiration later in the summer (Figure B.11). Although the later part of the summer showed a decrease in riparian transpiration, the amount of transpiration was consistent from approximately July through the end of the summer. Hillslope sap flux, although not shown in Figure B.11, had a similar

temporal trend with a larger reduction in the daily peak transpiration occurring late in the summer.

Hillslope Evapotranspiration

Reference ET

Canopy reference ET (ET_{can}) and grass reference ET (ET_{gr}) were calculated on an hourly timescale at each hillslope meteorological site from May 24th, 2014 to October 16th, 2014. The Lower Weather meteorological site calculated the highest values of hourly grass reference ET (ET_{gr}) of all the meteorological sites, followed by Treeline, Lower Deer Point, and Bogus Ridge Sites (Figure B.12). The largest canopy reference ET (ET_{can}) for the season was calculated at the Treeline weather station, followed by the Lower weather station (Figure B.13). Lower Deer Point and Bogus Ridge calculated similar hourly canopy reference ET (ET_{can}) for the season.

The grass and canopy reference ET showed similar temporal trends of maximum ET in July. The highest daily peak of ET in July is followed by a reduction in evapotranspiration for both grass and canopy reference ET. The smallest estimate of ET occurs in October where grass and canopy reference ET are reduced substantially from their high daily peaks in July.

Growing Season

The soil moisture varied with elevation throughout the watershed, which determined the growing season for grass reference ET. The beginning of the growing season occurred before analysis for all meteorological sites within DCEW, which was May 24th, 2014. The end of the growing season was relatively dependent on elevation. The end of the growing season was calculated to occur earlier at lower elevations due to

lack of hillslope soil moisture earlier in the season. The higher elevation had a relatively longer growing season due to cooler temperatures and a longer subsistence of soil moisture. Bogus Ridge was the exception with the meteorological station being at a high elevation but producing a short growing season (Table A.8).

The soil moisture analysis showed there was a response to precipitation events during the summer. The soil profile was affected by precipitation events in late summer that infiltrated through the soil profile therefore evapotranspiration was calculated after the end of the growing season at some sites.

ET and Elevation Relationship

An evapotranspiration and elevation relationship was computed for each sub-watershed separately based on calculations of vegetation cover and growing season. The largest reference ET values still occurred at the Lower Weather site, but Lower Weather ET estimates were greatly reduced due to the growing season modification. Table A.9 shows the average linear trend for the model used to calculate a theoretical hillslope ET ($ET_{v,i}$) at each elevation band.

Hillslope ET Results

The hypsometric and vegetation model showed the largest hillslope ET (ET_h), ranging from approximately 1 to 4 mm/day, occurred over the entire watershed (Table A.7). The smallest hillslope ET (ET_h) was calculated in Confluence 1 West sub-watershed ranging from approximately 0.1 to 0.5 mm/day (Table A.4).

The hillslope ET varied throughout the baseflow season for each sub-watershed. The highest hillslope ET values occurred in June and July for each sub-watershed (Table A.3 – Table A.7). The lowest values were calculated around September with a slight

recovery in October (Figure B.14 – Figure B.18).

The uncertainty for hillslope ET estimates was calculated at approximately 6-8% of the spatially distributed watershed scale ET. The uncertainty was based on estimates of instrument error from Graham et al. (2010), with the instrument error treated as a systematic error and propagated through the error calculation.

Riparian Evapotranspiration

Riparian Area

The riparian area makes up approximately 5% of the entire watershed based on the modeled riparian zone area. Riparian ET was converted from a value of volume per time to length per time by distributing the missing streamflow across the riparian zone area of influence. The riparian zone area of influence was calculated as the riparian area and was determined to be approximately 5% of each watershed's respective watershed area (Table A.2). The only sub-watershed not at 5% was Confluence 1 East, which calculated 4% of the watershed as the riparian zone area. Applying this zone of influence to the diel signals allowed the "missing streamflow" to be converted to a length per time, which could be compared to a watershed scale ET estimate.

Riparian ET

The riparian evapotranspiration, calculated using the "missing streamflow," was spatially and temporally variable throughout the watershed. However, there were consistent trends within the sub-watersheds throughout the summer. These trends showed that riparian ET (ET_r) values, for precipitation-free time periods, were the largest early in the baseflow season during the recession of the hydrograph for all sites (Table A.3-Table A.7). The May and June baseflow periods produced the largest amount of daily riparian

ET with daily values ranging between 0.3 (Table A.7) and 1.2 mm/day (Table A.3). The smallest contribution of riparian ET occurred during the August and September baseflow periods for all sites. The August and September values ranged between 0 mm/day with gauges that had no streamflow (Table A.4) to approximately 0.7 mm/day (Table A.3).

The largest contribution of riparian ET (ET_r) occurred from the higher elevation gauges. Confluence 1 East and Confluence 1 West had values ranging around 1 mm/day when water was flowing in each stream. Riparian ET calculated using the lower elevation gauges had much lower average daily ET rates.

Watershed Evapotranspiration

Watershed ET had similar trends to hillslope ET with large amounts of ET occurring early in the summer and decreasing throughout the summer. The hillslope ET, being weighted by approximately 95%, dominated the watershed ET results, while riparian ET, weighted by approximately 5%, had little influence on the overall watershed ET estimate both temporally and spatially. Table A.3-Table A.7 showed those trends for each sub-watershed.

Evapotranspiration Comparison

Riparian evapotranspiration accounted for 1-11% of the watershed scale ET during the summer for the gauging sites within DCEW. The higher elevation watersheds generally had weighted riparian ET (ET_rW_r) that accounted for larger percentages of watershed scale ET (ET_c). Higher elevation gauges, such as Confluence 1 East, had times throughout the summer where the weighted riparian ET (ET_rW_r) accounted for up to 11% of the catchment ET (ET_c) (Table A.3). The higher percentage of riparian ET occurred particularly during the beginning (May) and end (October) of the analysis period. Lower

elevation gauges tended to account for a smaller amount of watershed scale ET (ET_c). Lower Gauge had weighted riparian ET range from 0.25% to 0.7% of watershed scale ET and the streamflow even ceased for a part of the baseflow (Table A.7).

Streamflow Diel Signal Controls

Diel signal properties were analyzed to determine spatial and temporal variability throughout the watershed. The fluxes from atmospheric, sap flux, and streamflow measurements were also analyzed to determine controls on streamflow diel signals in DCEW.

Diel Signal Lag

Average lag time was calculated for each precipitation-free period and this average lag time increased throughout the baseflow for all catchments until late summer when baseflow rebounded and lag times decreased. Table A.3-Table A.7 shows that most lag times increased throughout the summer. The lag times had no correlation to watershed area, which were similar to the findings of Graham et al. (2013) and Szeftel (2010). The LG site produced an average lag time of approximately 7 hours (Table A.3), while the upper catchment C1E produced an average lag time of approximately 10 hours (Table A.7). Although there was spatial variability within the watershed, the lag times at each gauging station were consistent in their change throughout the baseflow season.

Diel Signal Amplitude

The amplitude for all gauging stations decreased throughout the summer and slowly recovered after early September (Figure B.19). The larger catchments tended to have larger amplitudes during high baseflow and amplitudes decreased as baseflow decreased. Two gauging stations (C1E and C2M) had constant discharge throughout the

summer and were compared for amplitude variability throughout the baseflow.

There was a high correlation between catchment size and amplitude early in the summer for precipitation-free periods. However, there was a lack of correlation between catchment size and amplitude during the middle and later part of the baseflow (Figure B.20). For example, during intermediate and low baseflow C1E had larger amplitudes than the C2M catchment. This is similar to the finding of Szeftel (2010) who described a high correlation between catchment scale and amplitude during high baseflow, but a decrease in the correlation with intermediate and low baseflow levels. A high correlation between amplitude could be seen within DCEW where the early summer had a significant relationship between C1E amplitude and C2M amplitudes, but the latter part of the summer showed no relationship (Figure B.21). The average amplitudes for all precipitation-free periods were normalized to drainage basin area for each sub-watershed and found that the upper catchments had the largest normalized amplitudes within the watershed (Figure B.22).

Meteorological and Sap Flux Comparison

Multiple relationships between meteorological, sap flux, and streamflow variables were found for precipitation-free periods during the baseflow in DCEW. A significant relationship was found between average daily sap flux estimates and average daily net radiation measurements within DCEW (Figure B.23). This relationship showed that with a high average daily net radiation there was also a high measurement of average daily sap flux. There was also a relationship between the average sap flux and the average actual ET estimate for each day without precipitation (Figure B.24). Although there was no significant relationship found between average daily sap flux and average daily

temperature for the entire summer (Figure B.25), it was found for a part of the summer. Figure B.26 showed that during the latter part of the summer, from July 25, 2014 to September 15, 2014, there was a strong positive linear relationship between the two variables. This plot showed that low temperatures coincided with low sap flux rates from riparian vegetation.

"Missing Streamflow" was not as strongly linked to sap flux as some of the meteorological variables. However, a weak linear relationship was found between the average "missing streamflow" for each day and the average sap flux for each day without precipitation during baseflow (Figure B.27).

Riparian and Hillslope Comparison

To gain a better understanding of evapotranspiration processes within a watershed, the riparian and hillslope fluxes were analyzed and compared. The difference between riparian ET and hillslope ET processes were analyzed using both meteorological and sap flux variables.

Meteorological Observations

Riparian zones and hillslopes were shown to have a difference in meteorological measurements at night. Riparian night-time temperature and night-time relative humidity were significantly different from hillslope meteorological values during the same time. Riparian temperatures were much lower at night throughout the summer months and relative humidity was relatively higher at night compared to all hillslope meteorological stations regardless of elevation (Figure B.28; Figure B.29). This meteorological measurement affected the Penman-Monteith evapotranspiration calculations of canopy reference ET and reference ET at the riparian site, which showed that little to no ET

occurred at night within the riparian zone (Figure B.30). The daytime meteorological variables were similar in all aspects and were well correlated with elevation, as expected.

Sap Flux Observations

To understand differences in riparian and hillslope transpiration, sap flux comparison were made between the same species (Douglas-fir) in both riparian and hillslope environments. Riparian sap flow and hillslope sap flow measurements showed transpiration in the early summer and then a decline in transpiration during the mid and late summer. Figure B.31 shows this comparison between two Douglas-fir trees of the same diameter. The riparian vegetation is shown to have more transpiration early in the summer and a decline in transpiration is observed later in the summer. The hillslope and riparian sap flux showed a decline in transpiration from approximately July through October. Soil moisture was also observed to decline during the summer as well. The soil moisture storage has been documented in DCEW before by Smith et. al (2011), who showed that there is limited soil moisture storage available within DCEW.

Analysis performed on sap flux showed a relationship between riparian sap flux and streamflow discharge, as well as hillslope sap flux and soil moisture. Figure B.32 shows there is a relationship between riparian sap flux and Confluence 1 East discharge for the summer of 2014. The relationship shown, along with the plot in Figure B.33 of streamflow discharge and sap flux, illustrates the decline in riparian sap flux coinciding with a decrease in streamflow discharge. A weaker relationship exists between hillslope sap flux and adjacent hillslope soil moisture for the entire summer as seen in Figure B.34. Refining the analysis to separate the data into two datasets shows that in the early summer soil moisture does not correlate well with sap flux, but a strong relationship is

observed later in the summer. Figure B. 35 shows the later part of the summer where the soil moisture has a very strong relationship with sap flux. This relationship can be observed when soil moisture and sap flux are plotted beside one another in Figure B.36.

4. DISCUSSION

Riparian Evapotranspiration

The riparian ET throughout the watershed accounted for approximately 1-11% of the watershed scale ET during low flows in DCEW (Table A.3-Table A.7). The calculated riparian ET based on the "missing streamflow" method was variable throughout the watershed due to the diel signal amplitude's spatial and temporal variability throughout the watershed.

Based on the analysis performed on the amplitude and lag time of the diel signal, it can be concluded that the most accurate estimates of riparian ET are in the headwaters of the watershed. The gauging station at Confluence 1 East and Confluence 1 West calculated the highest riparian ET ranging from 3.5% - 11% throughout the summer months (Table A.3; Table A.4). This estimate provided a better understanding of riparian zone ET. However, when taking into account the uncertainty within the watershed scale ET estimate, it can be decided that the riparian zone evapotranspiration is not a significant contribution to the watershed scale ET estimate.

Previous diel signal studies have shown a temporal trend of a decrease in evapotranspiration estimates, calculated from diel signal methods, over the summer (Lautz 2008; Gribovszki et al. 2008). However, these studies did not compare to a larger scale watershed ET, so it is unknown if the diel signal ET estimates were significant relative to the watershed scale ET. This diel signal study provided insight into the overall contribution of riparian ET and showed that with the use of streamflow diel signals there

was no significant contribution. We concluded this to be a function of two processes. Either the diel signal method was not an accurate method to estimate ET or the riparian zone truly has less evapotranspiration occurring from within the region. We found a combination of these two conclusions to be the reason for a small riparian zone ET contribution at a watershed scale.

Diel Signal

To understand the effectiveness of the streamflow diel signal method, we analyzed the controls on the streamflow diel signals. Analyzing the diel signal spatially and temporally provided a better understanding of the limitations and effectiveness of the method for estimating riparian ET.

The characteristics of the diel signals within DCEW varied in both space and time. The variability of the diel signal's lag time and amplitude were determined to have affected the calculation of "missing streamflow." The amplitude had been shown within various studies to decrease throughout the summer as baseflow decreased. This had been attributed to mainly the dampening of downstream diel signal (Wondzell et al. 2007). The reason for the amplitude decreasing at low baseflow is not well understood and could be due to various factors such as the processes of signal transfer from the vegetation to the streamflow. The amplitude decrease over time could be due to an accurate representation of the diel signal that is controlled by groundwater, vegetation uptake, atmospheric demand, or a combination of the three. To decipher between the multiple causes, riparian zone processes from sap flux and meteorological stations were analyzed to determine diel signal temporal and spatial variability.

Diel Signal Temporal Variability

Explanations for the amplitudes temporal variability were explored. The explanations for amplitude variability could be a factor of either limited water availability due to a decreasing groundwater table through the summer, vegetation regulating transpiration, or the atmospheric demand decreasing throughout the summer. A decreasing groundwater table would make it harder for vegetation to transpire water to the atmosphere via the riparian zone, and would support multiple theories on diel signal transfer brought up in the background. However, Wondzell et al. (2007) rejected this idea of a decreasing groundwater table through the summer in their study because it was not observed within groundwater piezometers. For this study, groundwater piezometers were not instrumented near the riparian zone, so it could not be determined whether this was the case or not within DCEW.

Variability in transpiration could be a possible reason for the temporal variability in diel signal amplitude. Sap flux data acquired within the riparian zone and hillslope showed a decrease in transpiration through the summer in instrumented deciduous and conifer trees. The riparian vegetation showed a general decrease through the summer, which could be the cause for the decrease in amplitude of the streamflow. The relationship between riparian sap flux and streamflow discharge (Figure B.32) supports the idea that vegetation uptake could be correlated to the amplitude. So this could be an explanation for amplitudes decreasing toward the latter part of the summer. Water availability and atmospheric controls are two controls on riparian vegetation that could affect transpiration and ultimately diel signal amplitudes

Groundwater is a reliable water source for vegetation in DCEW, particularly in

the riparian zone. In the past, the riparian vegetation has been shown to have utilized predominately soil water for most of the summer (McCutcheon 2015). When comparing the riparian zone vegetation to the hillslope vegetation, it has been observed that riparian vegetation utilizes groundwater more relative to hillslope vegetation within DCEW. This could help to elucidate the difference between hillslope and riparian sap flux. The hillslope relying almost solely on soil moisture could not transpire when the soil reached a permanent wilting point. However, riparian sap flux showed that there was still transpiration occurring, although minor, during the driest part of the baseflow when hillslope transpiration shuts down (Figure B.31). The previous work completed within DCEW helped to reveal possible controls on riparian vegetation and subsequently controls on diel signal amplitude.

Atmospheric demand was shown to increase early in the summer and then decrease through the later part of the summer. A proxy for atmospheric demand, vapor pressure deficit (VPD), was calculated for each precipitation-free period and averaged over that time period. The data showed that the highest VPD corresponded to the lowest amplitudes during the summer. There was a decrease late in the summer, but that decrease did not coincide with the decrease in amplitude that occurred through the summer. Although the atmospheric demand declined through the summer, it did not correspond with the decline in sap flux. However, there were other meteorological variables that corresponded well to sap flux.

A correlation was observed between sap flux and net radiation throughout the summer, as well as temperature and sap flux late in the summer. This could support the idea that the atmospheric variables play a role in the decline of streamflow amplitude,

through the summer, via vegetation. Past studies have shown vegetation to be able to control transpiration with water storage and the stomata regulation (Cermák et al. 2007; Whitehead 1998). However, the sap flux's connection to meteorological variables demonstrates that meteorological variables could be controlling the amplitude's temporal variations within DCEW.

Another factor affecting the temporal variability could be the active riparian area. The active riparian area has been shown to shrink during the summer in some watersheds (Bond et al. 2002). For this study, the modeled riparian zone was calculated as an average riparian area and used as a constant throughout the summer. The model was based on the slope and relative distance to the stream channel within the riparian zone and provided an adequate riparian area estimate. However, the variability within the riparian area zone of influence during the summer could be controlling the vegetation that interacts with the riparian subsurface water. Therefore, less vegetation transpiring could ultimately affect the diel signal amplitude over time. Future studies would benefit from more research into groundwater availability to the riparian zone area of influence and how the active riparian area changes throughout the summer in DCEW.

Although lag time and amplitude vary temporally, a pattern of recovery is observed within this study, as well as previous studies. Previous research within DCEW has shown that the lag times at various gauging stations increases throughout the summer until late summer when lag times recover back to early summer levels (Graham et al. 2013). The same pattern of recovery was seen within the discharge and amplitudes at nearly all sites in DCEW. This is due to the recovery of the streamflow at the end of the baseflow season where discharge increases either from increased precipitation or a

decrease in vegetation uptake (Frye 2013). Daily sap flux calculations compared with daily temperature values support that a decrease in vegetation uptake occurs when there is a decrease in temperature late in the baseflow season (Figure B.26). A significant positive relationship between net radiation and sap flux for precipitation-free periods supports the idea that vegetation transpiration decreases along with a decrease in atmospheric measurements (Figure B.23; Figure B.24). These correlations may provide an explanation for the recovery of baseflow and diel signal characteristics.

Diel Signal Spatial Variability

The ability to compare diel signals in spatial detail and determine relationships along the stream channel provides a nested catchment design an advantage over an independent gauging station. The nested catchment design allowed for analysis and comparison of spatial variability of diel characteristics, such as amplitude and lag time, throughout the watershed. The influence from incremental watersheds, within a complex mountainous watershed, provided insight into spatial diel signals processes. Analyzing these smaller sub-watersheds within a watershed allows for a more spatially refined analysis that provides greater insight into catchment-streamflow connectivity (Szeftel 2010).

There was a large spatial variation of diel signal amplitudes within the watershed. The amplitudes within DCEW correlated well with watershed area early in the summer, but the relationship became weaker through the summer (Figure B.20). This data would support the idea of slower velocities in streamflow later in the summer causing a mixing of the upstream signals, therefore, decreasing the amplitude of the downstream signal. However a recent study by, Szeftel (2010) found data contrary to the idea of a mixing of

an upstream signal affecting downstream amplitudes. The results of that study showed that the amplitude actually increased downstream and pointed out that this is contrary to the idea of signal mixing as the signals move downstream. One would expect downstream gauges to have lower amplitudes if this was the case.

There were similar results within DCEW where downstream gauges tended to have higher amplitudes. The only location this was not applicable was between the C2M gauging station and LG station. Previous work done within DCEW has shown that this section of the stream can be classified as a losing stream (Frye 2013) and the decrease in discharge could be the reason for consistently lower amplitudes at Lower Gauge station.

A possible explanation, within DCEW, for downstream gauges having higher amplitudes, but still being reduced by upstream amplitudes, would be that the magnitude of discharge occurring at downstream stations is much larger than upstream gauges. Throughout the watershed, there is a strong relationship between amplitude and discharge. The larger discharge downstream allows for a larger diel signal since the diel signal is not constrained. The upstream gauges would, therefore, have amplitudes that are limited by the magnitude of discharge at that gauging station. The idea that the downstream signals are reduced is still possible because the amount of discharge is much larger downstream compared to upstream.

Although the spatial variability of amplitude and lag time throughout the watershed could be controlled by streamflow discharge, there are also two other factors that may affect amplitude. One possible factor that could explain the variability of lag times and amplitude within DCEW is the vegetation distribution within the watershed. The upper elevation hillslopes of the watershed are highly vegetated with conifers and

this is where the largest normalized amplitudes are observed within the diel signal. The lower elevations have smaller normalized amplitudes and have less hillslope vegetation. The larger vegetation in the higher elevations has been observed to have deeper root systems (Mauer & Palátová. 2012) that could tap into subsurface water that would otherwise enter the stream channel. Therefore, the near riparian areas could be affecting diel signals within the higher elevation watersheds that are highly vegetated. On the other hand, the lower elevation hillslopes are steeper and occupied by grasses and shrubs that are less likely to access subsurface water that is entering the stream via the riparian zone. So the larger influence of riparian area could have a greater effect on the diel signals in the higher elevations of the catchment.

The second possible factor is the theory of upstream signals mixing and affecting lower elevation diel signals within DCEW. The timing of the diel signal within DCEW was observed to vary throughout the watershed. This timing could impact downstream gauges and be the cause of lower amplitudes in the lower elevations of the watershed. The upstream signals generally reach minimum streamflow late in the day, relative to downstream gauges that generally reached minimum streamflow earlier in the day. So since the timing of the diel signals are not coinciding with one another, they become destructive as they move downstream.

The evidence for the mixing of diel signals was observed in the lag times throughout the summer and the amplitudes being normalized for each sub-watershed. The normalized amplitudes showed that the amplitudes were much lower than expected for lower elevation gauges. Based on the amplitudes, it could be determined that lower elevation gauges within DCEW were heavily affected by the mixing of diel signals from

higher elevation gauges. The variability in lag times of upstream signals dampens the diel signal as it moves downstream. Since amplitude is a characteristic of the diel signal, reducing the overall amplitude of the diel signal affects the riparian ET calculation. When the average amplitude was normalized to the area of the catchment, it was observed that the higher elevation catchments have normalized amplitudes that are up to twice as large as downstream catchments. For example, the normalized amplitude at the C1E gauging site was two times greater than at the C2M gauge (Figure B.22). This analysis was consistent throughout the summer with the higher elevation gauges having higher normalized amplitudes in comparison to lower elevation gauges. The reason for this discrepancy is the mixing of the diel signal from upstream sites. Utilizing diel signals from downstream gauges may not be the most accurate representation of riparian ET in the lower elevations of DCEW. The results from this analysis would suggest that downstream gauges underestimate riparian zone evapotranspiration for Dry Creek Experimental Watershed due to the mixing of upstream diel signals.

Although amplitude destruction is occurring throughout the summer, the downstream diel signals are observed to be affected even more so later in the summer. Correlating amplitudes between C1E and C2M show a significant relationship in the early summer followed by no relationship later in the summer. This supports the theory of stream velocity affecting the diel signals. This theory suggests that when streams are at high velocities early in the summer there is a correlation between amplitudes of upstream and downstream gauges. As the summer progresses, the relationship weakens due to a decrease in streamflow velocity and mixing of diel signals. Figure B.21 shows this idea by splitting the dataset of daily amplitudes for precipitation-free periods into early and

late summer.

The analysis of lag times and amplitudes of the diel signal within a nested catchment provided an explanation for the spatial variability of the diel signal within DCEW. The nested catchment allowed for comparison of linked stream gauges to determine the influences on diel signal characteristics. This theory, along with vegetation cover and streamflow discharge, plays a role in the amplitude and lag time variability throughout the watershed. Based on this data, we can conclude that the headwaters of the watershed produce the most reliable representation of the true diel signal and, therefore, the most accurate estimate of riparian zone ET.

Investigating Controls on Riparian Evapotranspiration

The minor contribution of riparian zone evapotranspiration, relative to watershed scale ET, can be explained by various observations in meteorological and sap flux measurements. The riparian zone is thought to be a water source for vegetation to use throughout the summer due to streamflow within the riparian zone. The data collected show that although there is water available, the vegetation may not be transpiring at its potential.

Data from meteorological stations show that during the day the fluxes between hillslopes and riparian zones are quite similar. However, the riparian zone experiences cold air drainage at night (Goulden et al. 2006) based on observations of temperature within the riparian zone. This cold air drainage causes a reduction in the amount of ET. In a comparison of models with the Penman-Monteith equation, hillslopes are able to transpire at night with warmer temperatures and lower relative humidity. Overall, the riparian zone experiences less ET at night throughout the year, when compared to

hillslopes, therefore, decreasing the overall potential for the riparian zone to evapotranspire over the summer.

The comparison of sap flux at riparian and hillslope sites showed that riparian zones are able to transpire for a longer period of time during the summer, but showed a decline toward the end of the summer. The hillslope vegetation had a limited amount of water storage within the soil profile and, therefore, a more restricted growing season, which can be seen in the decreased transpiration at low water storage (Figure B.36). Riparian zones experience a similar decline in transpiration during low baseflow, but the decline was less significant when compared to hillslope transpiration. The relationship between average riparian sap flux and average daily streamflow discharges shows that riparian vegetation may not be significantly transpiring at all times during the baseflow. The data show that there is a point in the summer when the riparian zone transpiration slows down substantially, and this may explain the reason for the limited estimate of riparian ET.

Although the riparian zone ET does not account for a significant amount of the watershed scale ET estimate, the timing of the loss is occurring at a crucial time when streamflow is at its lowest during the year. Since the riparian zone serves as a major ecosystem for the watershed during the summer months, it is a crucial area to understand. Although the diel signals do not have a large impact on the overall watershed ET, the diel signals do play a key role in water availability in the riparian zone for vegetation and biota during summer months.

The effect of diel signals on low flows has a substantial impact on the ecosystem within the riparian zone. The time of year that these processes are occurring is when

streamflow is the lowest in DCEW and the most crucial for the ecosystem. Table A.3-Table A.7 show that the “missing streamflow” calculated from the diel signal can account for up to 88% of the actual streamflow during particular periods of the summer months. Recent work within DCEW has shown a pure genetic redband trout species that exists within the stream and relies on low flows throughout the summer in DCEW (Richins 2014). This example of fish relying on streamflow processes illustrates that it is important to understand the impact that climate has on riparian processes and how the climate affects streamflow during these baseflow events.

5. CONCLUSION

The ecological importance of riparian zones outweighs their proportional area of the watershed because of the location within the watershed and the connection between vegetation and hydrologic processes, particularly during the summer months. The riparian zone accounts for at most 11% of the watershed scale ET, within DCEW, during baseflow. Although it was expected that the riparian zone, with a sufficient supply of water, would have a significant impact on the watershed scale ET, that was not the case within DCEW. However, the riparian zone is an important ecohydrologic region of the watershed during the summer months and it is important to understand the processes that are occurring within this ecosystem.

The spatial and temporal variability in the amplitude and lag time of the streamflow diel signals was a product of diel signal mixing and possibly vegetation cover. The variability and destructive mixing of upstream signals altered the downstream amplitude, diminishing downstream diel signals throughout the baseflow season. The data provided from a nested catchment design helped to conclude that the upper reaches of the watershed were the most accurate representation of riparian ET within DCEW.

Hillslope and riparian meteorological measurements showed significant differences between hillslope and riparian zones with a comparison of night-time measurements. At night, temperatures were much lower within the riparian zone, causing an increase in relative humidity compared to hillslope meteorological sites. This was a function of cold air drainage and it was observed that no evapotranspiration was able to

occur at night within the riparian zone.

Sap flux comparison between hillslope and riparian vegetation showed that riparian transpiration of Douglas-fir declined, although there was still water available within the stream. Although not as drastic, this observation was similar to the decline in hillslope transpiration when soil moisture reached a wilting point and the hillslope vegetation stopped transpiration. This has implications on watershed scale ET measurements, since the riparian zone is observed to reduce transpiration when it could be thought to still be transpiring due to riparian water availability.

Strong correlations were found between net radiation, temperature, and sap flux for most of the baseflow season. However, there was no significant relationship found between the sap flux and "missing streamflow" from diel signals. This may be due to various factors of tree storage (Cermák et al. 2007) or possible stomata regulation occurring within the species (Whitehead 1998). This would be an area upon which future studies to expand to better understand the link between vegetation and streamflow diel signals.

Obtaining a better understanding of riparian zone processes and their influences on the watershed has helped to determine the significances that diel signals have on water availability during the summer. Water availability during the summer months is crucial to vegetation and fish species within DCEW. Baseflows are necessary to sustain life during the summer in semi-arid watersheds. Therefore, it is important to study riparian zone processes, when water is limited, to understand the effects diel signals could have on water availability within the stream.

Further research on diel signal processes within the riparian zone would allow for

a better understanding of how these signals are transmitted to the stream and what impacts they could have on the ecosystem with a changing climate. Increase understanding of sap flow, both spatially and temporally, would also add insight into riparian zone processes for future studies. Studies on subsurface processes within DCEW would also allow for further insight into diel signal processes and the mechanism of diel signal transfer from the vegetation to the stream.

6. REFERENCES

Aishlin, P., and McNamara, J.P., 2011, Bedrock infiltration and mountain block recharge accounting using chloride mass balance: Hydrological Processes, v. 25, p. 1934–1948, doi: 10.1002/hyp.7950.

Allen, R., Pereira, L.S., Raes, D., and Smith, M., 1998, Crop evapotranspiration: Guidelines for computing crop requirements: Irrigation and Drainage Paper No. 56, FAO, p. 300, doi: 10.1016/j.eja.2010.12.001.

Allen, R.G., Pruitt, W.O., Wright, J.L., Howell, T. a., Ventura, F., Snyder, R., Itenfisu, D., Steduto, P., Berengena, J., Yrisarry, J.B., Smith, M., Pereira, L.S., Raes, D., Perrier, A., et al., 2006, A recommendation on standardized surface resistance for hourly calculation of reference ETo by the FAO56 Penman-Monteith method: Agricultural Water Management, v. 81, p. 1–22, doi: 10.1016/j.agwat.2005.03.007.

Bancalari, M. a. E., Perry, D. a., and Marshall, J.D., 1987, Leaf area – sapwood area relationships in adjacent young Douglas-fir stands with different early growth rates: Canadian Journal of Forest Research, v. 17, p. 174–180, doi: 10.1139/x87-030.

Barnard, H.R., Graham, C.B., Van Verseveld, W.J., Brooks, J.R., Bond, B.J., and McDonnell, J.J., 2010, Mechanistic assessment of hillslope transpiration controls of diel subsurface flow: a steady state irrigation approach: Ecohydrology, p. 133–142, doi: 10.1002/eco

Blaney, H.F., Taylor, C.A., Young, A.A., 1930. Rainfall penetration and consumptive use of water in the Santa Ana River Valley and Coastal Plain. California Department of Public Works, Division of Water Resources, Bulletin 33, p. 162.

Blaney, H.F., 1965, Consumptive use and water requirements in New Mexico: U.S. Department of Agriculture, Soil and Water Conservation Research Division and Department of Agricultural Engineering, v. 36, p. 82.

Bond, B.J., Jones, J. a., Moore, G., Phillips, N., Post, D., and McDonnell, J.J., 2002, The zone of vegetation influence on baseflow revealed by diel patterns of streamflow and vegetation water use in a headwater basin: Hydrological Processes, v. 16, p. 1671–1677, doi: 10.1002/hyp.5022.

Boronina, A., Golubev, S., and Balderer, W., 2005, Estimation of actual evapotranspiration from an alluvial aquifer of the Kouris catchment (Cyprus) using continuous streamflow records: Hydrological Processes, v. 19, p. 4055–4068, doi: 10.1002/hyp.5871.

Bren, J., 1997, Effects of slope vegetation removal on the diurnal variations of a small mountain stream: Water Resources Research, v. 33, p. 321–331.

Burt, T.P. 1979. Diurnal variations in stream discharge and throughflow during a period of low flow. Journal of hydrology, v. 41 p. 291.

Butler, J.J., Kluitenberg, G.J., Whittemore, D.O., Loheide, S.P., Jin, W., Billinger, M. a., and Zhan, X., 2007, A field investigation of phreatophyte-induced fluctuations in the water table: Water Resources Research, v. 43, p. n/a–n/a, doi: 10.1029/2005WR004627.

Cadol, D., Kampf, S., and Wohl, E., 2012, Effects of evapotranspiration on baseflow in a tropical headwater catchment: Journal of Hydrology, v. 462-463, p. 4–14, doi: 10.1016/j.jhydrol.2012.04.060.

Chauvin, G.M., Flerchinger, G.N., Link, T.E., Marks, D., Winstral, a. H., and Seyfried, M.S., 2011, Long-term water balance and conceptual model of a semi-arid mountainous catchment: Journal of Hydrology, v. 400, p. 133–143, doi: 10.1016/j.jhydrol.2011.01.031.

Cermák, J., Kucera, J., Bauerle, W.L., Phillips, N., and Hinckley, T.M., 2007, Tree water storage and its diurnal dynamics related to sap flow and changes in stem volume

in old-growth Douglas-fir trees.: Tree physiology, v. 27, p. 181–198, doi: 10.1093/treephys/27.2.181.

Constantz, J., Thomas, C.L., and Zellweger, G., 1994, Influence of diurnal variations in stream temperature on streamflow loss and groundwater recharge: Water Resources Research, v. 30, p. 3253–3264.

Czikowsky, M., and Fitzjarrald, D., 2004, Evidence of seasonal changes in evapotranspiration in eastern US hydrological records: Journal of Hydrometeorology, p. 974–988.

Dahm, C.N., Cleverly, J.R., Allred Coonrod, J.E., Thibault, J.R., Mcdonnell, D.E., and Gilroy, D.J., 2002, Evapotranspiration at the land/water interface in a semi-arid drainage basin: Freshwater Biology, v. 47, p. 831–843, doi: 10.1046/j.1365-2427.2002.00917.x.

DCEW, 2015, Watershed Description, Retrieved from http://earth.boisestate.edu/drycreek/watershed-description/

Dunford, E.G., and Fletcher, P.W., 1947, Effect of removal of stream-bank vegetation upon water yield: EOS Transactions AGU, v. 28, p. 105– 110.

Emanuel, R.E., Epstein, H.E., McGlynn, B.L., Welsch, D.L., Muth, D.J., and D'Odorico, P., 2010, Spatial and temporal controls on watershed ecohydrology in the northern Rocky Mountains: Water Resources Research, v. 46, p. n/a–n/a, doi: 10.1029/2009WR008890.

Fahle, M., and Dietrich, O., 2014, Estimation of evapotranspiration using diurnal groundwater level fluctuations: Comparison of different approaches with groundwater lysimeter data: Water Resources Research, v. 50, p. 273–286, doi: 10.1002/2013WR014472.

Federer, C., 1973, Forest transpiration greatly speeds streamflow recession: Water Resources Research, v. 9.

Frye, A.D., 2013, The persistence of losing and gaining stream reaches: Boise State University

Goulden, M.L., Miller, S.D., and da Rocha, H.R., 2006, Nocturnal cold air drainage and pooling in a tropical forest: Journal of Geophysical Research: Atmospheres, v. 111, p. 1–14, doi: 10.1029/2005JD006037

Goodrich, D., Scott, R., Qi, J., and Goff, B., 2000, Seasonal estimates of riparian evapotranspiration using remote and in situ measurements: Agricultural and Forest …, v. 105, p. 281–309.

Graham, C.B., Barnard, H.R., Kavanagh, K.L., and McNamara, J.P., 2013, Catchment scale controls the temporal connection of transpiration and diel fluctuations in streamflow: Hydrological Processes, v. 27, p. 2541–2556, doi: 10.1002/hyp.9334.

Graham, C.B., van Verseveld, W., Barnard, H.R., and McDonnell, J.J., 2010, Estimating the deep seepage component of the hillslope and catchment water balance within a measurement uncertainty framework: Hydrological Processes, v. 24, p. 3631–3647, doi: 10.1002/hyp.7788.

Granier, A., 1987, Evaluation of transpiration in a Douglas-fir stand by means of sap flow measurements. Tree physiology, v. 3, p. 309–20.

Gregory, S. V, Swanson, F.J., Mckee, W.A., Kenneth, W., Swanson, J., and Cummins, K.W., 1991, An Ecosystem Perspective of Riparian Zones: BioScience, v. 41, p. 540–551, doi: 10.2307/1311607.

Gribovszki, Z., Kalicz, P., Szilágyi, J., and Kucsara, M., 2008, Riparian zone evapotranspiration estimation from diurnal groundwater level fluctuations: Journal of Hydrology, v. 349, p. 6–17, doi: 10.1016/j.jhydrol.2007.10.049.

Gribovszki, Z., Kalicz, P., Kucsara, M., 2006. Streamflow characteristics of two forested catchments in Sopron Hills. Acta Silvatica et Lignaria Hungarica 2, 81– 92. <http://aslh.nyme.hu/>

Gribovszki, Z., Szilágyi, J., and Kalicz, P., 2010, Diurnal fluctuations in shallow groundwater levels and streamflow rates and their interpretation–A review: Journal of Hydrology, v. 385, p. 371–383, doi: 10.1016/j.jhydrol.2010.02.001.

Lautz, L.K., 2008, Estimating groundwater evapotranspiration rates using diurnal water-table fluctuations in a semi-arid riparian zone: Hydrogeology Journal, v. 16, p. 483–497, doi: 10.1007/s10040-007-0239-0.

Lawrence, R.E., 1990, The interaction between the environment land use and hydrology of the Bogong High Plains area from 1850 to 1985. PhD Thesis, Geography Department, The University of Melbourne.

Loheide, S.P., 2008, A method for estimating subdaily evapotranspiration of shallow groundwater using diurnal water table fluctuations: Ecohydrology, v. 66, p. 59–66, doi: 10.1002/eco.

Loughridge, R. 2014, Identifying Topographic Controls of Terrestrial Vegetation Using Remote Sensing Data in a Semiarid Mountain Watershed, Idaho, USA: Boise State University

Lundquist, J., and Cayan, D., 2002, Seasonal and spatial patterns in diurnal cycles in streamflow in the western United States: Journal of Hydrometeorology, p. 591–603.

Mauer, O., and Palátová, E., 2012, Root system development in douglas fir (Pseudotsuga menziesii [Mirb.] Franco) on fertile sites: Journal of Forest Science, v. 58, p. 400–409.

McCutcheon, R.J., 2015, Stable isotopes reveal a disconnect between biotic and abiotic hydrological processes in a seasonally-dry, semi-arid watershed: Boise State University.

McDonnell, J.J., 2014, The two water worlds hypothesis: ecohydrological separation of water between streams and trees? Wiley Interdisciplinary Reviews: Water, v. 1, p. n/a–n/a, doi: 10.1002/wat2.1027.

Moore, G.W., Jones, J. a., and Bond, B.J., 2011, How soil moisture mediates the influence of transpiration on streamflow at hourly to interannual scales in a forested catchment: Hydrological Processes, v. 25, p. 3701–3710, doi: 10.1002/hyp.8095.

Muntzner, R., Weijs, S.W., Tarolli, P., Calaf, M., Oldroyd, H.J., and Parlange, M.B., 2015, Controls on the diurnal streamflow cycles in two subbasins of an alpine headwater catchment: AGU Water Resources Research, p. 3403–3418, doi: 10.1016/0022-1694(68)90080-2.

Oishi, a. C., Oren, R., Novick, K. a., Palmroth, S., and Katul, G.G., 2010, Interannual Invariability of Forest Evapotranspiration and Its Consequence to Water Flow Downstream: Ecosystems, v. 13, p. 421–436, doi: 10.1007/s10021-010-9328-3.

O'Loughlin, E.M., Cheney, N.P., and Burns, J., 1982, The Bushranger Experiment: Hydrological response of a eucalypt catchment to fire, *in* O'Loughlin, E.M. and Bren, L.J. eds., The First National Symposium on Forest Hydrology, Canberra, Australia, p. 132–139.

Parham, W.B., 2015, Spatial and temporal storage dynamics moderate the ecohydrological significance of evapotranspiration in semi-arid mountainous terrain: Boise State University.

Reigner I.C., 1965, Method of Estimating Steam flow Loss by Evapotranspiration From the Riparian Zone: Forest Science,

Renée Brooks, J., Barnard, H.R., Coulombe, R., and McDonnell, J.J., 2009, Ecohydrologic separation of water between trees and streams in a Mediterranean climate: Nature Geoscience, v. 3, p. 100–104, doi: 10.1038/ngeo722

Richins, S., 2014, Ecology of Columbia River Redband Trout, *Oncorhynchus mykiss gairdneri*, in Dry Creek, Idaho (Lower Boise River Drainage): The College of Idaho, 1 - 75 p.

Schaeffer, S., Williams, D., and Goodrich, D., 2000, Transpiration of cottonwood/willow forest estimated from sap flux: Agricultural and Forest …, v. 105, p. 257–270.

Smith, T.J., McNamara, J.P., Flores, a. N., Gribb, M.M., Aishlin, P.S., and Benner, S.G., 2011, Small soil storage capacity limits benefit of winter snowpack to upland vegetation: Hydrological Processes, v. 25, p. 3858–3865, doi: 10.1002/hyp.8340.

Snyder, K., and Williams, D., 2000, Water sources used by riparian trees varies among stream types on the San Pedro River, Arizona: Agricultural and Forest Meteorology, v. 105, p. 227–240.

Stratton, B.T., Sridhar, V., Gribb, M.M., McNamara, J.P., and Narasimhan, B., 2009, Modeling the Spatially Varying Water Balance Processes in a Semiarid Mountainous Watershed of Idaho: JAWRA Journal of the American Water Resources Association, v. 45, p. 1390–1408, doi: 10.1111/j.1752-1688.2009.00371.x.

Sulistyowati, R., Hapsari, R.I., Syamsudin, F., Mori, S., Oishi, S.T., and Yamanaka, M.D., 2014, Rainfall-Driven Diurnal Variations of Water Level in the Ciliwung River, West Jawa, Indonesia: Sola, v. 10, p. 141–144, doi: 10.2151/sola.2014-029

Szeftel, P., 2010, Stream-Catchment Connectivity and Streamflow Dynamics in a Montane Landscape: 166 p.

Tabacchi, E., Lambs, L., Guilloy, H., Planty-Tabacchi, A.M., Muller, E., and Décamps, H., 2000, Impacts of riparian vegetation on hydrological processes: Hydrological Processes, v. 14, p. 2959–2976, doi: 10.1002/1099-1085(200011/12)14:16/17<2959::AID-HYP129>3.0.CO;2-B.

Tschinkel, H., 1963, Short term fluctuation in streamflow as related to evaporation and transpiration: Journal of Geophysical Research, v. 68.

van Meerveld, H.J., Seibert, J., and Peters, N.E., 2015, Hillslope-riparian-stream connectivity and flow directions at the Panola Mountain Research Watershed: Hydrological Processes, v. 3574, doi: 10.1002/hyp.10508.

Wain, A.S., 1994, Diurnal River Flow Variations and Development Planning in the Tropics: The Geographical Journal, v. 160, p. 295–306, doi: 10.2307/3059611.

White, W.N., 1932, A method of estimating ground-water supplies based on discharge by plants ..., *in* Contributions to the Hydrology of the United States, p. 1–105.

Whitehead, D., 1998, Regulation of stomatal conductance and transpiration in forest canopies. Tree physiology, v. 18, p. 633–644, doi: 10.1093/treephys/18.8-9.633.

Williams, C., and McNamara, J.P., 2009, Controls on the temporal and spatial variability of soil moisture in a mountainous landscape: the signature of snow and complex terrain: Hydrology and Earth …, p. 1325–1336.

Wilson, K., and Hanson, P., 2001, A comparison of methods for determining forest evapotranspiration and its components: sap-flow, soil water budget, eddy covariance and catchment water balance: Agricultural and Forest …, v. 106, p. 153–168.

Wondzell, S.M., Gooseff, M.N., and McGlynn, B.L., 2010, An analysis of alternative conceptual models relating hyporheic exchange flow to diel fluctuations in discharge during baseflow recession: Hydrological Processes, v. 24, p. 686–694, doi: 10.1002/hyp.7507.

Wondzell, S.M., Gooseff, M.N., and McGlynn, B.L., 2007, Flow velocity and the hydrologic behavior of streams during baseflow: Geophysical Research Letters, v. 34, p. L24404, doi: 10.1029/2007GL031256.

APPENDIX A

Tables

Table A.1 Vegetation cover for each sub-watershed within DCEW

Watershed	Grass/Shrub (W_{gr})	Canopy (W_{can})
C1E	15%	85%
C1W	35%	65%
C2E	48%	52%
C2M	41%	59%
LG	46%	54%

Table A.2 Table of the riparian area calculated for each sub-watershed from the modeled riparian zone in ArcMap 10.3. Shows the weight of the hillslope and riparian zone used to weight the $ET_{r,h}$ calculations to determine catchment ET (ET_c)

Watershed	$Area_{Total}$ (km^2)	$Area_{rip}$ (km^2)	Percent Riparian Area (W_r)	Percent Hillslope Area (W_h)
C1E	8.6	0.34	4%	96%
C1W	3.8	0.19	5%	95%
C2E	7.5	0.38	5%	95%
C2M	23.9	1.2	5%	95%
LG	26.9	1.43	5%	95%

Table A.3 Table of variables within Confluence 1 East watershed for precipitation-free periods during the summer of 2014

Confluence 1 East						
	5/29-6/13	6/20-6/25	6/28-7/19	7/25-8/05	9/01-9/15	10/01-10/10
Period Length	15	6	22	12	15	10
ET_h (mm/day)	0.84	0.86	0.98	0.74	0.39	0.31
ET_r (mm/day)	1.2	0.60	0.62	0.73	0.69	0.89
ET_c (mm/day)	0.85	0.85	0.97	0.74	0.40	0.33
ET_rW_r/ ET_c (%)	5.8%	2.8%	2.6%	3.9%	6.9%	10.7%
Average Lag (hrs)	-9.0	-10.0	-9.0	-10.0	-11.0	-12.0
Avg. Amplitude (L/s)	17	11	10	11	11	12
Missing Streamflow / Streamflow	14%	11%	25%	74%	55%	16%

Table A.4 Table of variables within Confluence 1 West watershed for precipitation-free periods during the summer of 2014. An asterisk (*) denotes a different time period length from the rest of the sub-watersheds due to no significant streamflow during the excluded dates.

Confluence 1 West						
	5/29-6/13	6/20-6/25	6/28-6/30*	7/25-8/05	9/01-9/15	10/01-10/10
Period Length	15	6	3	12	15	10
ET_h (mm/day)	0.47	0.48	0.48	0.29	0.13	0.15
ET_r (mm/day)	0.64	0.35	0.24	0	0	0
ET_c (mm/day)	0.48	0.48	0.46	0.28	0.13	0.15
ET_rW_r/ ET_c (%)	6.7%	3.7%	2.6%	0%	0%	0%
Average Lag (hrs)	-4	-5	-4	N/A	N/A	N/A
Avg. Amplitude (L/s)	5.9	3.1	2.1	N/A	N/A	N/A
Missing Streamflow / Streamflow	22%	39%	41%	N/A	N/A	N/A

Table A.5 Table of variables within Confluence 2 East watershed for precipitation-free periods during the summer of 2014. An asterisk (*) denotes a different time period length from the rest of the sub-watersheds due to no significant streamflow during the excluded dates.

Confluence 2 East						
	5/29-6/13	6/20-6/25	6/28-7/08*	7/25-8/05	9/12-9/15*	10/01-10/10
Period Length	15	6	11	12	4	10
ET_h (mm/day)	1.1	1.1	1.2	0.52	0.21	0.30
ET_r (mm/day)	0.43	0.28	0.20	0	0.11	0.09
ET_c (mm/day)	1.1	1.1	1.1	0.49	0.21	0.29
ET_rW_r/ ET_c (%)	2.0%	1.3%	0.92%	0%	2.7%	1.6%
Average Lag (hrs)	-4	-5	-5	N/A	-3	-4
Avg. Amplitude (L/s)	7.6	4.8	3.1	N/A	1.8	1.6
Missing Streamflow / Streamflow	30%	44%	83%	N/A	88%	25%

Table A.6 Table of variables within Confluence 2 Main watershed for precipitation-free periods during the summer of 2014

Confluence 2 Main						
	5/29-6/13	6/20-6/25	6/28-7/19	7/25-8/05	9/01-9/15	10/01-10/10
Period Length	15	6	22	12	15	10
ET_h (mm/day)	3.2	3.3	3.1	1.7	0.75	0.96
ET_r (mm/day)	0.67	0.46	0.34	0.14	0.07	0.17
ET_c (mm/day)	3.1	3.1	2.9	1.7	0.72	0.92
ET_rW_r/ ET_c (%)	1.1%	0.74%	0.59%	0.44%	0.52%	0.93%
Average Lag (hrs)	-5	-5	-6	-6	-5	-4
Avg. Amplitude (L/s)	36	25	16	7.2	4.2	9.7
Missing Streamflow / Streamflow	19%	22%	32%	55%	23%	12%

Table A.7 Table of variables within Dry Creek Experimental Watershed (LG) for precipitation-free periods during the summer of 2014

Lower Gauge						
	5/29-6/13	6/20-6/25	6/28-7/19	7/25-8/05	9/01-9/15	10/01-10/10
Period Length	15	6	22	12	15	10
ET_h (mm/day)	3.9	4.0	3.7	1.9	0.77	1.1
ET_r (mm/day)	0.50	0.32	0.17	0	0	0.07
ET_c (mm/day)	3.8	3.8	3.5	1.8	0.73	1.1
ET_rW_r/ ET_c (%)	0.70%	0.44%	0.25%	0%	0%	0.36%
Average Lag (hrs)	-7	-7	-8	N/A	N/A	-8
Avg. Amplitude (L/s)	33	22	9.9	N/A	N/A	4.7
Missing Streamflow / Streamflow	15%	19%	32%	N/A	N/A	8.7%

Table A.8 Table of the end of the growing season within DCEW at each corresponding meteorological site

Weather Station	End of Growing Season
Lower Weather	7/15/2014
Treeline	7/5/2014
Lower Deer Point	8/9/2014
Bogus Ridge	7/2/2014

Table A.9 The average linear relationship between evapotranspiration and elevation for each meteorological station within DCEW

Watershed	Linear Relationship	R^2
C1E	-0.063x+373.05	0.38
C1W	-0.0709x+402.08	0.44
C2E	-0.0773x+428.69	0.36
C2M	-0.0732x+410.78	0.41
LG	-0.0758x+420.22	0.37

APPENDIX B

Figures

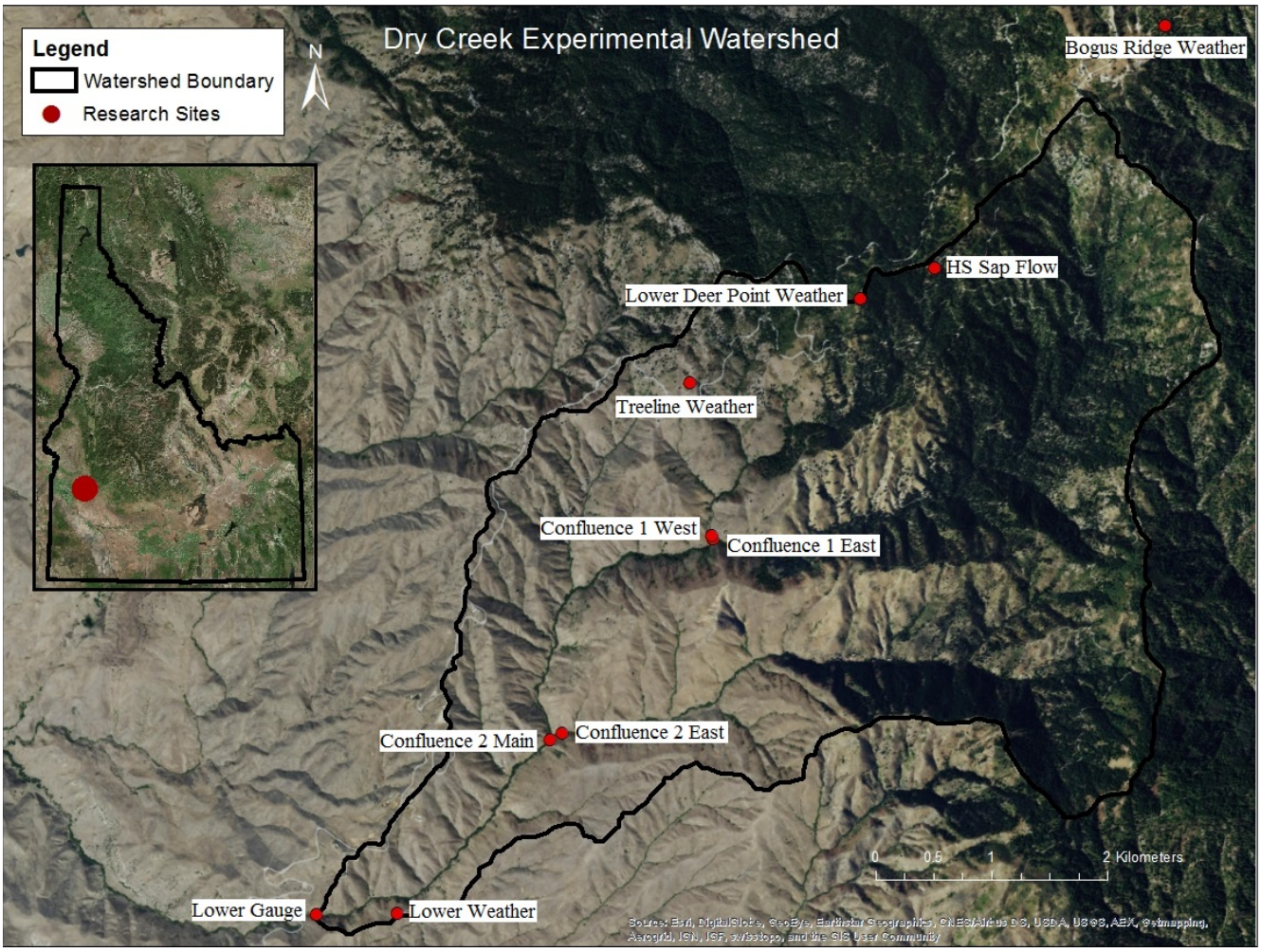

Figure B.1 The streamflow gauging stations and weather stations in Dry Creek Experimental Watershed that were utilized for this study with inset of location within Idaho.

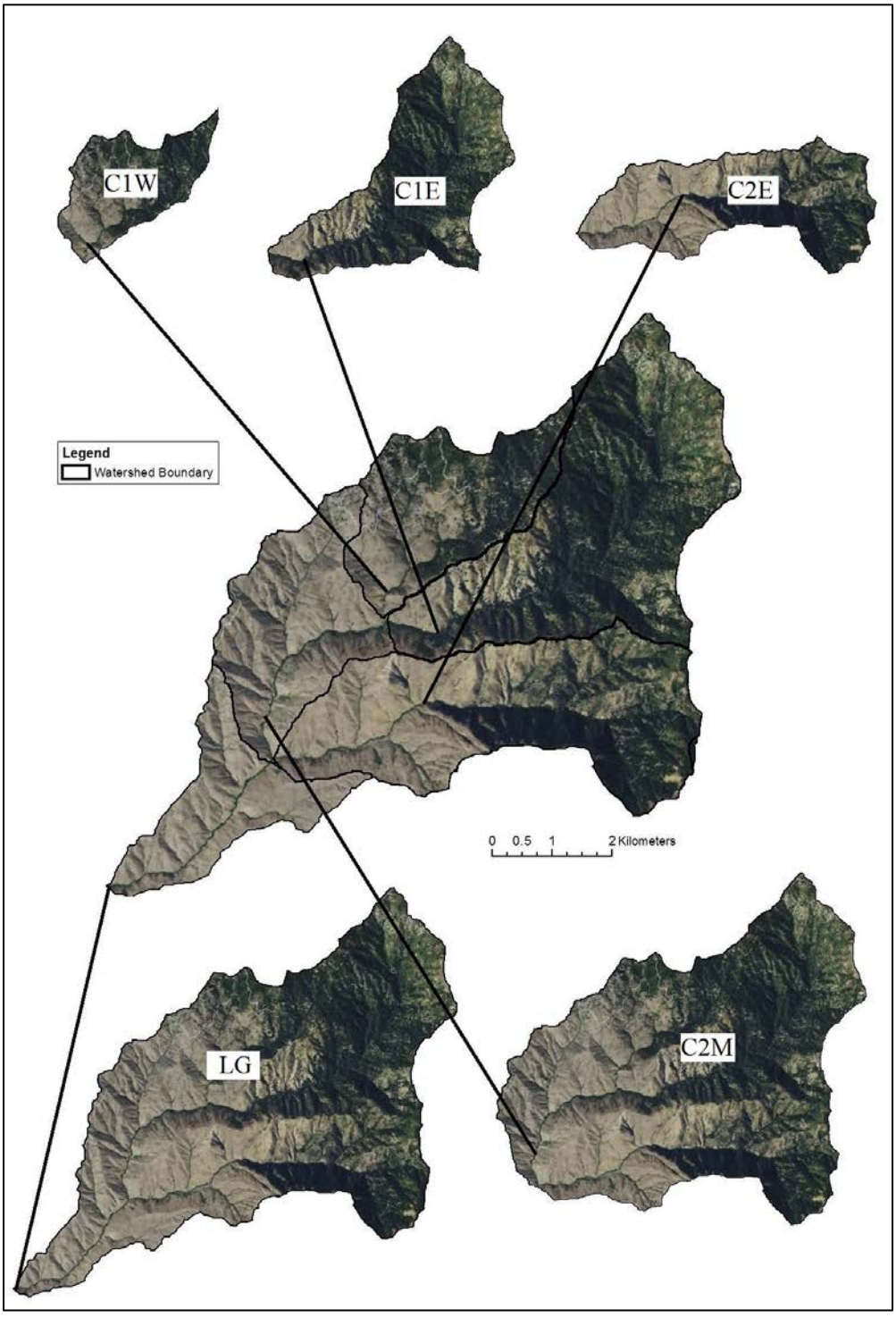

Figure B.2 The sub-watersheds used for the analysis of diel signal and the ET model. Note that C2M includes C2E, C1W, and C1E. Lower Gauge includes all sub-watersheds and is the entirety of the watershed.

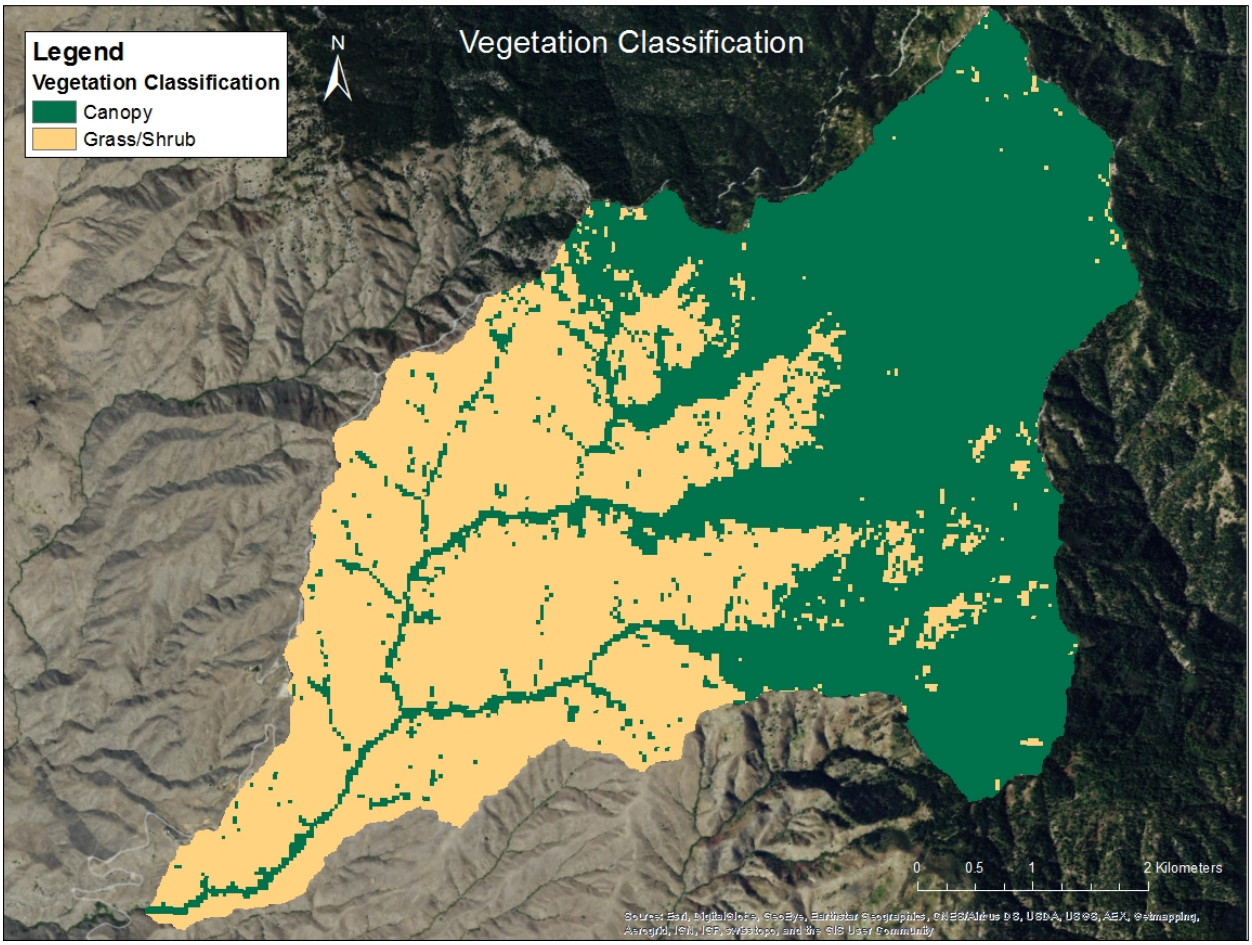

Figure B.3 The vegetation distribution within DCEW using Landsat 8 Data and a mahalanobis classification method to determine the weight of canopy ET (Wcan) and grass/shrub ET (Wgr).

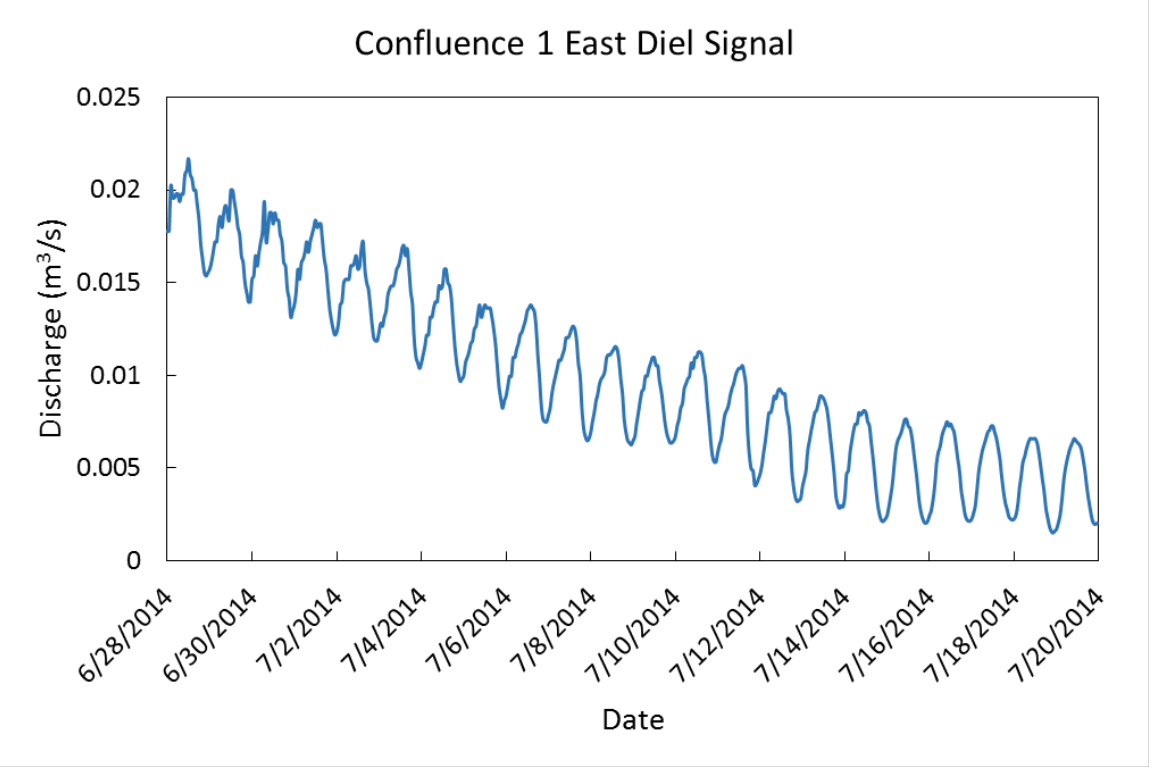

Figure B.4 Figure of Confluence 1 East discharge from June 28, 2014 to July 20, 2014 showing the presence of the diel signal within the streamflow hydrograph.

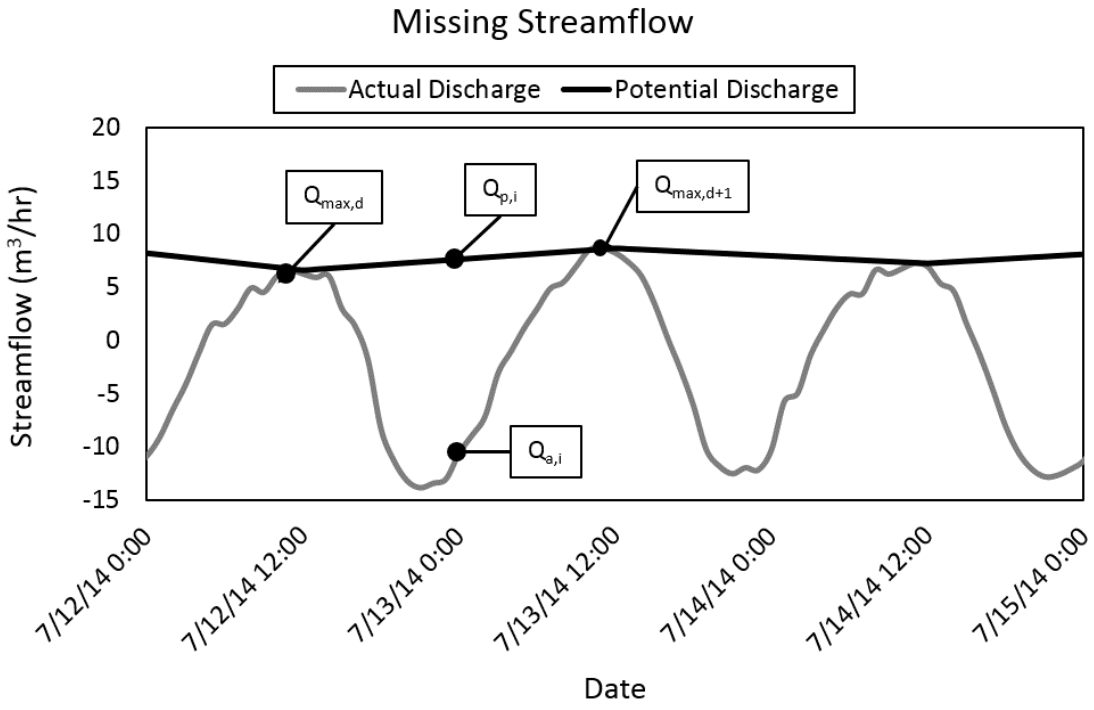

Figure B.5 An example calculation of "missing streamflow," which is the difference between the potential discharge ($Q_{p,i}$) and the actual discharge ($Q_{a,i}$). Also, note the actual streamflow is in units of m^3/hr and is detrended before the maximum values are interpolated.

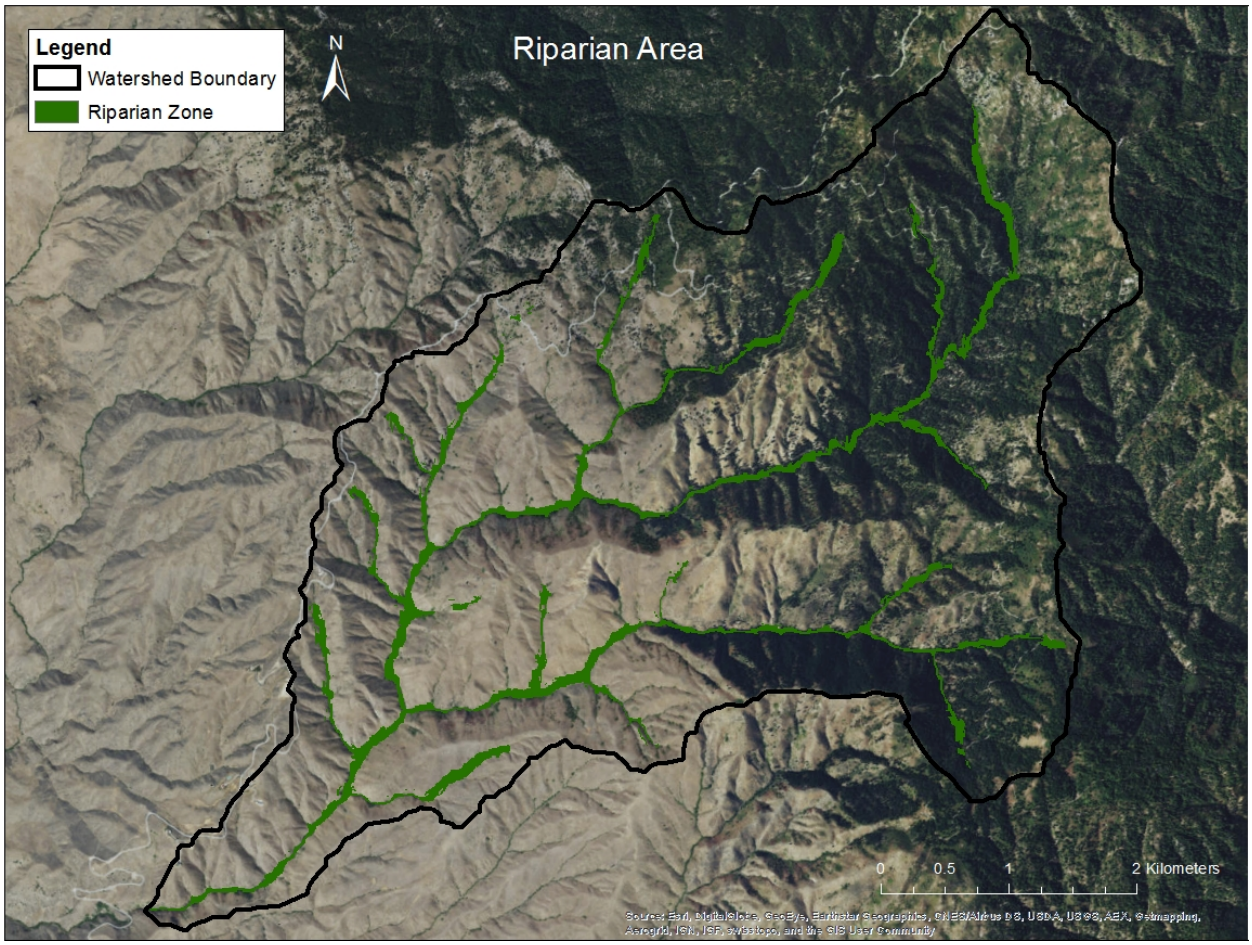

Figure B.6 A map showing the riparian zone area estimate based on a thirty-meter buffer and a slope of less than twenty-five degrees.

Figure B.7 Confluence 1 Sites with locations of gauging stations, temporary meteorological station, and sap flux instrumentation utilized for this study.

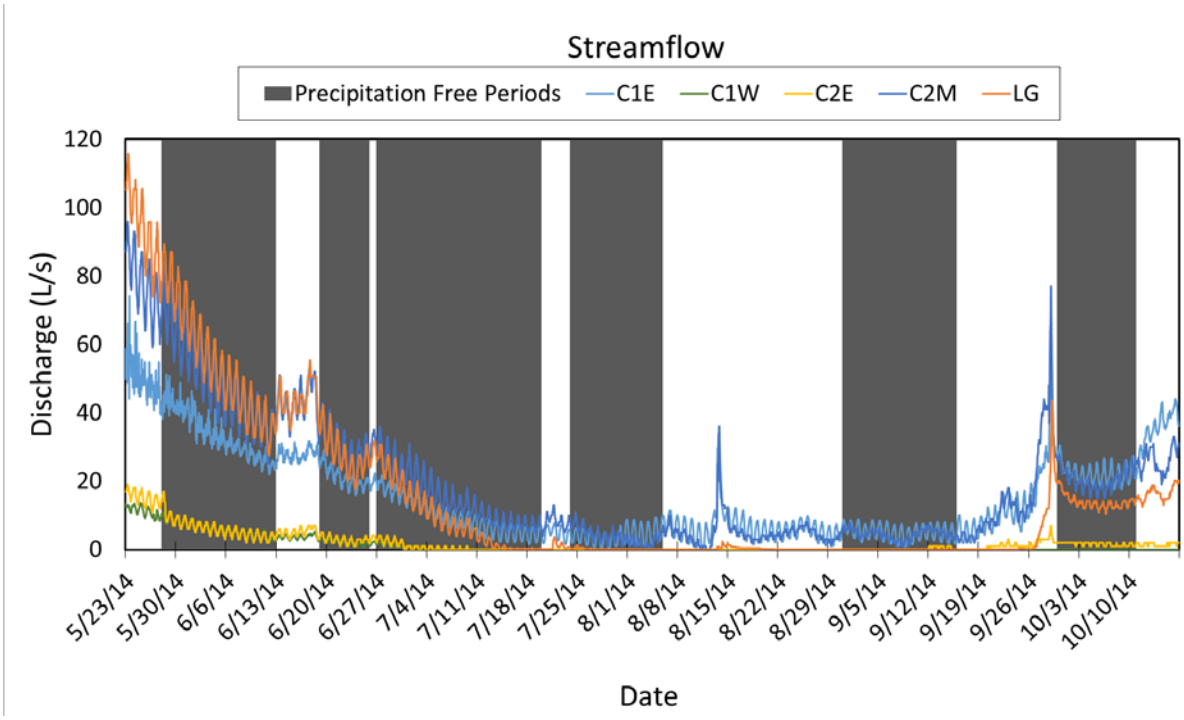

Figure B.8 The precipitation-free periods used for analysis of diel signals with discharge from all streamflow gauging stations.

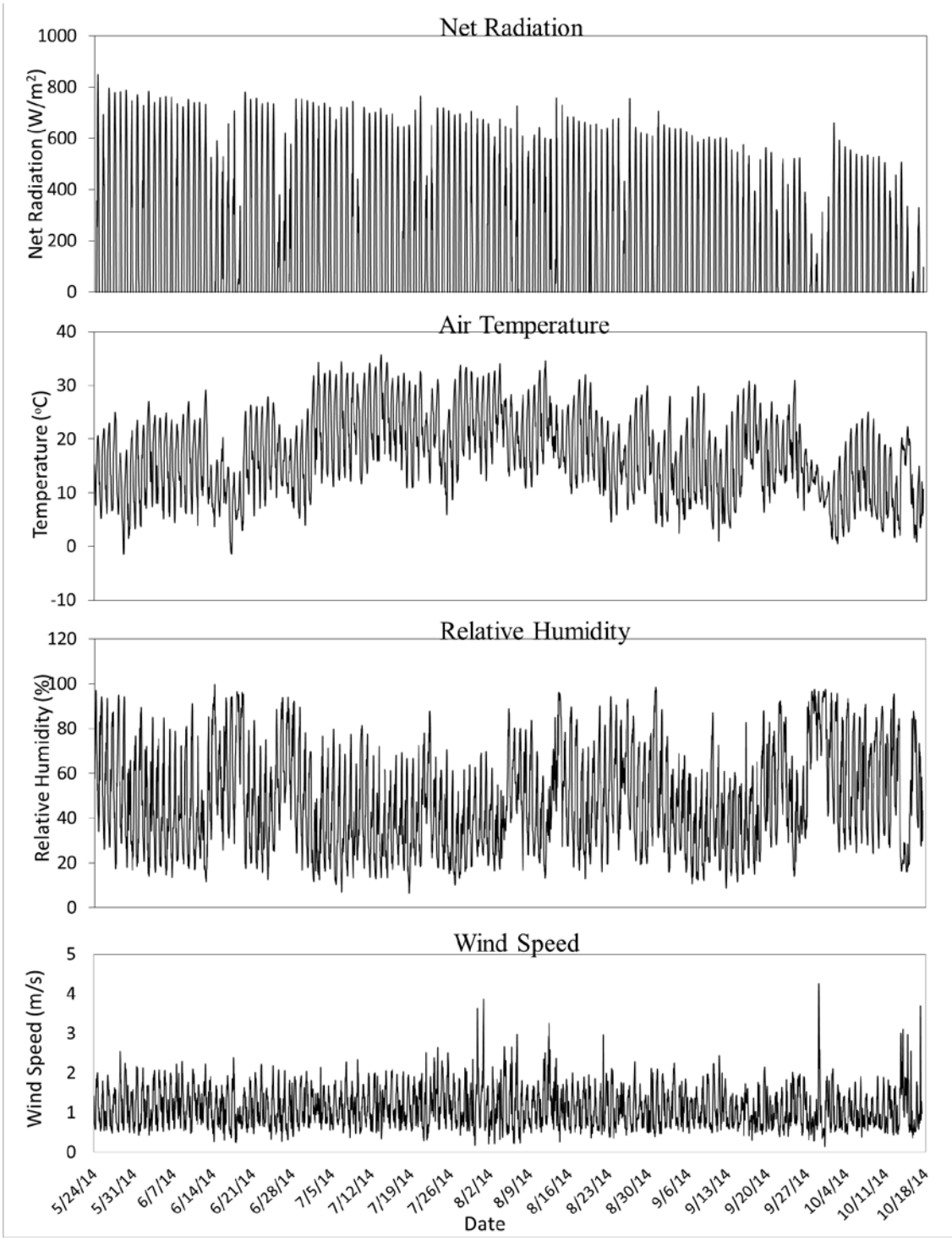

Figure B.9 Meteorological variables recorded at meteorological stations for evapotranspiration calculations and diel signal controls. The data shown is the measurement observed at Confluence 1 Meteorological site in the riparian zone. The figure shows the temporal trend of the meteorological variables during the summer on an hourly timescale.

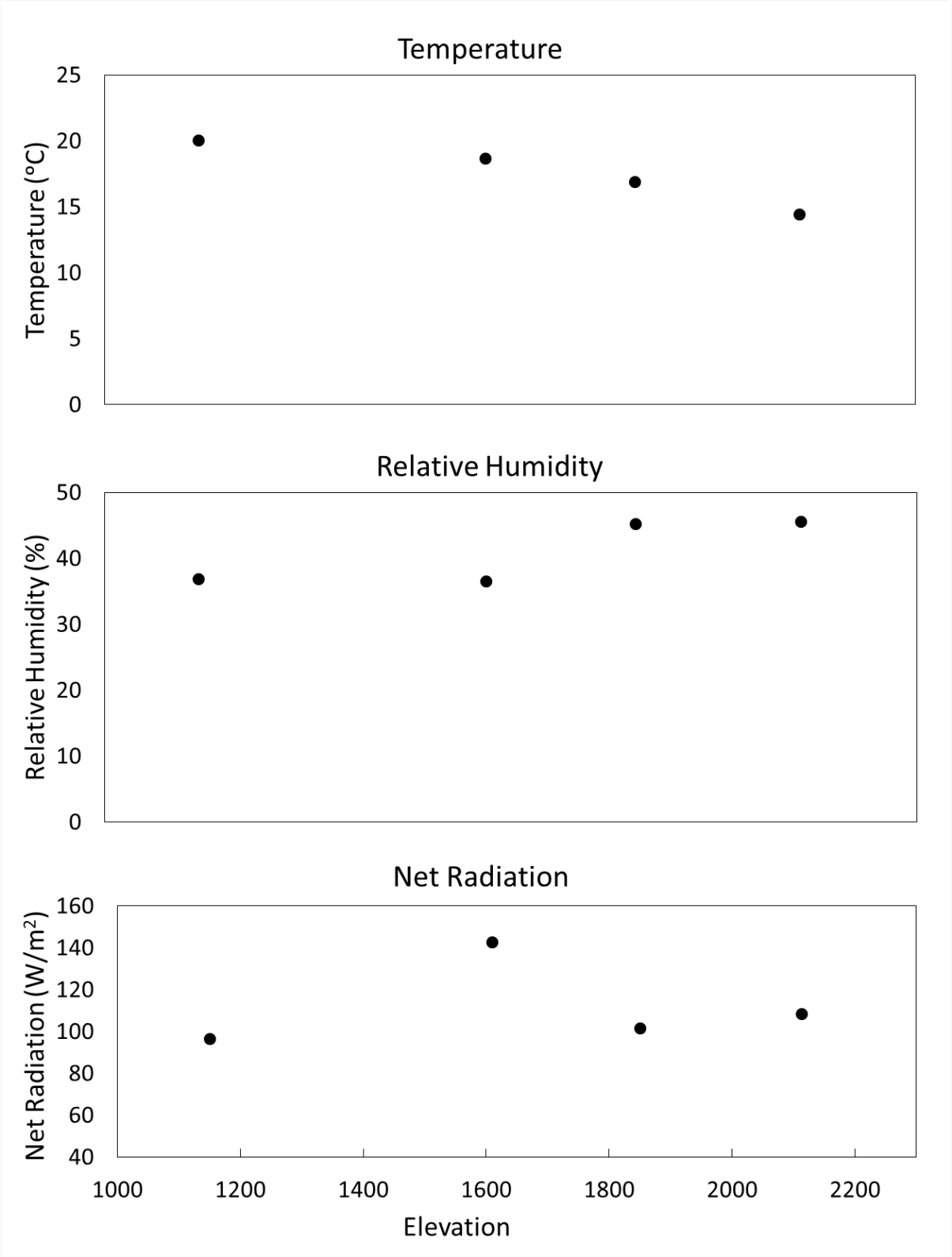

Figure B.10 The average summer values for four meteorological stations in Dry Creek Experimental Watershed at a range of elevations.

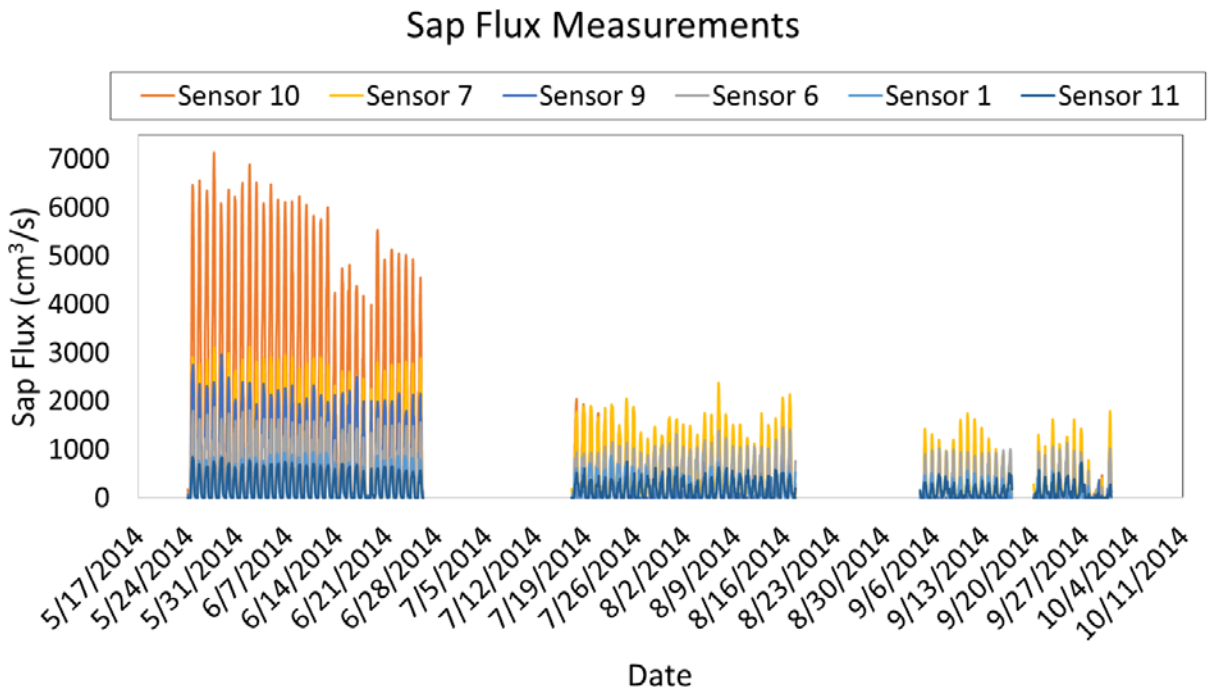

Figure B.11 Figure of sap flux hourly measurements for riparian zone sensors. The data shows the temporal trend of sap flow throughout the summer season with high values early in the season to lower values later in the summer. The data also shows missing sap flux values for date where there was insufficient power supply.

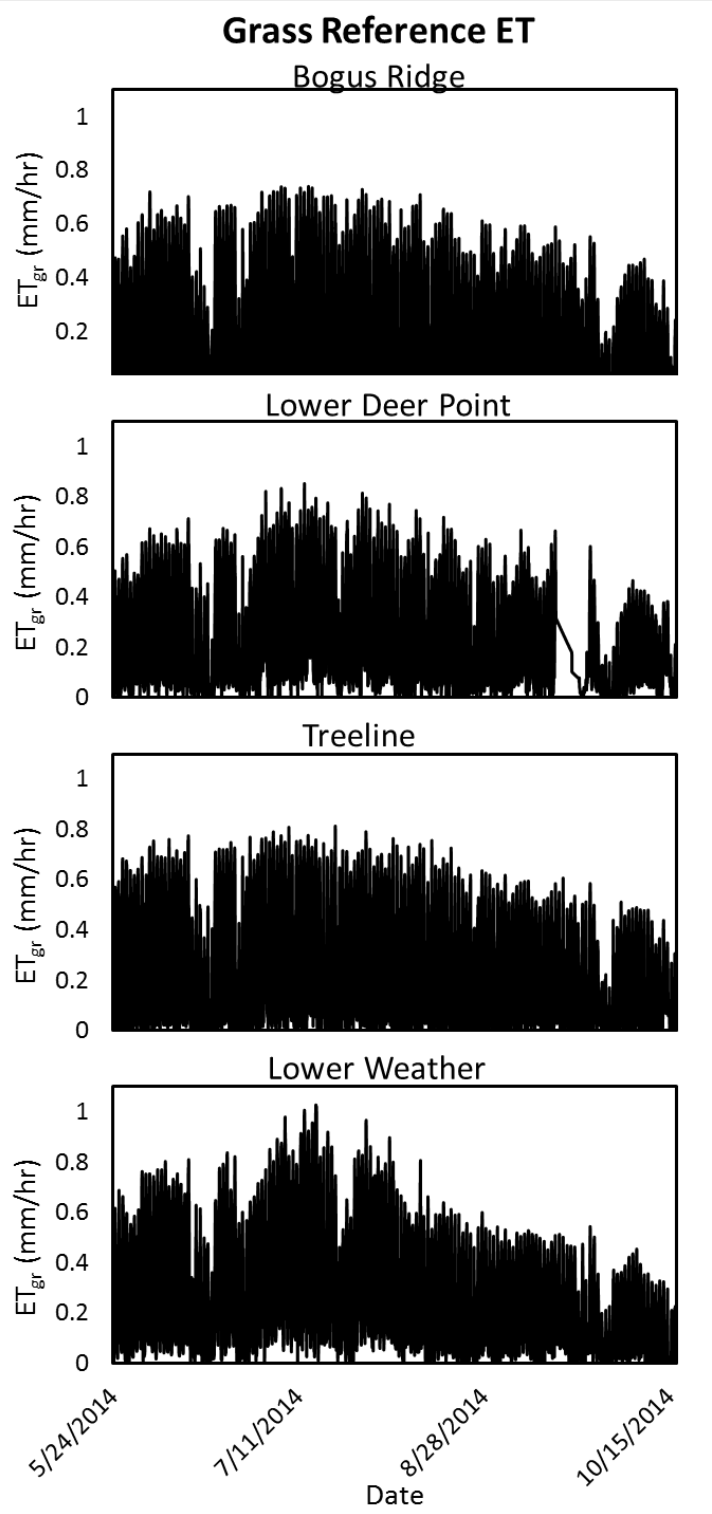

Figure B.12 Hourly grass reference ET (ET_{gr}) for all meteorological site for the entire analysis period. The highest values of ET_{gr} occur at Lower Weather (LW) meteorological site. This data is not moderated for the growing season, so this is technically the potential evapotranspiration for grass reference ET (ET_{gr}).

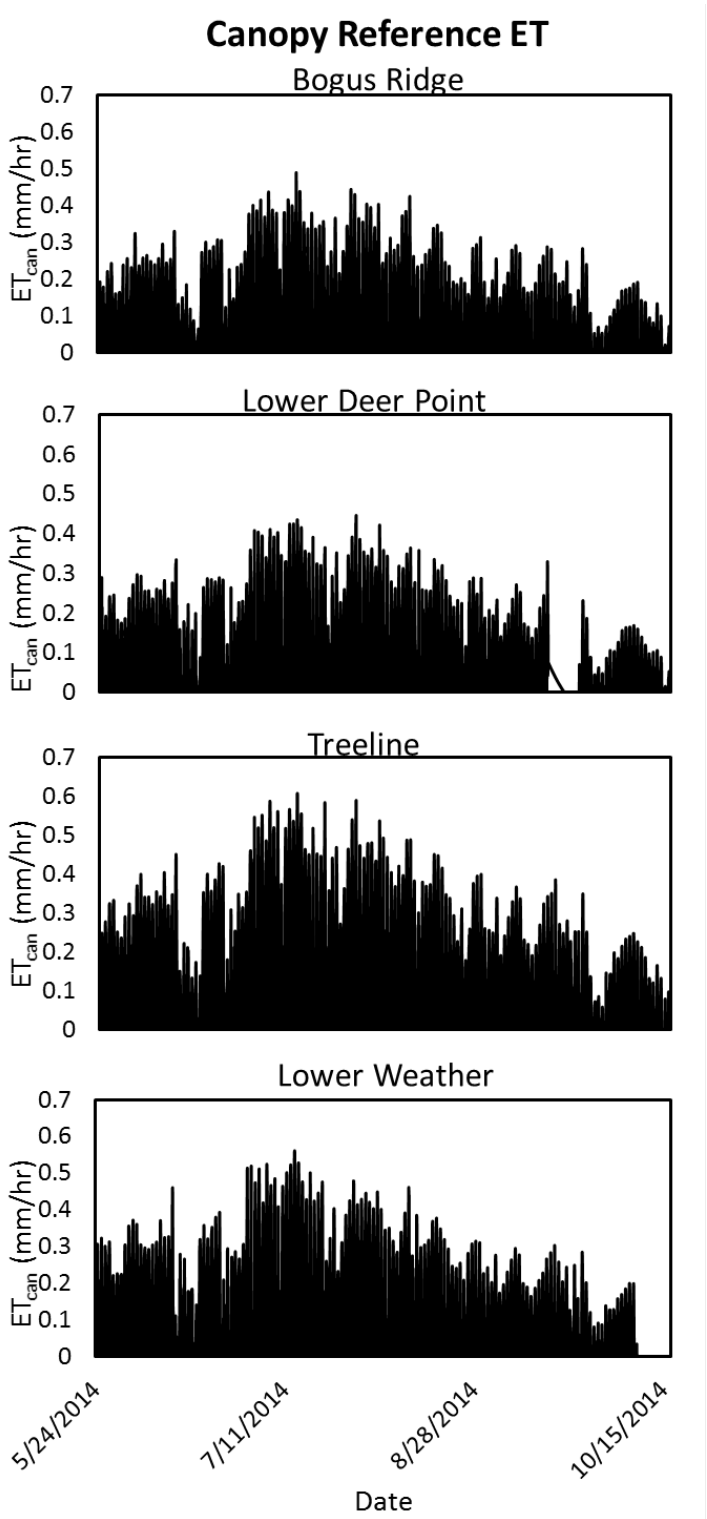

Figure B.13 Hourly canopy reference ET (ET_{can}) for all meteorological site for the entire analysis period. The highest values of ET_{can} occur from Treeline meteorological site.

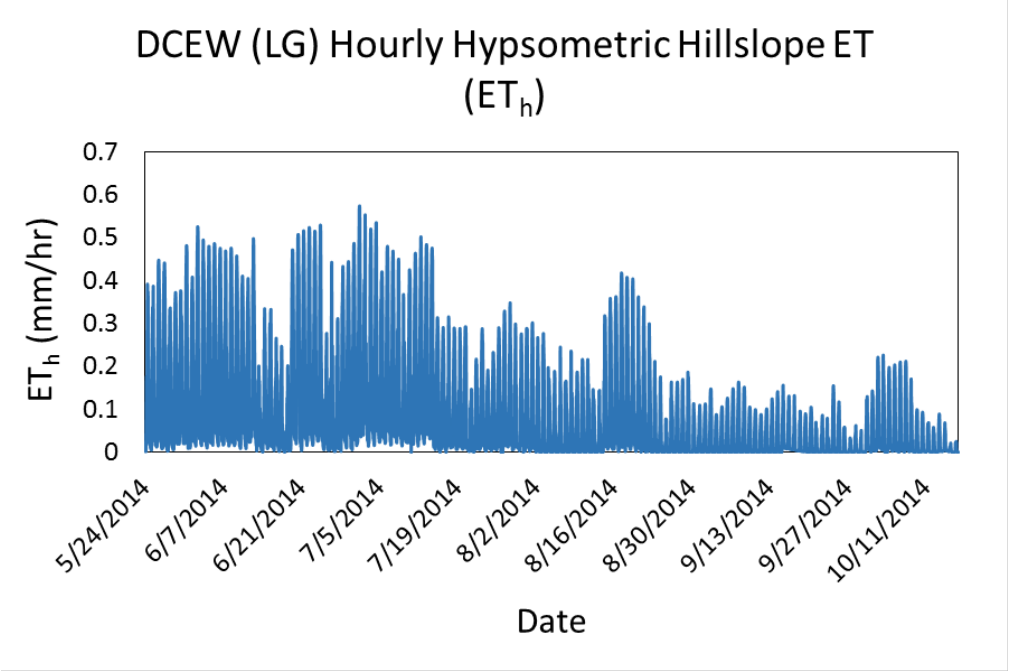

Figure B.14 Hourly hillslope ET (ET_h) estimates calculated using a spatially distributed hypsometric method for the entire DCEW (Lower Gauge).

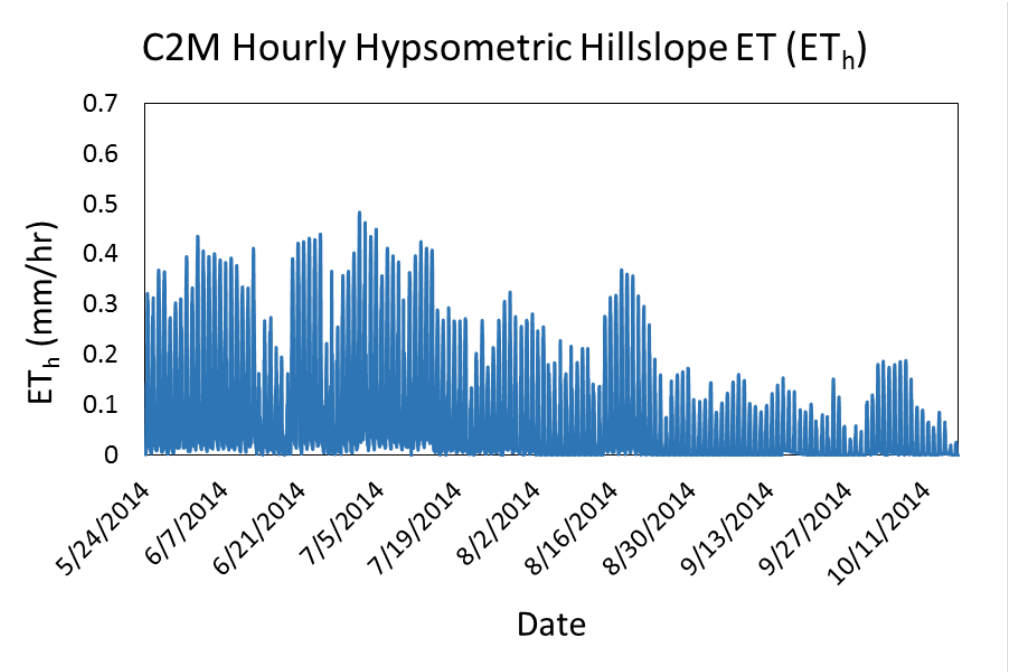

Figure B.15 Hourly hillslope ET (ET_h) estimates calculated using a spatially distributed hypsometric method for the C2M sub-watershed within DCEW.

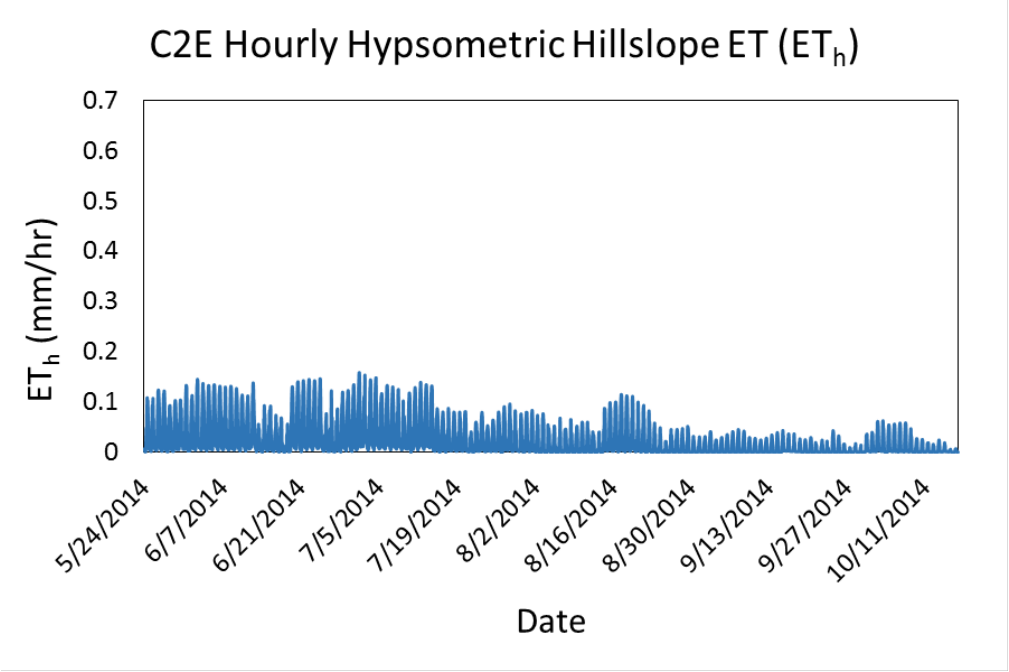

Figure B.16 Hourly hillslope ET (ET_h) estimates calculated using a spatially distributed hypsometric method for the C2E sub-watershed within DCEW.

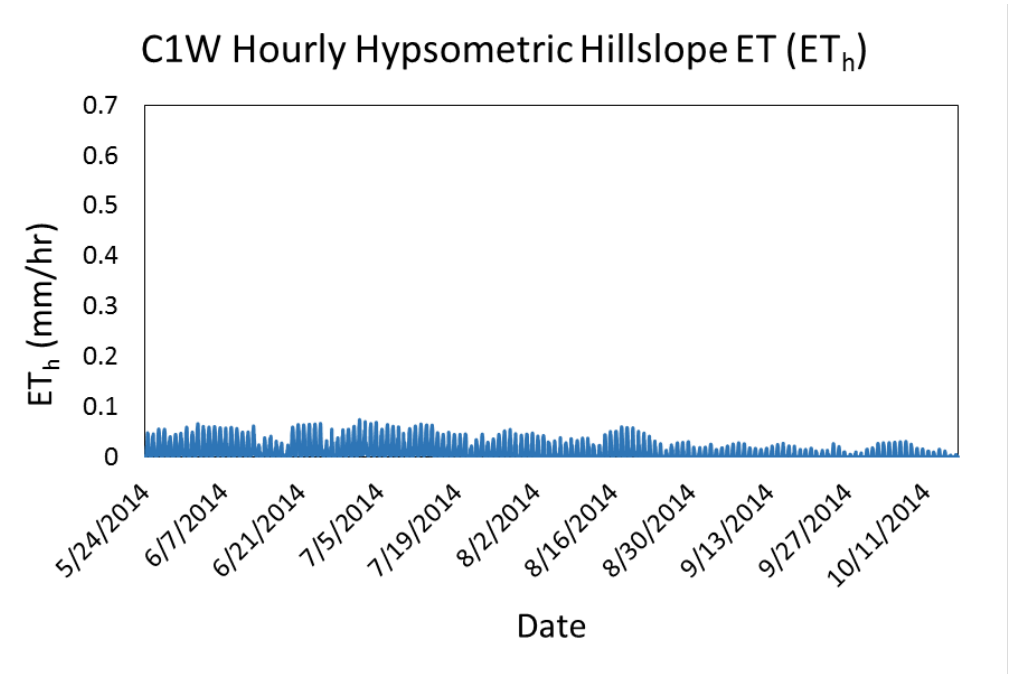

Figure B.17 Hourly hillslope ET (ET_h) estimates calculated using a spatially distributed hypsometric method for the C1W sub-watershed within DCEW.

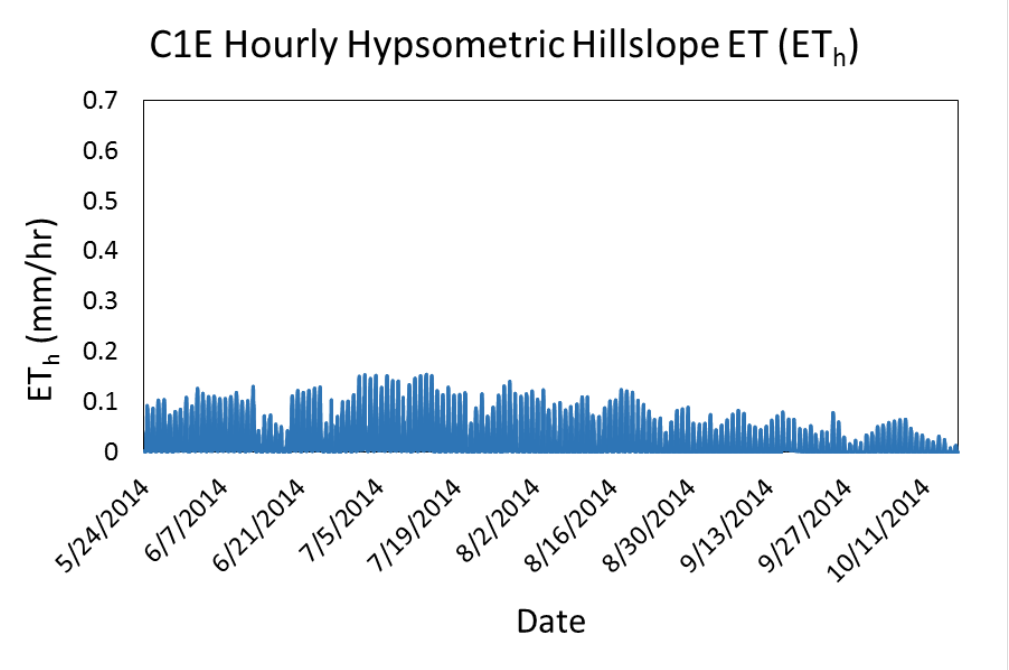

Figure B.18 Hourly hillslope ET (ET_h) estimates calculated using a spatially distributed hypsometric method for the C1E sub-watershed within DCEW.

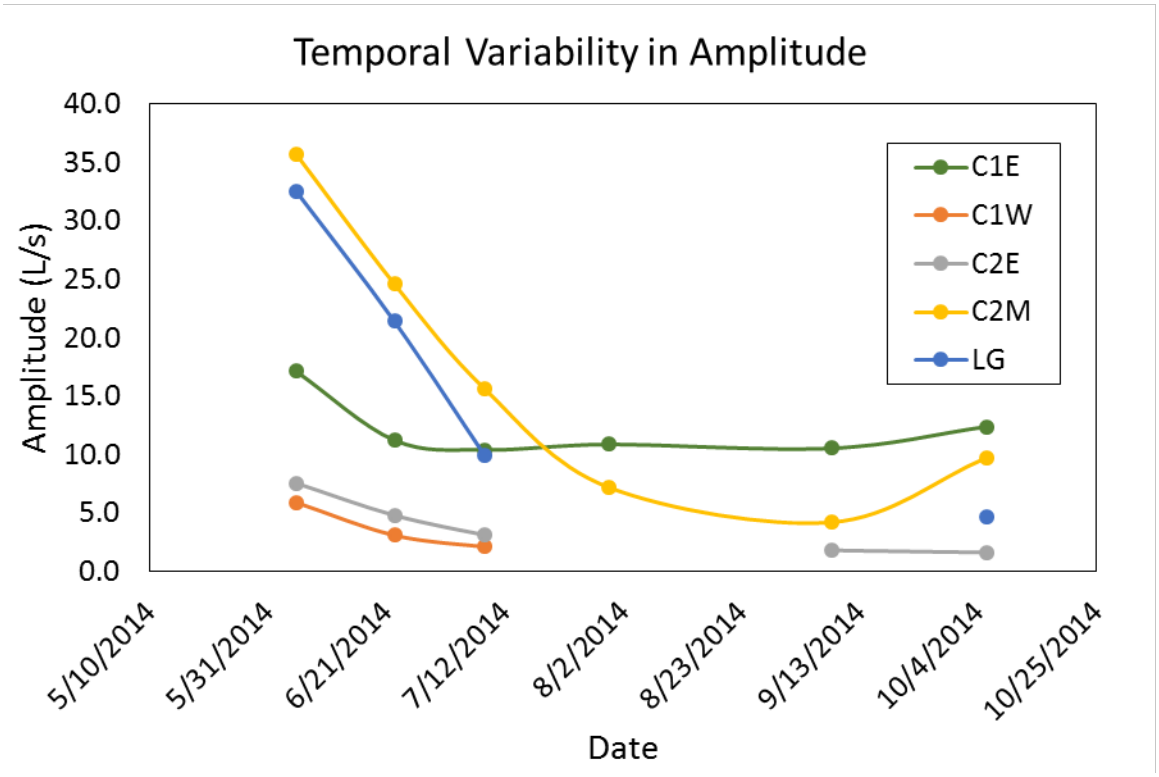

Figure B.19 The average amplitude for precipitation-free periods during the 2014 baseflow period. The data shows a decline in amplitude as baseflow decreases during the summer with a rebound occurring at the end of the summer for most streamflow gauges.

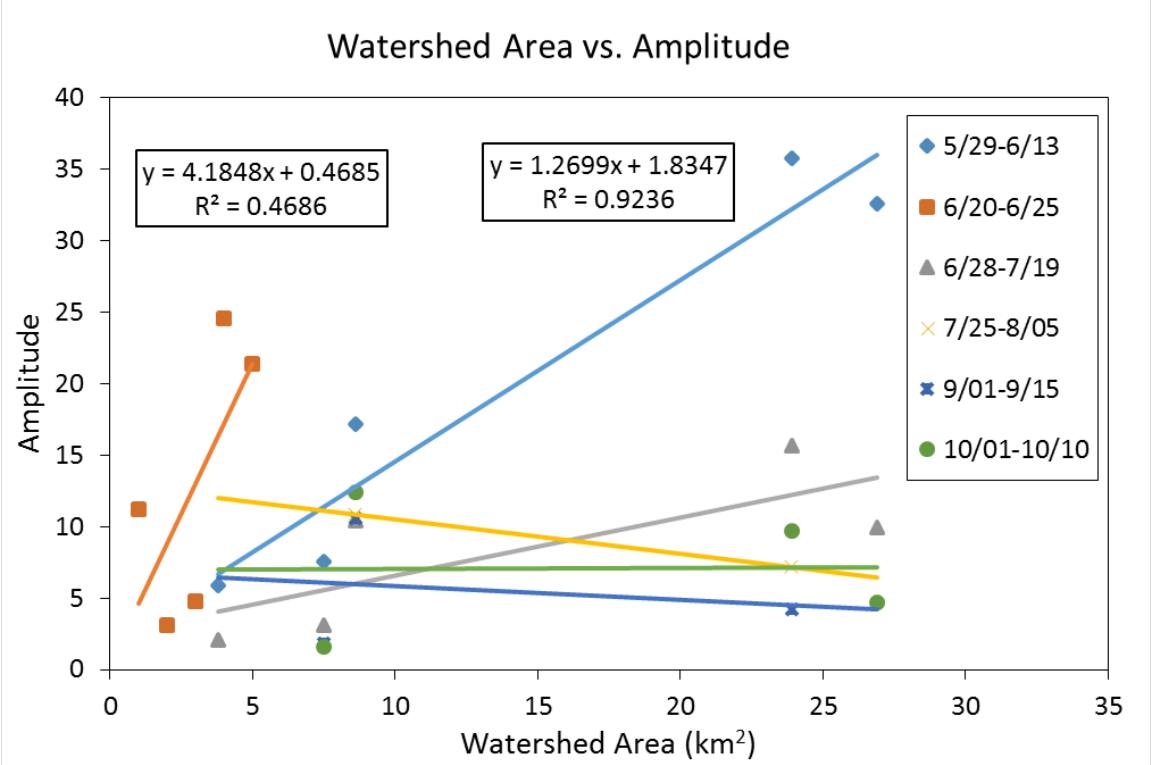

Figure B.20 Plot of watershed area and average amplitudes for the corresponding watershed for each precipitation-free period. Periods with no flow were not plotted. The plot shows that early season amplitudes were highly correlated to watershed area. Only 2 equations are shown because after June 28 a significant relationship no longer existed. R^2 values for periods after June 28 were not significant.

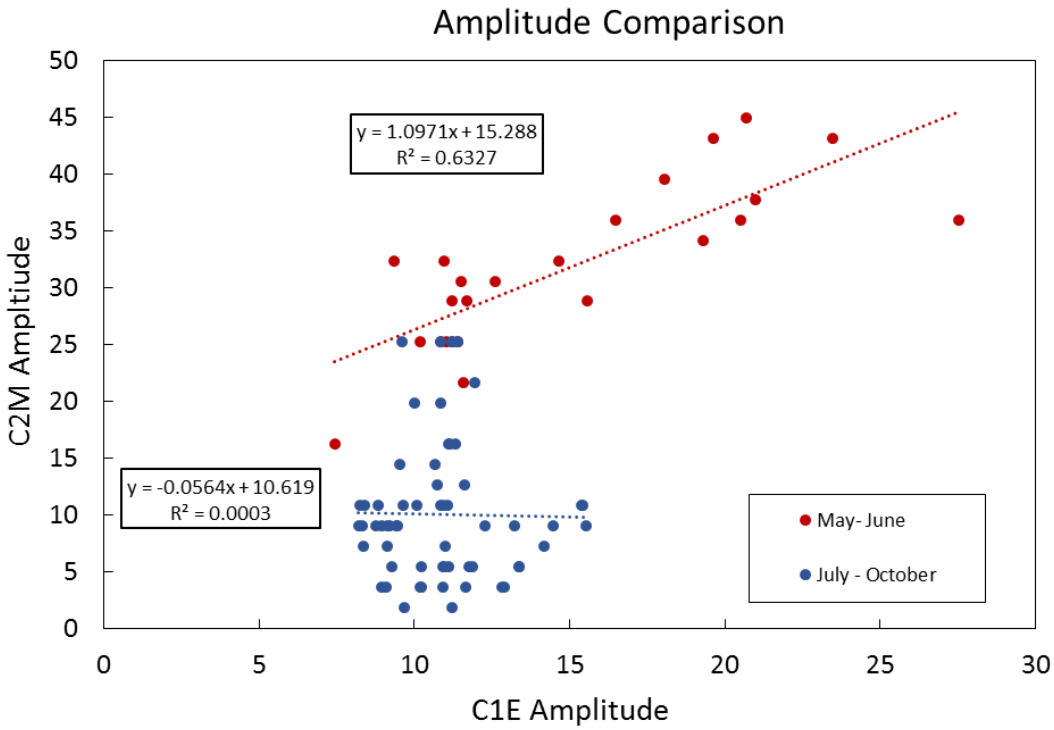

Figure B.21 A scatter plot of Confluence 2 Main and Confluence 1 East split into two separate datasets for the summer of 2014. The early summer (May-June) shows a strong relationship between the two revealing that amplitudes seem to be related in early summer. As the summer progresses (July-October), the data no longer has a relationship showing the possibility of upstream diel signals mixing and having an effect on the downstream streamflow diel signals (C2M)

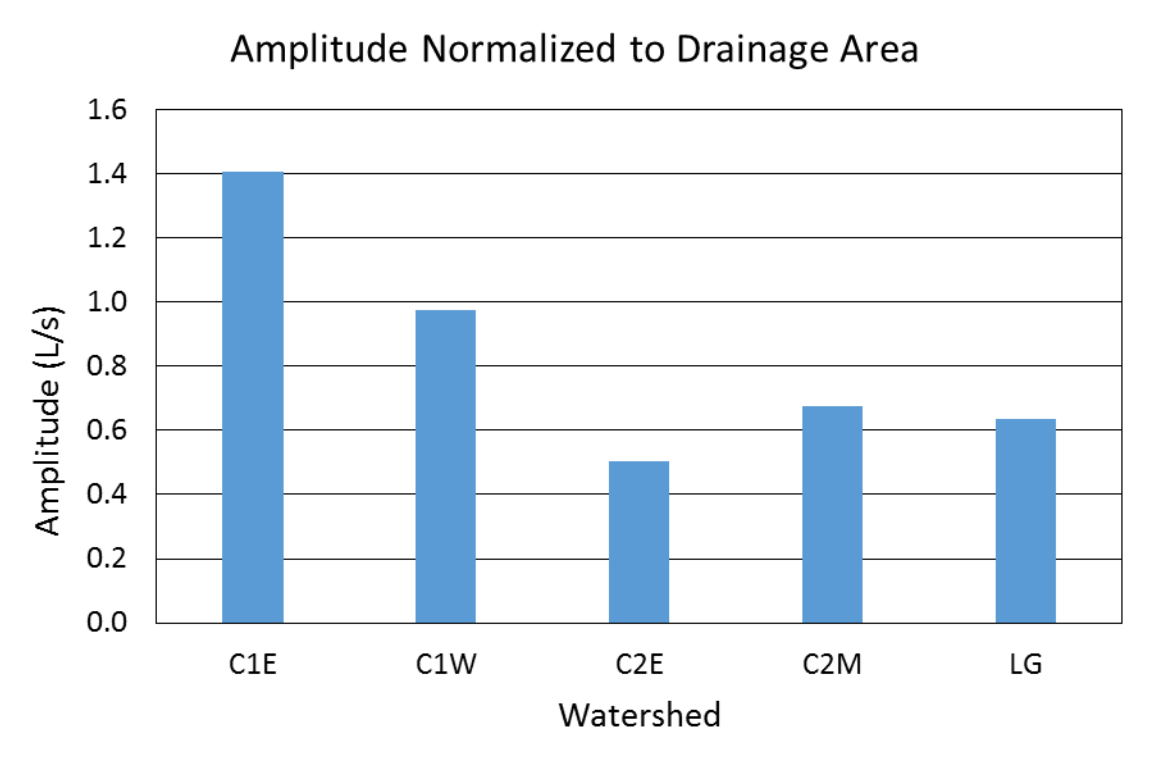

Figure B.22 The amplitude normalized to the sub-watershed drainage area. The data show the upstream outlet points have the largest amplitude. This normalizes the drainage area so that the amount of discharge occurring within the stream is not skewed because of the size of the drainage area. This helps to compare amplitudes to one another and provide details on where the largest amplitudes are occurring within the watershed.

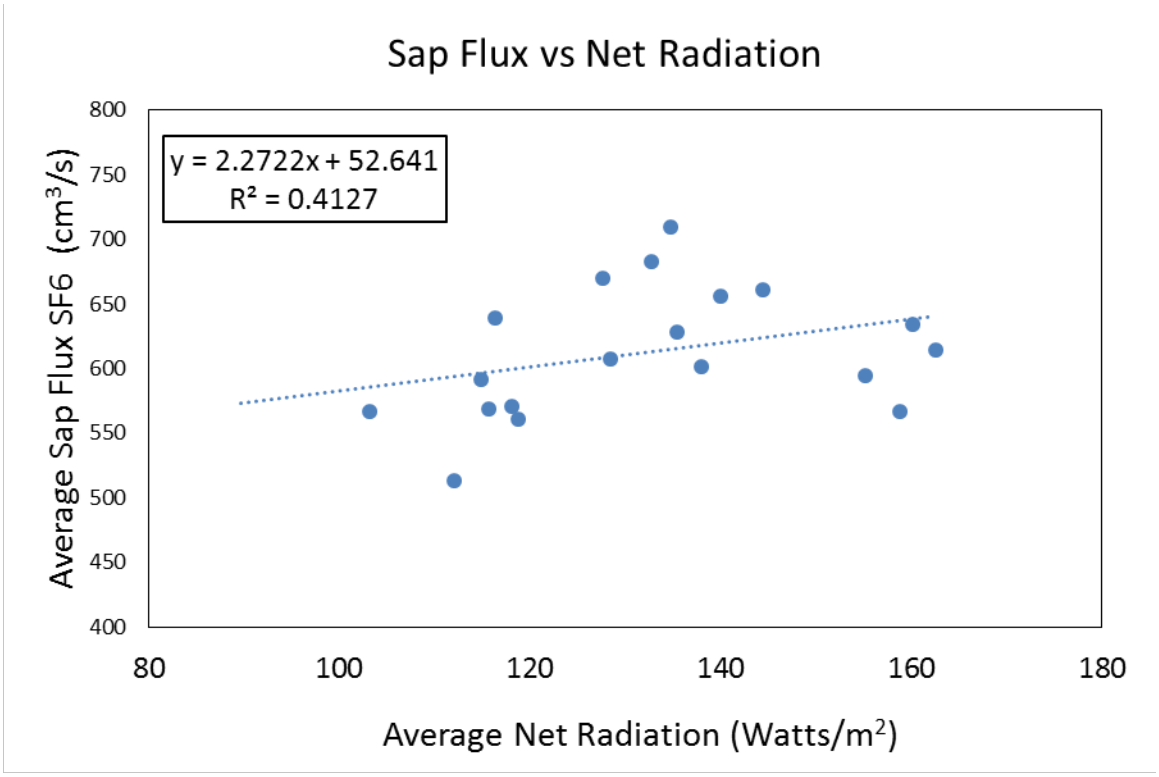

Figure B.23 A scatter plot of average net radiation at C1E and riparian Douglas-fir sap flux for precipitation-free periods during baseflow of 2014. Shows there is a linear relationship between the two measurements

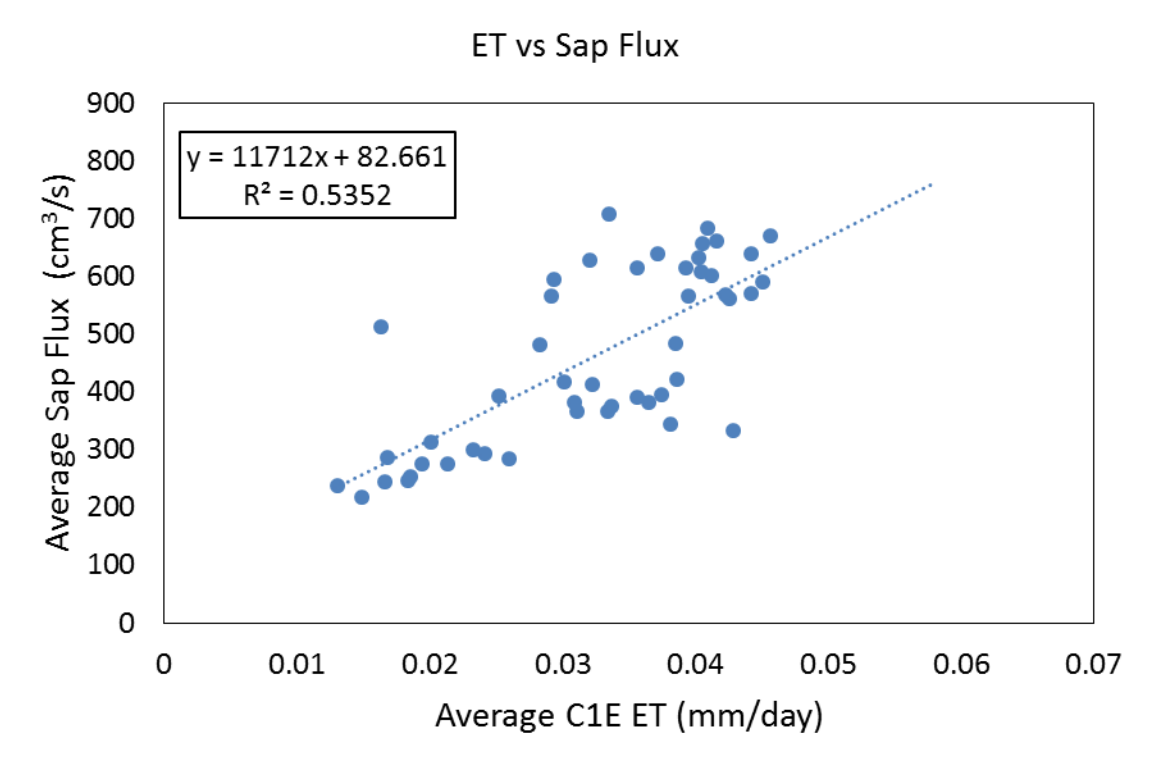

Figure B.24 A scatter plot of average daily sap flux and average actual ET at C1E sub-watershed for precipitation-free periods during baseflow of 2014. Shows there is a positive linear relationship between the two measurements.

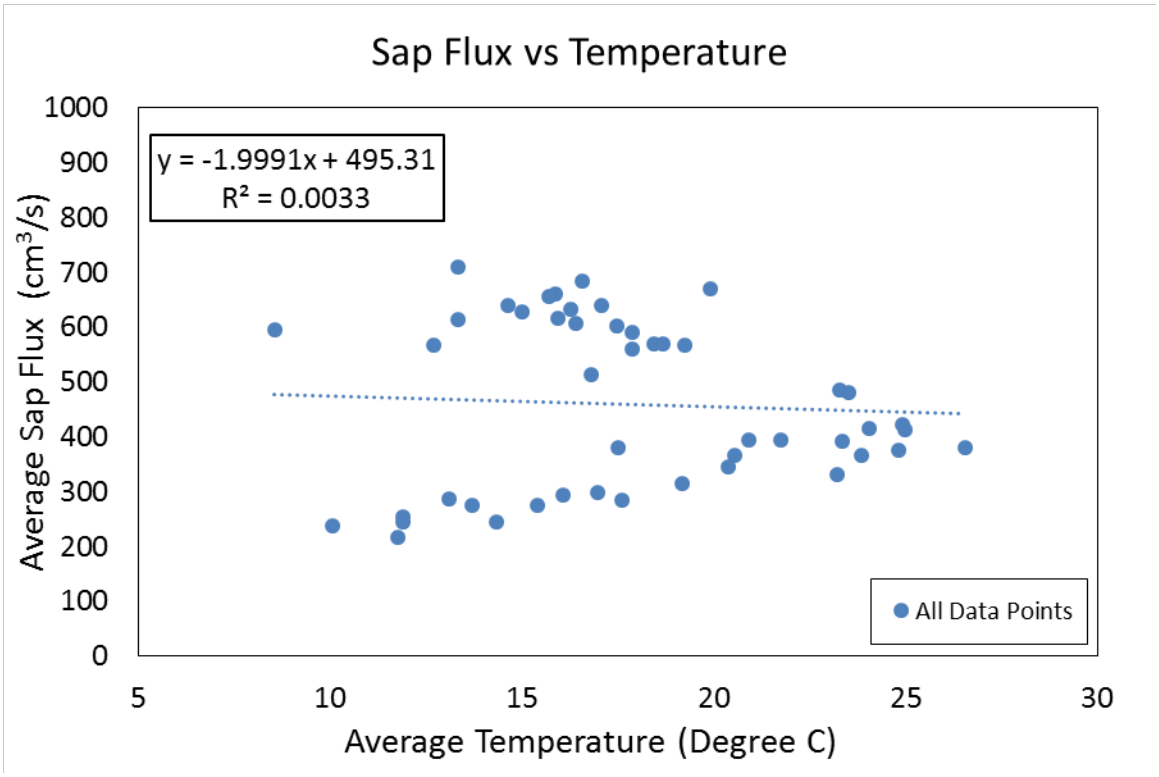

Figure B.25 A scatter plot of average daily sap flux and average daily temperature measurement for all precipitation-free periods during baseflow. Showing no relationship between the two when the whole baseflow is taken into account.

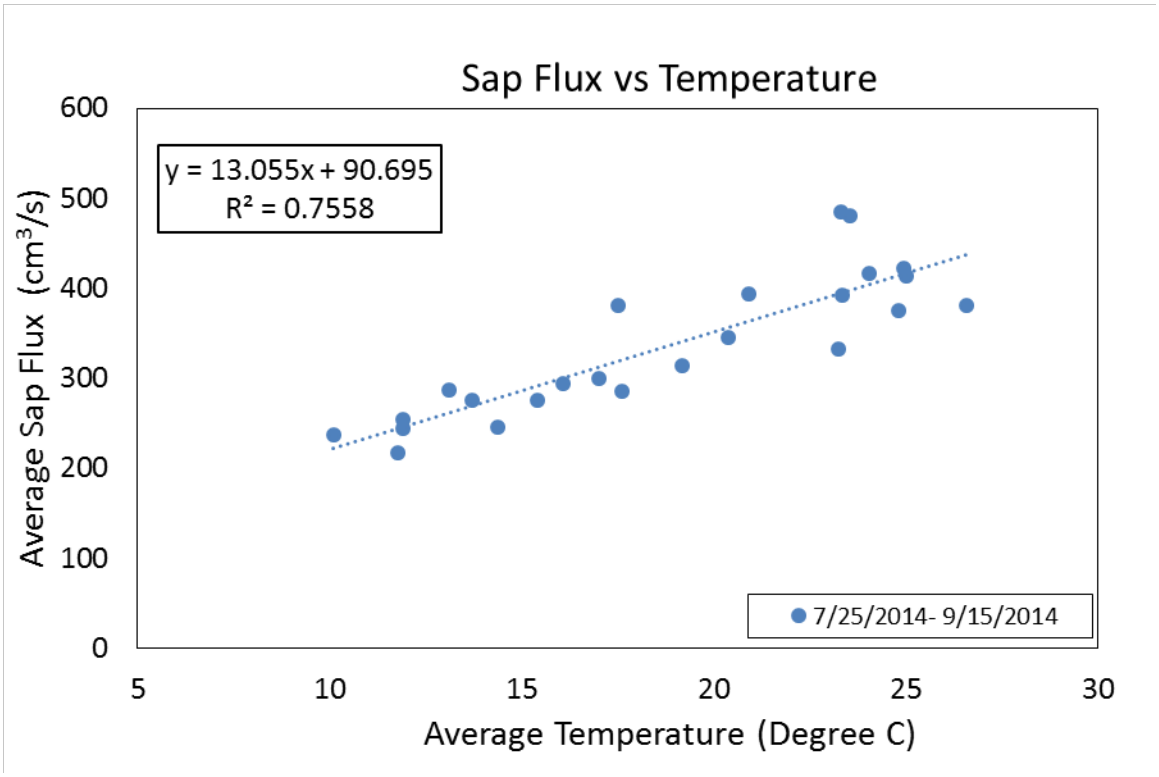

Figure B.26 A scatter plot of average daily sap flux and average daily temperature measurements for precipitation-free periods between July 25th and September 15. The data shows a positive linear relationship and that a decrease in temperature correlates well with a decrease in sap flux.

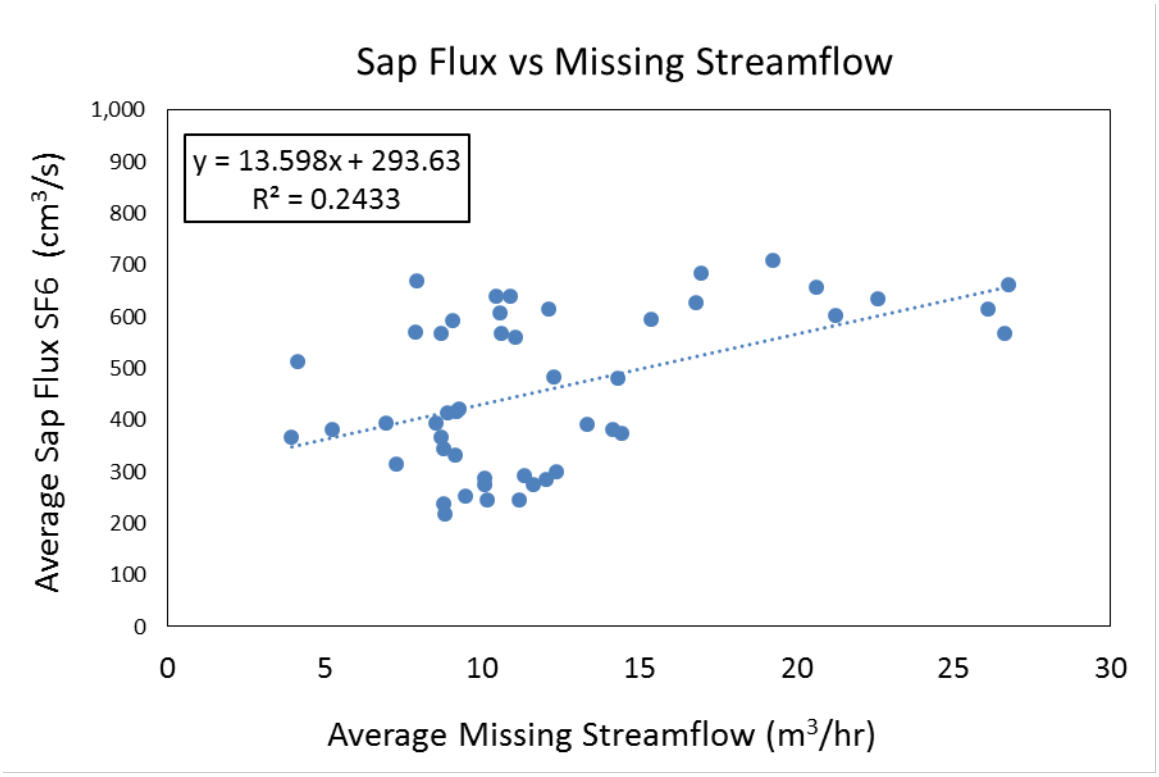

Figure B.27 A scatter plot of average daily sap flux and average daily "missing streamflow" for precipitation-free periods during baseflow of 2014. There is a weak linear relationship showing some correlation between the two.

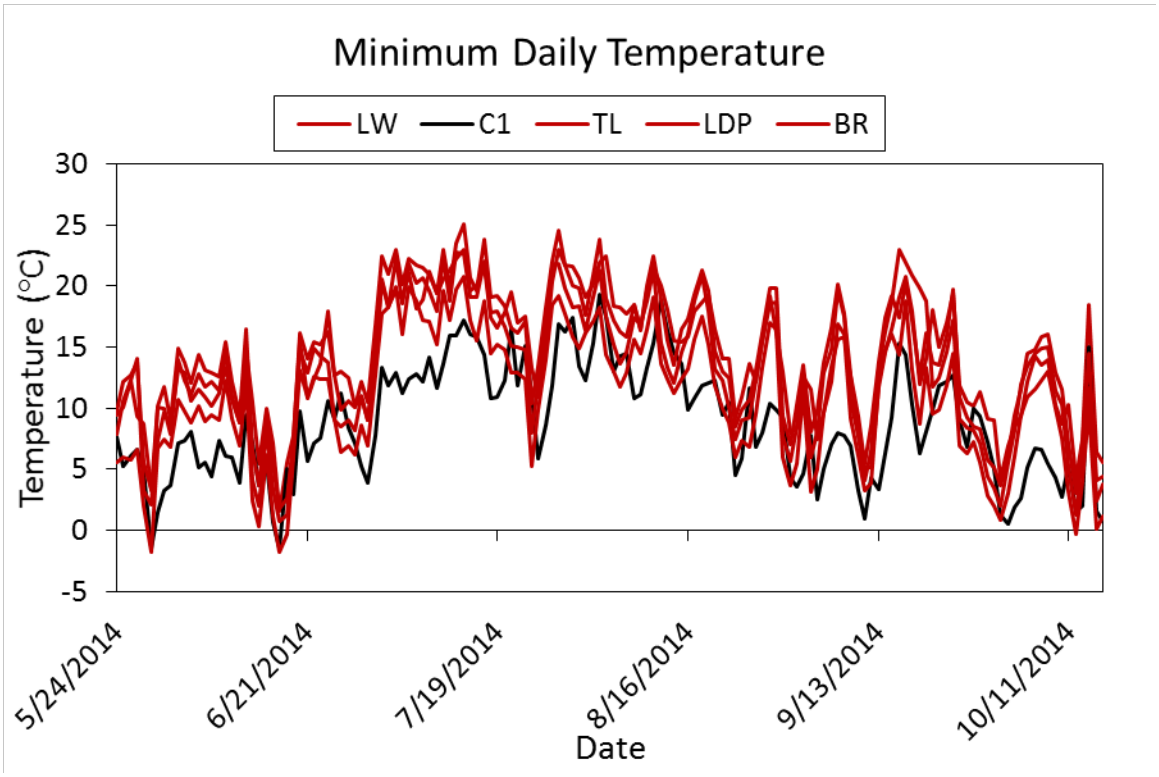

Figure B.28 Plot of average daily minimum temperature for all meteorological stations. The riparian meteorological station (C1) shows the lowest daily temperatures compared to hillslopes. This occurred at night due to cold air drainage.

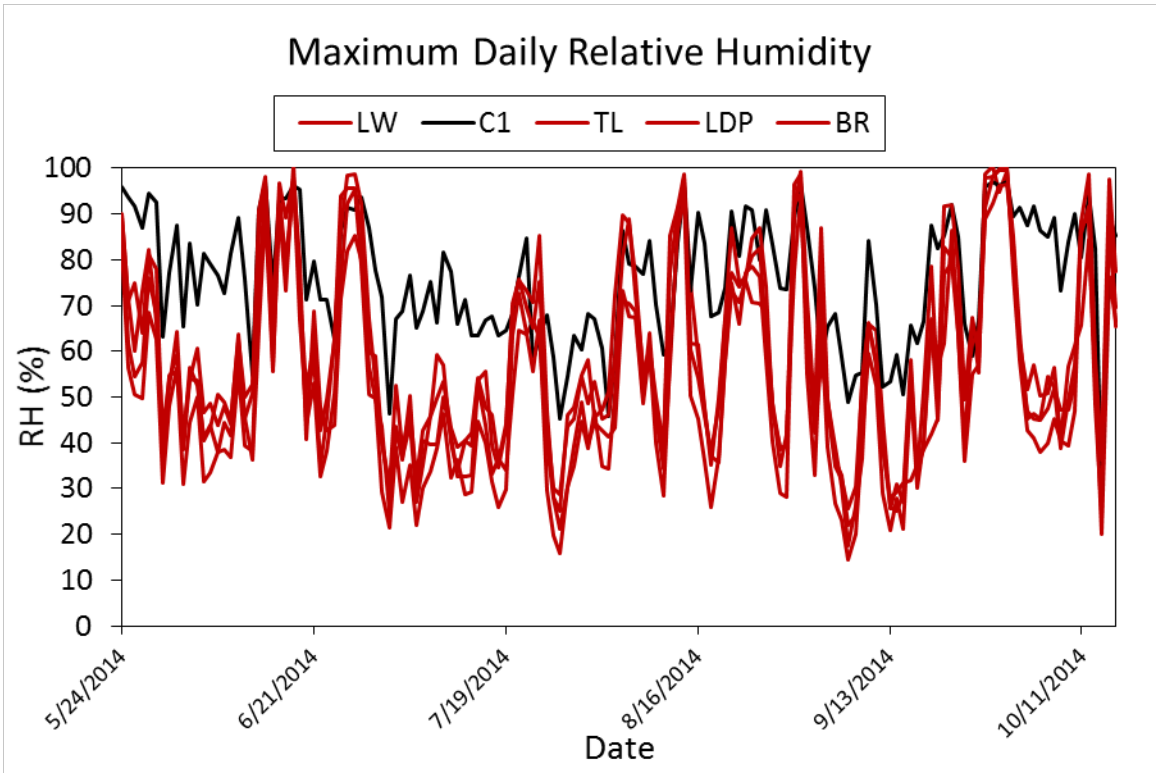

Figure B.29 Plot of average daily maximum relative humidity for all meteorological stations. Riparian meteorological station (C1) shows the highest relative humidity compared to all hillslope meteorological stations. This occurred at night in conjunction with the colder riparian zone temperatures.

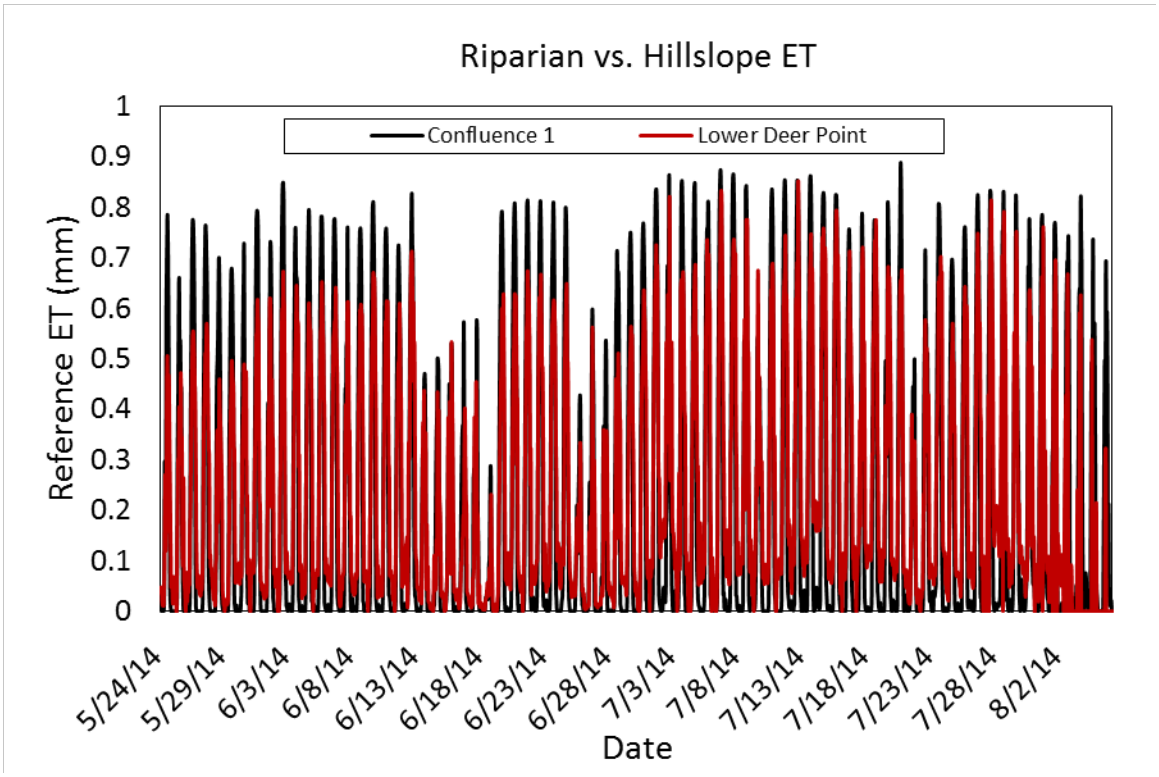

Figure B.30 Plot of Confluence 1 meteorological station reference ET and Lower Deer Point meteorological station reference ET. The nighttime Penman-Monteith Reference ET is lower for riparian meteorological station due to lower temperature and higher relative humidity at night.

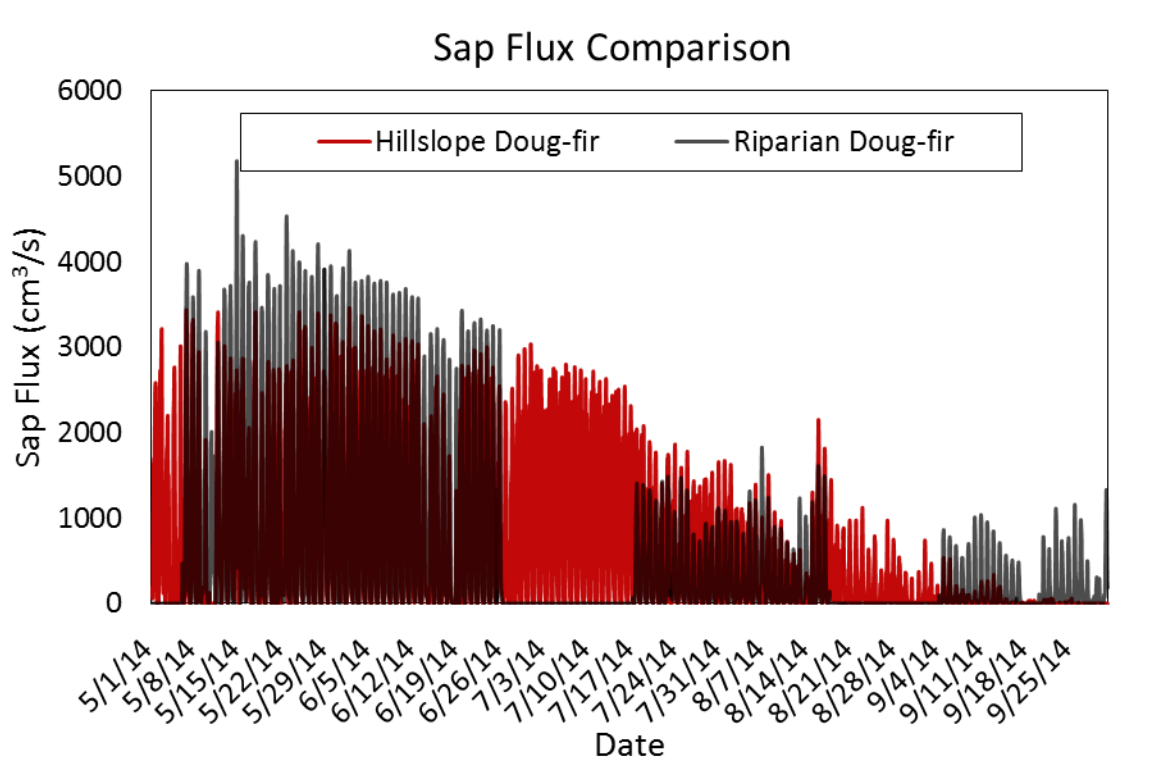

Figure B.31 A comparison of sap flux between riparian and hillslope regions. The trees are the same species (Douglas-fir) and same diameter (approximately 27.5 cm). Hillslope and riparian sap flux are comparable in June and July but differ during August, September, and October. This is thought to be due to the decrease in water availability on the hillslopes affecting transpiration rates of vegetation. Both measurements show a decline in transpiration through the summer. This shows the riparian zone also is affected by a decrease in water availability. Missing data within riparian sap flux in July and August are due to an insufficient power supply to maintain sap flux measurements on an hourly timescale.

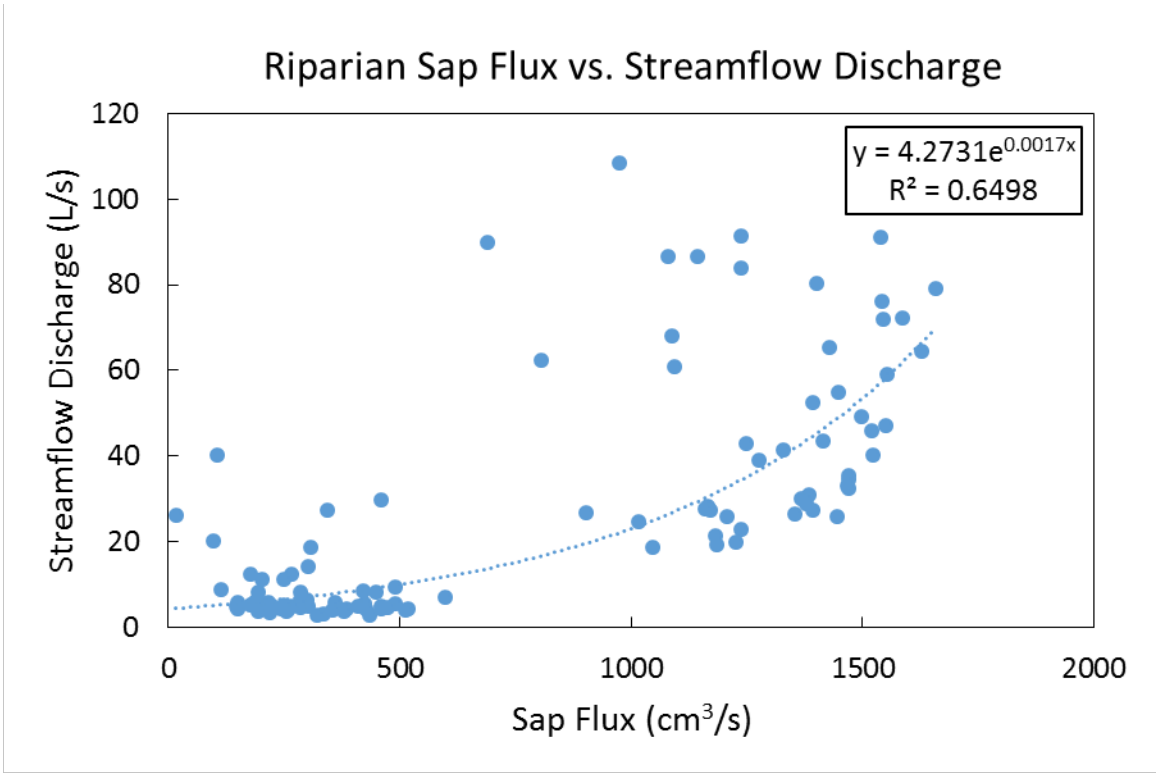

Figure B.32 A scatter plot of the average daily riparian sap flux and the average daily streamflow discharge for precipitation-free periods during summer 2014. The data show a significant exponential relationship between the two. High sap flux usually occurs when streamflow is at high discharge.

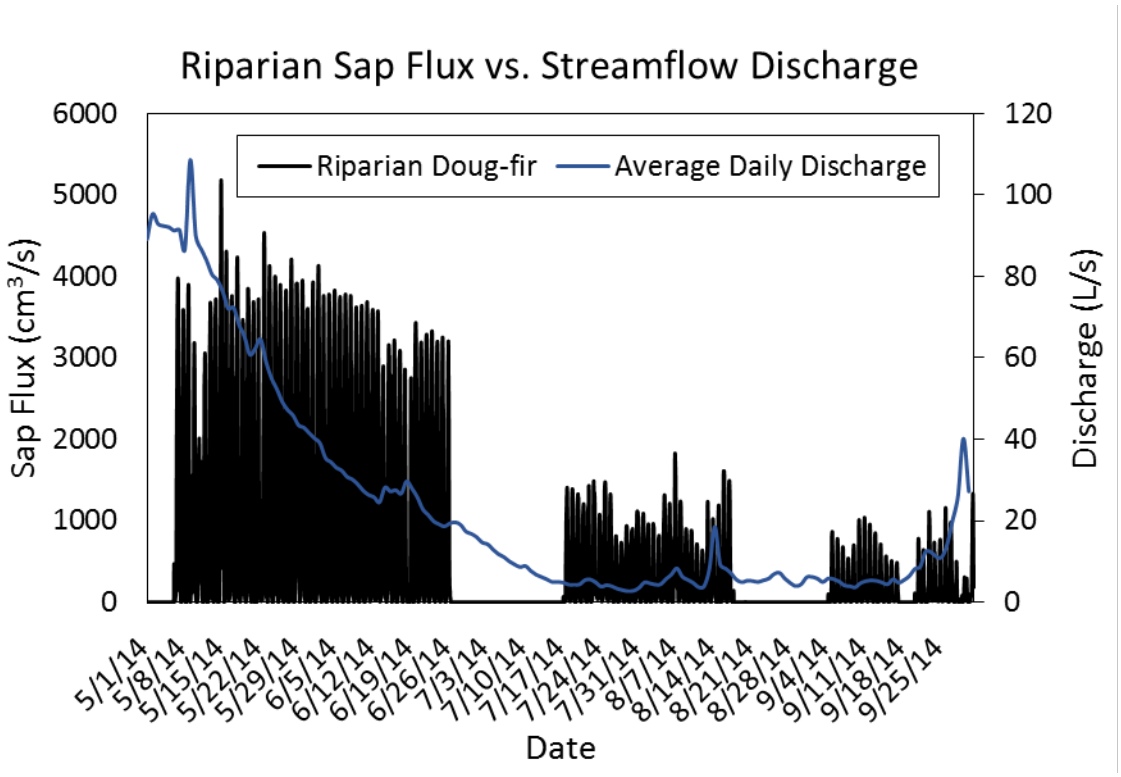

Figure B.33 Plot of riparian sap flux and the average daily streamflow at Confluence 1 East gauge. The plot shows a decrease in streamflow coinciding with a decrease in sap flux within the riparian zone.

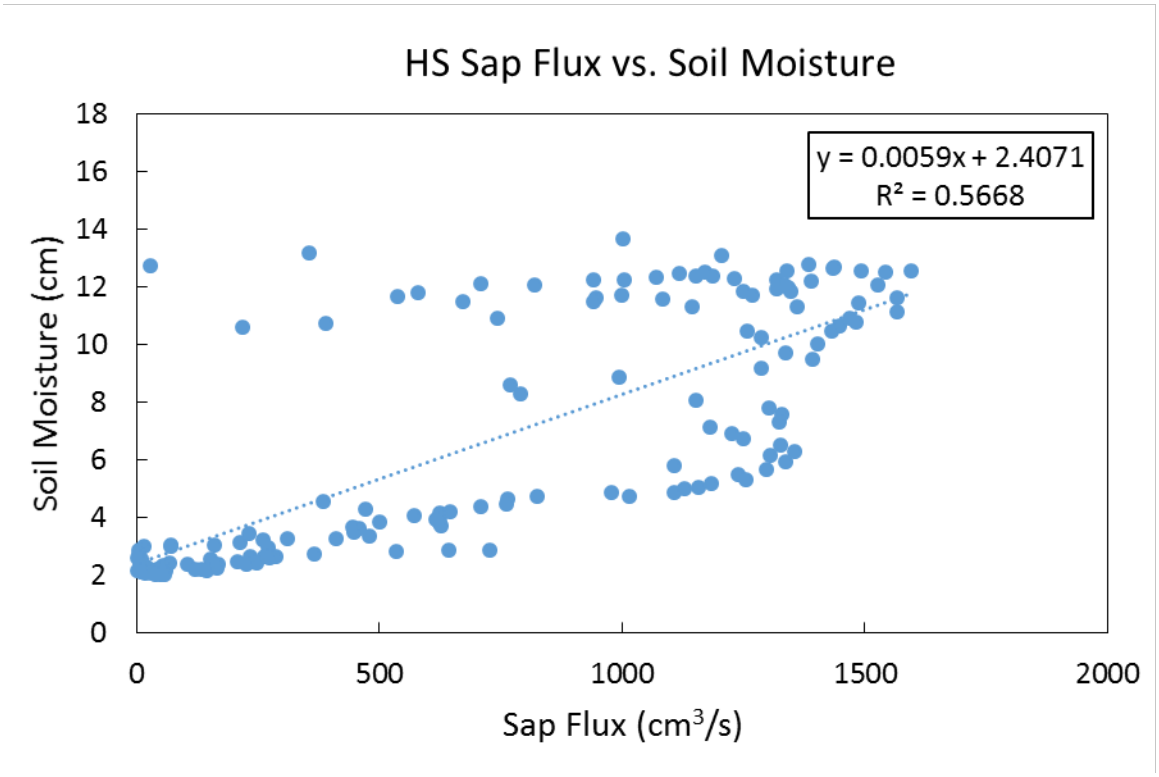

Figure B.34 A scatter plot of hillslope sap flux and soil moisture showing no clear relationship between the two. There is a trend of separate datasets within data.

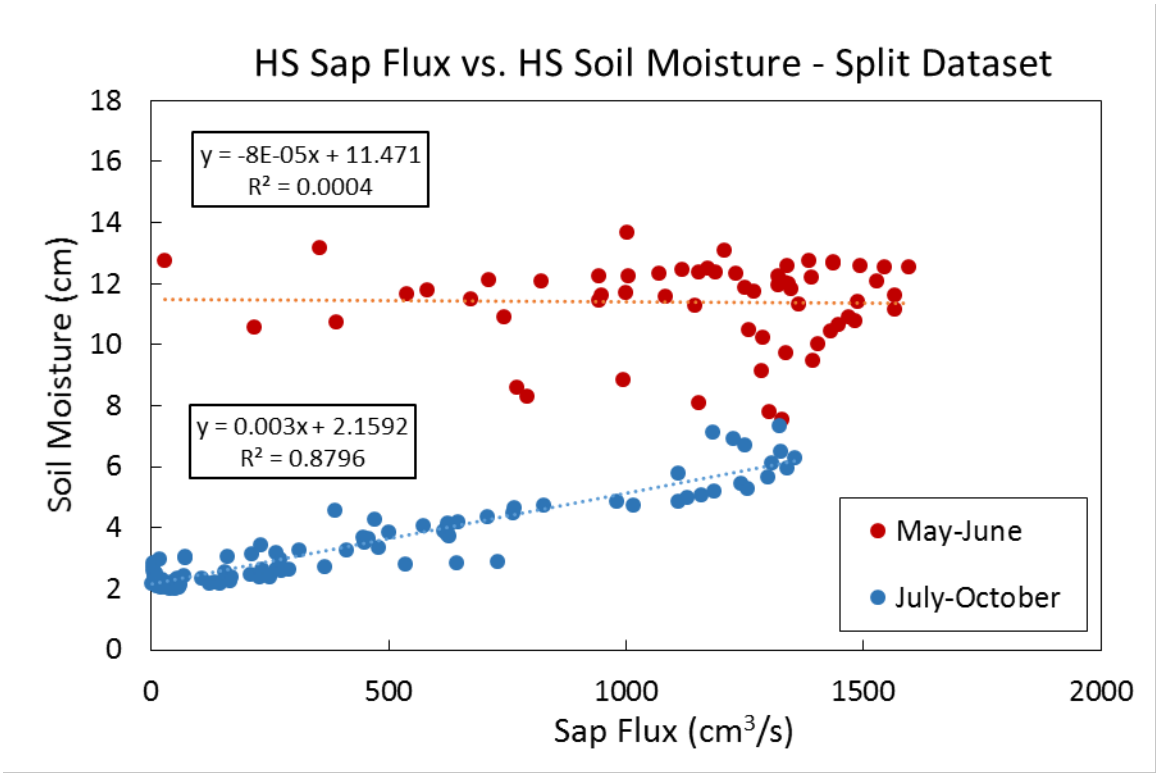

Figure B. 35 Scatter plot of hillslope sap flux and soil moisture showing the early summer compared to the later part of the summer. When the data is split there is a clear linear relationship between sap flux and soil moisture from July to October. Sap flux is low when there is little soil moisture present within the soil profile.

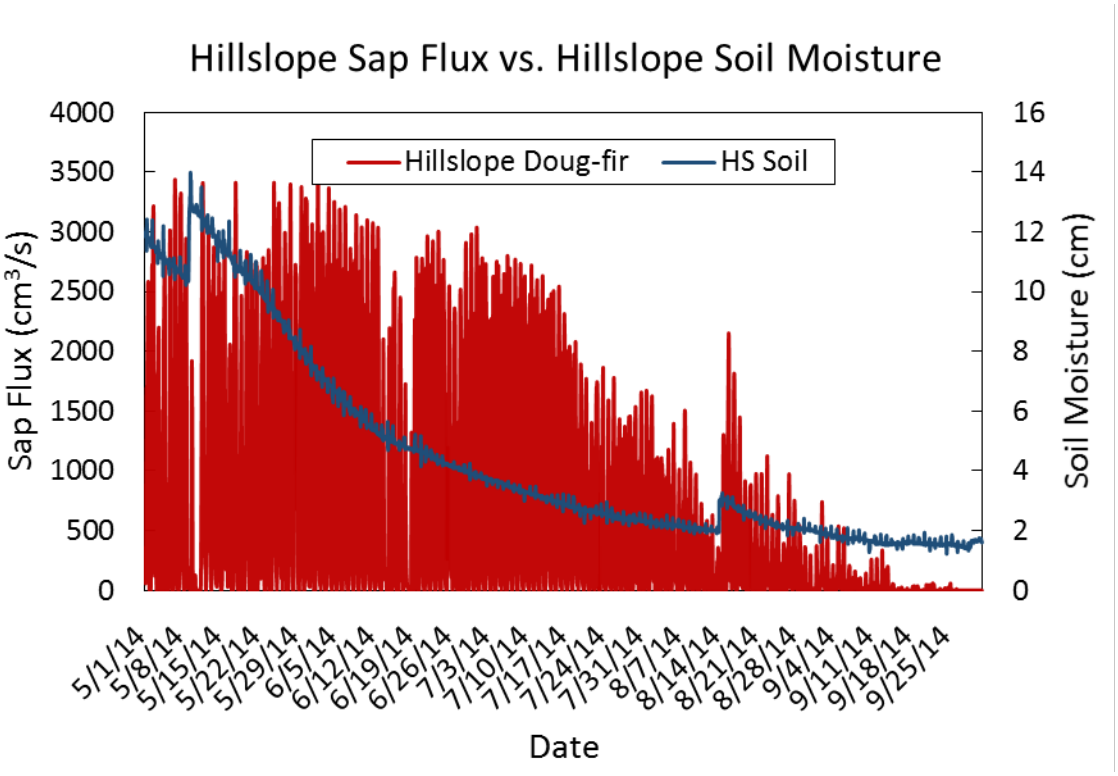

Figure B.36 Plot of hillslope sap flux and adjacent hillslope soil moisture. Shows a decline in both sap flux and soil moisture with responses to rain events late in the summer around August 20th, 2014.

APPENDIX C

Growing Season

The figures do show that there are responses to rain events within the soil profile that can allow ET to occur within the model after the results end of growing season. This occurs particularly often at the Bogus Ridge soil moisture site, which shows multiple large responses to precipitation inputs throughout the summer. With those responses, there is an ability for vegetation to transpire the soil moisture within the subsurface, since it is above the threshold for vegetation to extract the water from the soil pores.

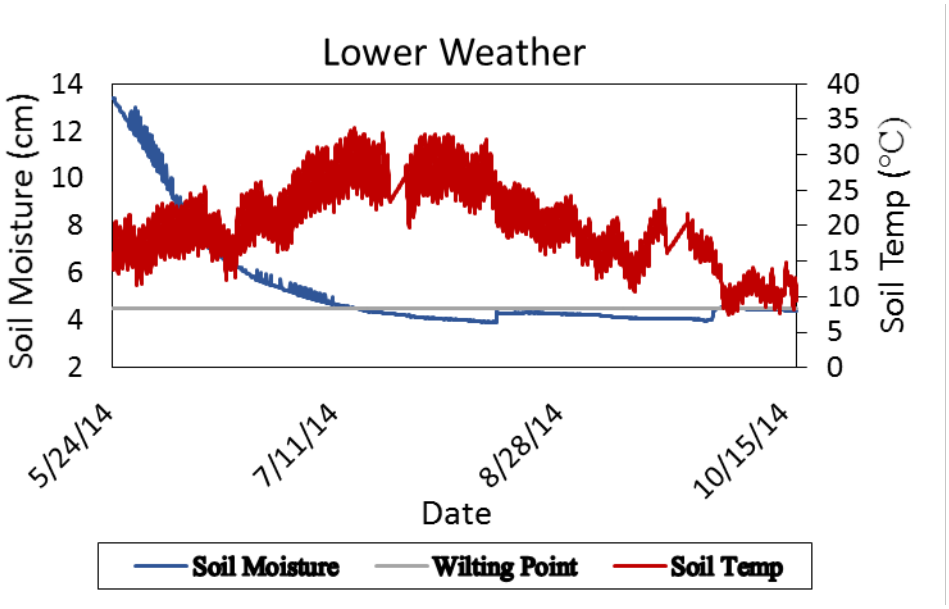

Figure C.1 The soil moisture and soil temperature plot for the Lower Weather meteorological site with the wilting point based on a change in slope of the soil moisture. When soil moisture was above the wilting point, ET was calculated for that meteorological station and when it was below the wilting point ET was set to 0.

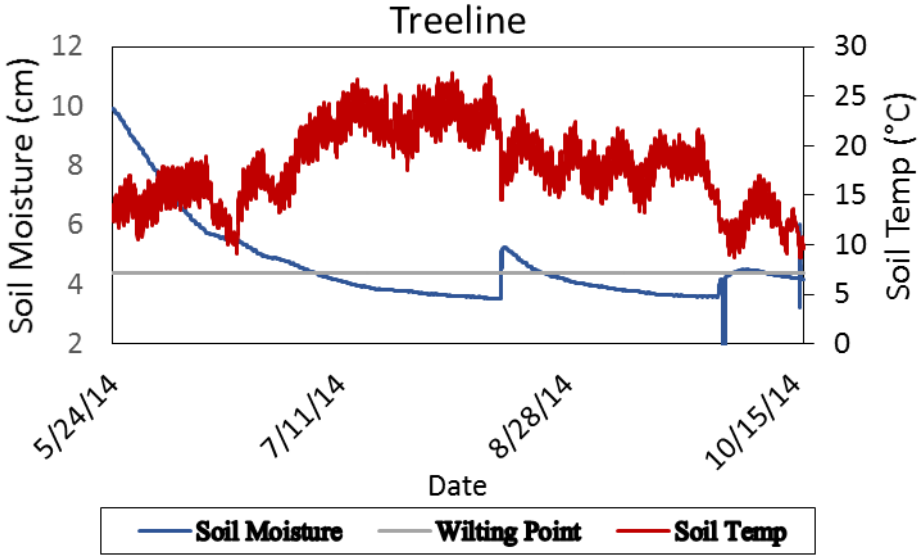

Figure C.2 The soil moisture and soil temperature plot for the Treeline meteorological site with the wilting point based on a change in slope of the soil moisture. When soil moisture was above the wilting point, ET was calculated for that meteorological station and when it was below the wilting point ET was set to 0.

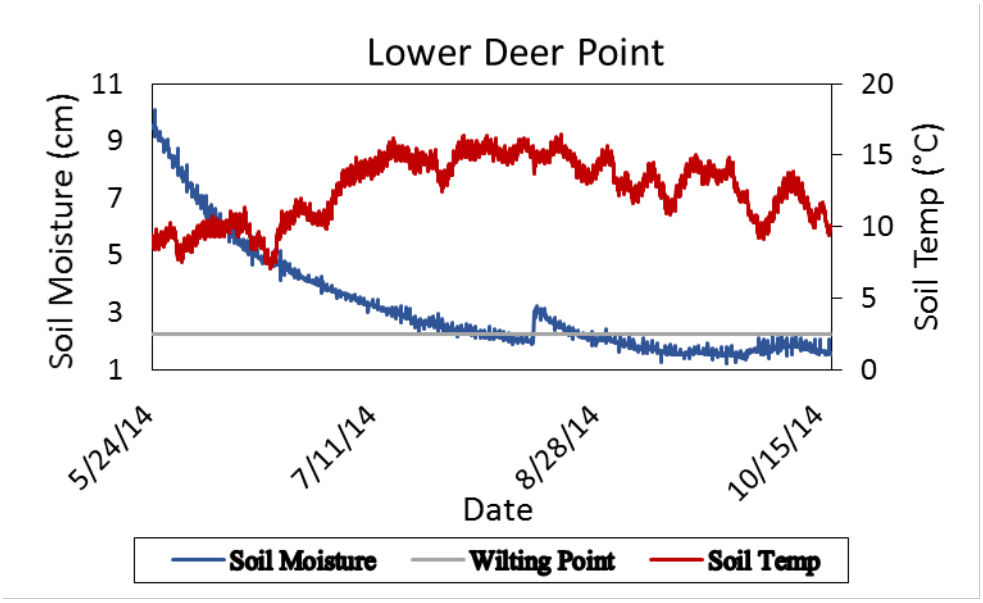

Figure C.3 The soil moisture and soil temperature plot for the Lower Deer Point meteorological site with the wilting point based on a change in slope of the soil moisture. When soil moisture was above the wilting point, ET was calculated for that meteorological station and when it was below the wilting point ET was set to 0.

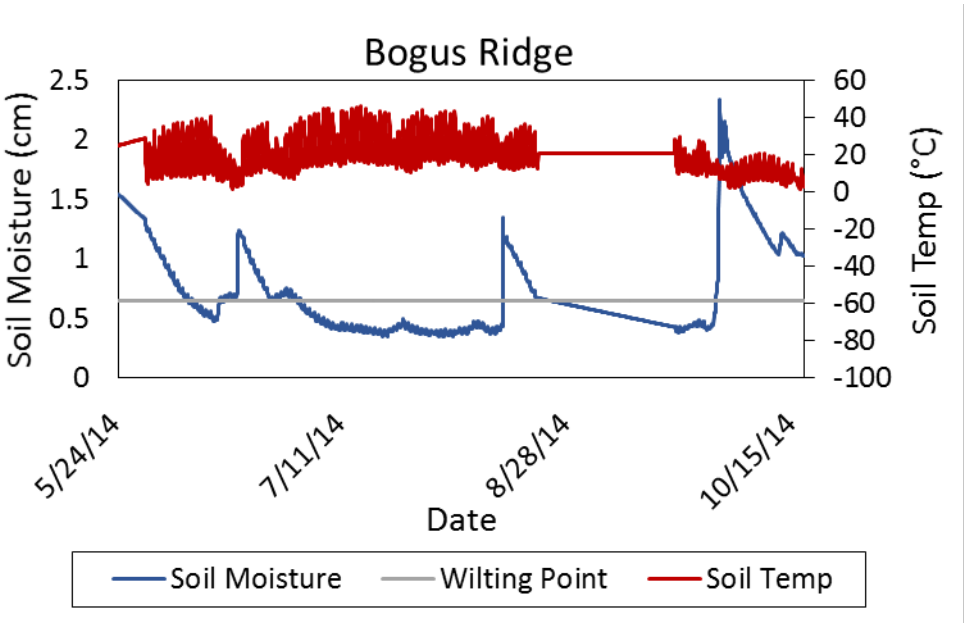

Figure C.4 The soil moisture and soil temperature plot for the Bogus Ridge meteorological site with the wilting point based on a change in slope of the soil moisture. When soil moisture was above the wilting point, ET was calculated for that meteorological station and when it was below the wilting point ET was set to 0.

APPENDIX D

Evapotranspiration Elevation Relationship

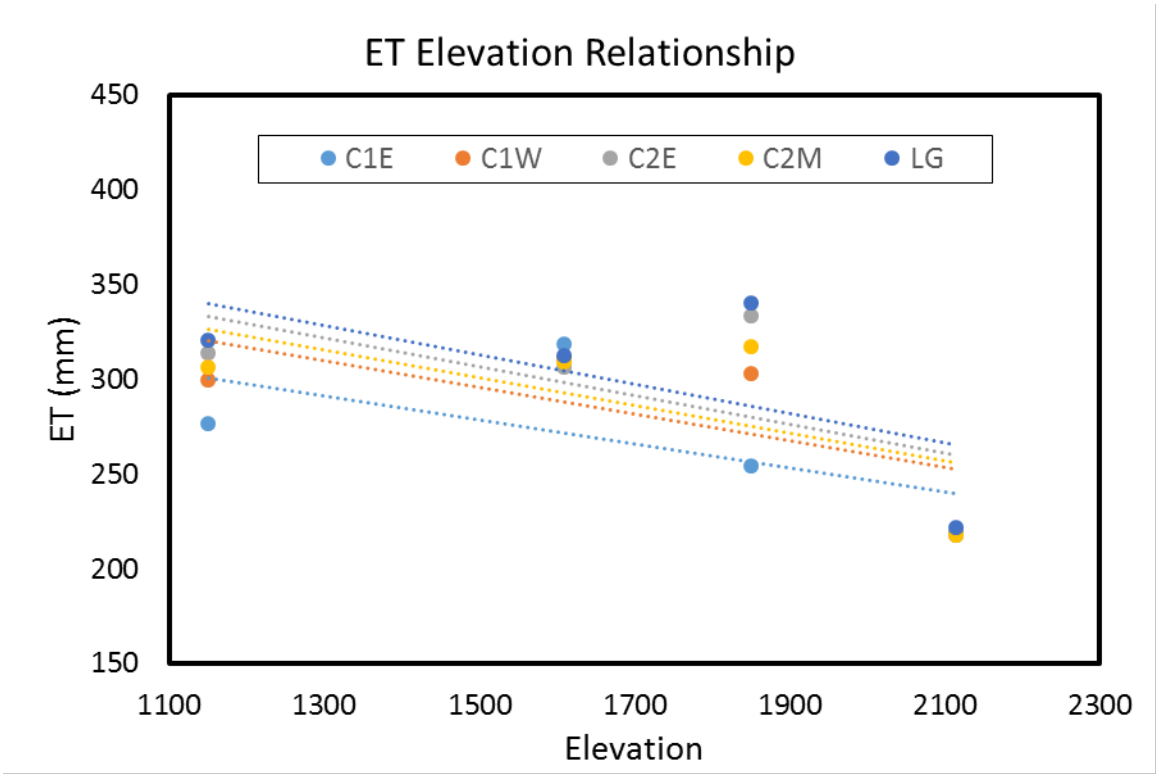

Figure D.1 Shows the ET_v values for each watershed at each meteorological site. ET_{gr} was moderated for growing season and ET_{gr} and ET_{can} were weighted based on vegetation cover.

APPENDIX E

Missing Streamflow Calculations

Table E.1 Confluence 1 East Daily Missing Streamflow

Date	Missing Streamflow (m^3/day)	Date	Missing Streamflow (m^3/day)
5/29/2014	370	7/18/2014	205
5/30/2014	639	7/19/2014	95
5/31/2014	626	7/25/2014	126
6/1/2014	462	7/26/2014	211
6/2/2014	510	7/27/2014	219
6/3/2014	407	7/28/2014	223
6/4/2014	543	7/29/2014	214
6/5/2014	642	7/30/2014	221
6/6/2014	495	7/31/2014	295
6/7/2014	403	8/1/2014	321
6/8/2014	254	8/2/2014	347
6/9/2014	251	8/3/2014	340
6/10/2014	291	8/4/2014	344
6/11/2014	262	8/5/2014	167
6/12/2014	190	9/1/2014	127
6/20/2014	189	9/2/2014	252
6/21/2014	266	9/3/2014	244
6/22/2014	209	9/4/2014	227
6/23/2014	218	9/5/2014	242
6/24/2014	255	9/6/2014	273
6/25/2014	100	9/7/2014	289
6/28/2014	141	9/8/2014	297
6/29/2014	240	9/9/2014	268
6/30/2014	214	9/10/2014	244
7/1/2014	209	9/11/2014	211
7/2/2014	237	9/12/2014	212
7/3/2014	239	9/13/2014	243
7/4/2014	247	9/14/2014	280
7/5/2014	198	9/15/2014	175
7/6/2014	226	10/1/2014	100
7/7/2014	238	10/2/2014	224
7/8/2014	213	10/3/2014	262
7/9/2014	215	10/4/2014	286
7/10/2014	205	10/5/2014	336
7/11/2014	246	10/6/2014	399
7/12/2014	230	10/7/2014	416
7/13/2014	231	10/8/2014	385
7/14/2014	222	10/9/2014	385
7/15/2014	237	10/10/2014	259
7/16/2014	216		
7/17/2014	209		

Table E.2 Confluence 1 West Daily Missing Streamflow

Date	Missing Streamflow (m^3/day)
5/29/2014	124
5/30/2014	140
5/31/2014	131
6/1/2014	138
6/2/2014	135
6/3/2014	124
6/4/2014	133
6/5/2014	136
6/6/2014	129
6/7/2014	106
6/8/2014	110
6/9/2014	117
6/10/2014	118
6/11/2014	129
6/12/2014	51
6/20/2014	76
6/21/2014	83
6/22/2014	81
6/23/2014	73
6/24/2014	63
6/25/2014	23

Table E.3 Confluence 2 East Daily Missing Streamflow

Date	Missing Streamflow (m^3/day)	Date	Missing Streamflow (m^3/day)
5/29/2014	278	10/2/2014	18
5/30/2014	178	10/3/2014	25
5/31/2014	160	10/4/2014	25
6/1/2014	176	10/5/2014	32
6/2/2014	142	10/6/2014	37
6/3/2014	134	10/7/2014	41
6/4/2014	158	10/8/2014	79
6/5/2014	166	10/9/2014	64
6/6/2014	147	10/10/2014	21
6/7/2014	157		
6/8/2014	170		
6/9/2014	151		
6/10/2014	161		
6/11/2014	153		
6/12/2014	86		
6/20/2014	114		
6/21/2014	127		
6/22/2014	118		
6/23/2014	134		
6/24/2014	131		
6/25/2014	14		
6/28/2014	49		
6/29/2014	54		
6/30/2014	34		
6/28/2014	102		
6/29/2014	131		
6/30/2014	140		
7/1/2014	114		
7/2/2014	54		
7/3/2014	37		
7/4/2014	43		
7/5/2014	50		
7/6/2014	61		
7/7/2014	65		
7/8/2014	38		
9/12/2014	30		
9/13/2014	49		
9/14/2014	63		
9/15/2014	23		
10/1/2014	0		

Table E.4 Confluence 2 Main Daily Missing Streamflow

Date	Missing Streamflow (m^3/day)	Date	Missing Streamflow (m^3/day)
5/29/2014	898	7/17/2014	211
5/30/2014	1008	7/18/2014	248
5/31/2014	986	7/19/2014	151
6/1/2014	876	7/25/2014	202
6/2/2014	815	7/26/2014	224
6/3/2014	848	7/27/2014	207
6/4/2014	853	7/28/2014	257
6/5/2014	869	7/29/2014	194
6/6/2014	838	7/30/2014	237
6/7/2014	767	7/31/2014	154
6/8/2014	768	8/1/2014	132
6/9/2014	777	8/2/2014	121
6/10/2014	733	8/3/2014	98
6/11/2014	672	8/4/2014	142
6/12/2014	364	8/5/2014	106
6/20/2014	593	9/1/2014	87
6/21/2014	697	9/2/2014	122
6/22/2014	634	9/3/2014	85
6/23/2014	604	9/4/2014	67
6/24/2014	550	9/5/2014	98
6/25/2014	225	9/6/2014	79
6/28/2014	495	9/7/2014	89
6/29/2014	600	9/8/2014	93
6/30/2014	619	9/9/2014	128
7/1/2014	500	9/10/2014	86
7/2/2014	642	9/11/2014	96
7/3/2014	538	9/12/2014	69
7/4/2014	551	9/13/2014	73
7/5/2014	508	9/14/2014	99
7/6/2014	454	9/15/2014	64
7/7/2014	477	10/1/2014	161
7/8/2014	423	10/2/2014	215
7/9/2014	326	10/3/2014	202
7/10/2014	387	10/4/2014	228
7/11/2014	357	10/5/2014	223
7/12/2014	311	10/6/2014	220
7/13/2014	318	10/7/2014	146
7/14/2014	328	10/8/2014	196
7/15/2014	300	10/9/2014	282
7/16/2014	275	10/10/2014	186

Table E.5 Lower Gauge Daily Missing Streamflow

Date	Missing Streamflow (m^3/day)	Date	Missing Streamflow (m^3/day)
5/29/2014	547	7/17/2014	12
5/30/2014	767	7/18/2014	12
5/31/2014	825	7/19/2014	9
6/1/2014	747	10/1/2014	74
6/2/2014	736	10/2/2014	148
6/3/2014	750	10/3/2014	98
6/4/2014	765	10/4/2014	78
6/5/2014	738	10/5/2014	105
6/6/2014	762	10/6/2014	150
6/7/2014	744	10/7/2014	104
6/8/2014	735	10/8/2014	136
6/9/2014	747	10/9/2014	90
6/10/2014	739	10/10/2014	25
6/11/2014	601		
6/12/2014	393		
6/20/2014	474		
6/21/2014	641		
6/22/2014	507		
6/23/2014	462		
6/24/2014	451		
6/25/2014	199		
6/28/2014	298		
6/29/2014	432		
6/30/2014	458		
7/1/2014	413		
7/2/2014	410		
7/3/2014	424		
7/4/2014	421		
7/5/2014	379		
7/6/2014	339		
7/7/2014	304		
7/8/2014	254		
7/9/2014	250		
7/10/2014	218		
7/11/2014	161		

APPENDIX F

Sap Flux Instrumentation

Future work would involve expanding the temporal and spatial monitoring of vegetation within the riparian zone. A larger spatial analysis would allow for an estimate of transpiration from an area of the riparian zone, which could provide the possibility of scaling up the estimates. An expanded temporal analysis would allow for a comparison between late summer and winter values to determine a baseline for little to no transpiration. It would also allow for analysis of the growing season since the vegetation would be monitored throughout the year. This would provide better estimates of ET and provide greater insight into hydrological processes. An expanded study of sap flux transpiration within the riparian zone would have to involve a larger battery supply and larger solar panels to charge the batteries. The current setup (as of December 2015) is not able to supply power over the winter or even at times during extended cloud cover in the summer.

Table F.1 Table of Sap Flux instrumentation showing location, sensor number, species, and tree diameter at breast height (DBH).

Location	Sensor #	Tree Species	DBH (cm)
Riparian	1	Water Birch	11.1
Riparian	2	Water Birch	10.2
Riparian	3	Water Birch	14.3
Riparian	4	Water Birch	11.1
Riparian	5	Douglas-fir	19.4
Riparian	6	Douglas-fir	19.4
Riparian	7	Douglas-fir	27.4
Riparian	8	Douglas-fir	27.4
Riparian	9	Douglas-fir	27.4
Riparian	10	Douglas-fir	27.4
Riparian	11	Douglas-fir	10.8
Riparian	12	Sagebrush	8.0
Hillslope	1	Douglas-fir	44.6
Hillslope	2	Douglas-fir	27.7